EXPERIMENTAL AND ANALYTICAL INVESTIGATION OF STEEL HARDENED CURTAIN WALL MULLIONS

Harshal Chavan

Thesis submitted to the University of Ottawa
in partial Fulfillment of the requirements for the
Master of Applied Science

Department of Civil Engineering
Faculty of Engineering
University of Ottawa

ABSTRACT

Glass facade/curtain wall assemblies are commonly used in modern building construction as part of building envelop. This system has a number of advantages, including pleasant architectural appearance, building energy optimization, acceptable fire resistance and low maintenance. However, they pose tremendous risk towards maliciously intended acts of terror in the form of bomb blasts. The literature review conducted revealed lack of previous research on mullion strengthening/hardening. The present study has the objective of developing hardening techniques for curtain wall mullions to withstand high-intensity impulsive blast loads.

Combined experimental and analytical research was conducted for the development of mullion retrofit techniques using the Shock Tube Facility of the University of Ottawa. The test program involved retrofitting existing, commercially used aluminum mullions with steel plates and subjecting them to different levels of blast loads. The mullions were retrofitted with three techniques with the help of steel L shaped angles, steel plates and with a combination of steel HSS sections and plates. The results indicated an increase of load carrying capacity of the mullions up to a factor of 2.2 with up to 30% reduction in mid-height displacements. It was shown that the steel hardening components developed full composite action with the existing aluminum section, indicating the effectiveness of the hardening technology.

The analytical research followed the experimental research with the main objective of validating experimental results, as well as validating the assumption of full composite action between the core aluminum mullion and the hardening plates. The first step was to develop resistance functions followed by the validation of main analytical tool RC-Blast and the UFC charted solution. Following excellent agreement between these two analytical tools, RC-Blast was further validated against the experimental results. In addition, Pressure-impulse (P-I) diagrams were developed as design aids for different pressure-impulse combinations.

The retrofit techniques developed were applied to a selected prototype building to assess their feasibility for use in practice. Two different blast threats were considered for this application. Conclusions were drawn regarding the effectiveness of the curtain wall hardening techniques for use in practice.

ACKNOWLEDGEMENT

In the first place I would like to thank my thesis supervisor Dr. Murat Saatcioglu, my father Mr. Mohan A. Chavan, my mother Mrs. Vibhavari M. Chavan and my younger sister Ms. Vedanti M. Chavan for constantly motivating me towards the completion of this entire process of the research and the writing of thesis.

The unweaving support, expert guidance and the financial help throughout my studies offered by my supervisor helped me to focus on my research and complete it smoothly and in a timely manner. I will be always grateful towards the lead and knowledge I acquired from you. Also, I want to thank Dr. Gamal Elnabelsya for their help in conducting the lab experiments which was one of the major parts of this entire thesis.

I express heartiest gratitude towards my family for upholding me all the time through their continual moral and financial efforts since the time I decided to pursue Master of Applied Sciences at the University of Ottawa.

I would also acknowledge my best true friends Logesh, Stacy, Aashu, Devang, Ankur and Amrit whom I met while completing my course and Tejraj, Preshit, Aditya, Sunil, Balraj, Ritu, Harshali and Akshay, my friends from India, for their help in everything. My well wishes are with you all.

NOTATIONS

P_r	-	Peak reflected pressure
I_r	-	Peak reflected impulse
T_d	-	Positive blast phase duration
f_y	-	Yield strength of material
E_A	-	Modulus of elasticity of Aluminum
E_s	-	Modulus of elasticity of Steel
M	-	Moment capacity of section
K_s	-	Stiffness for simply supported beam
K_f	-	Stiffness for fixed supported beam
I	-	Moment of Inertia
y	-	Maximum distance of tension fibers from neutral axis
R_{y1}	-	Initial yield resistance
u_{y1}	-	Initial yield displacement
k_f	-	Fixed support stiffness
R_{y2}	-	Final yield resistance
u_{y2}	-	Final yield displacement
k_s	-	Simple support stiffness
R_m	-	Elastic yield resistance
u_y	-	Equivalent yield resistance
K_{eff}	-	Equivalent stiffness
K_{LM}	-	Load mass factor
T_s	-	Time period of structure
m	-	Mass of structure
F_1	-	Blast load acting on tributary area
μ	-	Ductility ratio
U_m	-	Maximum inelastic displacement

ACRONYMS

SDOF	-	Single Degree of Freedom
MDOF	-	Multiple Degrees of Freedom
FEA	-	Finite Element Analysis
DIC	-	Digital Image Correlation
DAS	-	Data Acquisition System
LVDT	-	Linear Variable Displacement Transducer
GAC	-	Global Affairs Canada
IGU	-	Insulated Glass Unit
TNT	-	Trinitrotoulene
UFC	-	Unified Facilities Criteria
FSI	-	Fluid Structure Interaction
SSCW	-	Steel Stud Curtain Wall
FE/BR	-	Forced Entry / Ballistic Resistance
ALR	-	Arbitrary Lagrangian Method
VE	-	Visco-elastic Damper
ADAS	-	Additional Damping and Stiffness Device
HSS	-	Hallow Steel Section

TABLE OF CONTENTS

LIST OF FIGURES

LIST OF TABLES

CHAPTER 1. INTRODUCTION

1.1 GENERAL

Glass façades/curtain walls are commonly used in modern building construction for functional and architectural reasons. These building envelopes often consist of glass panes supported by aluminum mullions. Critical government facilities and office buildings may be at high risk for ill intended terrorist attacks, such as bomb blasts. Recent experience with such blast loads on critical infrastructure indicated that there exist needs for detailed experimental and analytical research for hardening of existing curtain walls and their aluminum mullions. In a recent experimental and analytical investigation at the University of Ottawa it was found that the aluminum mullions of glazed curtain walls suffer significant damage due to lack of strength and deformability of the mullions. The two primary factors that contribute to the undesirable performance of such walls included i) lack of mullion strength and ii) weak connections between the vertical and horizontal mullions under blast loads. Figure 1-1 illustrates the poor performance of curtain wall assemblies during a shock tube test, when a catchment system is used for blast protection of the occupants (Saatcioglu et al. 2017a and 2017b).

Figure 1 - 1 : Typical curtain wall failure during shock tube tests

1.2 OBJECTIVES & SCOPE

The objective of the current research project is to develop a blast-resistant hardening technology for curtain wall mullions to mitigate blast risk in critical infrastructure. The technology involves the use of steel plates of different form to increase strength and stiffness of existing aluminum mullions. This objective is attained by following the steps involved in the scope outlined below:

- Literature review of curtain wall hardening techniques and research conducted to date.
- Selection of three different sizes of aluminum mullions commonly used in building construction for testing using the University of Ottawa Shock Tube.
- Selection of three different hardening techniques involving the use of steel sections and/or steel plates.
- Testing of six mullions (three pairs) at the University of Ottawa Shock Tube Facility under simulated blast loading. The first test in each pair includes reference mullion with a different size, simulating curtain wall components in practice. Tests of three companion mullions of the previously selected sizes, hardened with steel plates of different configurations under progressively increasing blast load intensity (reflected pressure and impulse).
- Dynamic analysis of mullions and validation against test results.
- Analytical parametric investigation of curtain wall mullions under the blast loading, where the parameters consist of the size and type of curtain walls, fixity of mullions, threat level and the type of hardening technique used for retrofitting.
- Selection of a prototype building to investigate the feasibility of implementing the hardening techniques and making recommendations for use in practice.

1.3 RESEARCH SIGNIFICANCE

The current research program is intended to fill research gaps in the area of critical infrastructure protection against maliciously intended acts of terror in the form bomb blasts. One of the commonly used building envelop component is glass curtain wall, which is commonly used in modern office buildings and government facilities. While the technology to protect glass panes in such walls is available in the form of protective films and interlayer for blast-resistant glass, the hardening practices for mullions that support the blast loads transferred from glass panes lack sufficient research. These mullions are commonly manufactured using hallow aluminum sections, which lack the required strength and stiffness. The use of steel plates/sections on existing mullions are likely to provide much needed solution to the problem. However, there has not been research data in the literature to show their effectiveness. The level of composite action between the two dissimilar materials brings.

1.4 THESIS BREAKDOWN

Chapter 1 - Introduction

- Brief introduction to the thesis research, need for research, objectives and scope.

Chapter 2 - Literature Review

- Introduction to the curtain wall system and its components.
- Review and summary of previous experimental and analytical research conducted on blast resistant design of curtain walls.
- Identifying research gaps from the available literature.

Chapter 3 - Experimental Research

- Detailed explanation of the experimental program, including the experimental setup, specimens used, and the hardening techniques implemented.
- Discussion and comparison of experimental results obtained for existing reference mullions and hardened mullions with respect to pressure-time relationships and deflection-time histories.

Chapter 4 - Analytical Research

- Description of the analytical tools and development of resistance functions for test specimens.
- Validation of analytical methods and the development of design charts in the form of pressure-impulse (P-I) diagrams to predict the behavior of unhardened and hardened mullions for different pressure-impulse combinations.

Chapter 5 – Application of the Steel Hardening Techniques to a Prototype Building

- Selection of a prototype building and the implementation of the retrofit techniques developed to the building.

Chapter 6 - Conclusion

- Presentation of conclusions drawn from the current combined experimental and analytical investigation.

CHAPTER 2. LITERATURE REVIEW

2.1 GENERAL

This chapter provides an overview of existing knowledge on blast-resistant curtain walls, and a review of previous research on the topic. The following sections are briefly explained and reviewed in the chapter:

- Section 2.2: Introduction to curtain walls and mullions.
- Section 2.3: Curtain wall design guidelines.
- Section 2.4: Previous research on blast resistance of curtain walls.
- Section 2.5: Summary of literature review identifying research needs/ gaps.

2.2 INTRODUCTION TO CURTAIN WALLS & MULLIONS

2.2.1 Composition of a Curtain Wall System

Curtain walls are non-structural elements used to cover building exterior and serve as elements of building envelop. They are intended to protect buildings against weather and wind effects. They are not designed to carry gravity loads for the building, other than carrying their own weight. Curtain walls are made of light-weight materials. They are often made out of glass, which brings additional advantages, such as natural light and architecturally pleasant looks, while maintaining resistance to water and air infiltration into the building. Glass curtain walls consist of glass panes supported by light aluminum frame elements, referred to as mullions. Vertical mullions may span between the floors and may be supported by slabs or spandrel beams. Hence, they transfer out-of-plane loads, typically due to wind, to the structural framing system. The curtain walls also have horizontal mullions, sometime referred to as transoms that allow the use of smaller glass panels and provide support in the horizontal direction. Horizontal mullions frame into main vertical mullions, transferring wind loads collected by glass panels to vertical mullions. Therefore, horizontal mullions are smaller in size than vertical mullions.

An important feature of glass panes used in curtain walls is their insulation property. Therefore, often multiple panes are used as panels supported by the mullions. Insulated glass units (IGU) are commonly used as multiple glass panes with air gaps in between. Glass used is often tempered for increased strength and performance. IGUs can have multiple glass panes, but

double-pane glass panels are common for use in buildings. Figure 2-1 shows a typical glass curtain wall covering the exterior of a multi-story building.

Figure 2 - 1 : Curtain walls with glass panels (Northview Inc. 2021)

Glass curtain walls are designed to maintain their integrity and functionality during strong out-of-plane loads, such as those caused by windstorms and earthquakes. However, they are often vulnerable to blast-induced shock waves imposed on buildings due to a nearby accidental explosion or maliciously intended terrorist bomb attacks. Curtain wall design against blast loads brings a new dimension to the design of curtain walls. First, glass panels must be protected either by using laminated blast-resistant panels of by protective film placed over the glass on the interior face, thereby glazing the glass against breakage. Secondly, the mullions that support the glass panes must be strengthened against blast loads that are transferred from the glass panels. The current research project has the objective of developing techniques for strengthening aluminum mullions against blast loads. Further discussion of curtain wall behavior under blast loads is presented in Section 2.4 as part of literature review.

2.2.2 Advantages of Glass Curtain Wall Systems

Curtain walls are used in the construction industry as light-weight non-structural cladding elements. Glass curtain walls have certain advantages over other light-weight building cladding, which are outlined below:

- *Architectural Appearance:* A unique and sophisticated look of a building is created by using glass curtain walls on a building.
- *Fire Resistance:* In case of fire in a building, fire transmission across the surface in between the floors commonly occurs. Curtain walls act as a barrier for floor to floor spread of fire due to zero fire transmission across the surface.
- *Effect on thermal efficiency of building:* Glass curtain walls are equipped with insulated glass units (IGU) that consist of multiple glass panes with insulating air gaps in between. This results in temperature stabilization within the building with reductions in the building operating cost. In addition, they may be glazed for increased UV resistance, which prevents the objects inside the building from fading and degrading quickly.
- *Increase in structural stability:* A curtain wall system, even though not a load bearing system, helps dispersing stresses evenly throughout the entire frame of the building. This system is more resistant to withstand high wind loads, which helps reduce the sway of the building.
- *Low maintenance cost:* Curtain walls provide an insulating cover for the building against weathering. Air and water are kept out of the structure. This results in reduced maintenance cost and increased durability.
- *Blast proof design:* Due to its unique structural components and their alignment, it is viable and efficient to design curtain walls against blast loads. Currently, many high-profile structures include blast-resistant curtain walls to mitigate risk associated with maliciously intended bomb attacks.

2.3 CURTAIN WALLS DESIGN GUIDELINES

Design guidelines for blast-resistant curtain walls are scarce in the literature. A commonly used approach is prescribed in the US Army document "Unified Facilities Criteria (UFC-3-340-02)." This approach is summarized below with references made to design aids and design expressions included in the document.

2.3.1 Allowable limits for frame (mullion) design

The allowable limits for frame design with respect to deflection, stress and fasteners are given as follows.

Deflection: The relative deflection of the frame members (vertical mullions) shall be the minimum of 1/264th of the entire span length or 0.125 inch.

Stress: The maximum stress in any member (vertical mullion) shall not exceed $f_Y/1.65$, where f_Y is the yield stress of material for the member.

Fasteners: The maximum stress in fasteners shall not exceed $f_Y/2.00$, where. f_Y is the yield stress of the material for the member.

2.3.2 Calculation of design load and line shear

The typical parameters such as geometry of curtain wall, blast loading, resistance function and equivalent SDOF system are represented as follows.

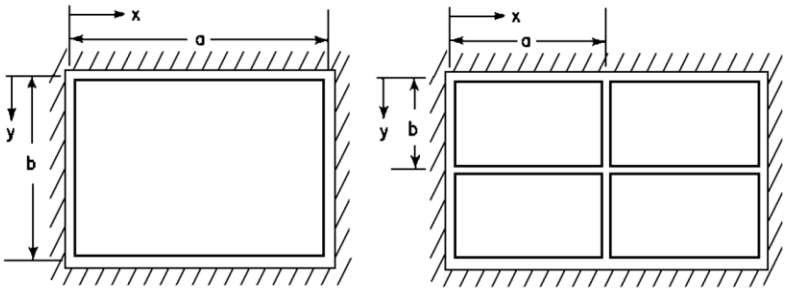

Figure 2 - 2 : Typical curtain wall geometry

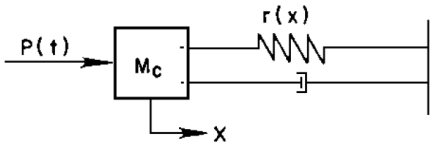

Figure 2 - 3 : Equivalent SDOF system

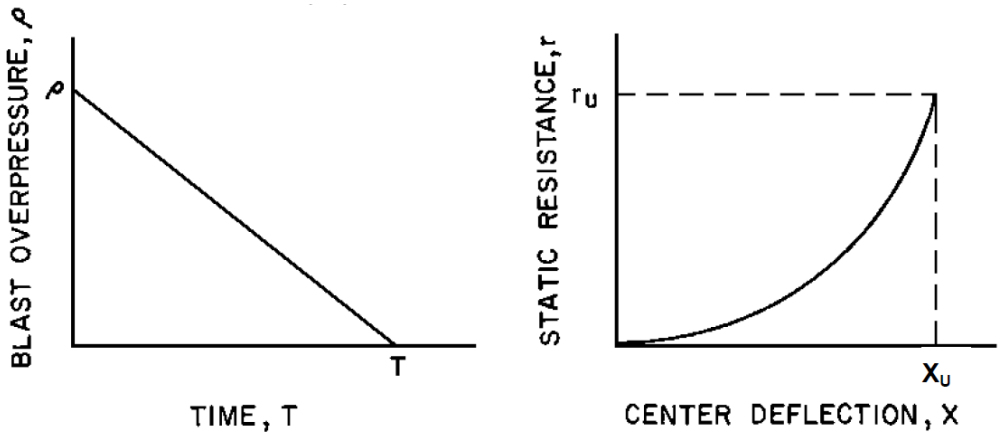

Figure 2 - 4 : Typical blast loading (left) and resistance of curtain wall (right)

The calculation of static design load r_u applied on the exposed frame members with a member width, w, tends to produce a line shear V_x acting along the longer side 'a', line shear V_y acting along the shorter side 'b' and the corner concentrated load 'R', produced by static design load are given as follows.

$$V_x = C_x r_u b \sin (\pi x/a) + r_u w, \text{ lb/in}$$

$$V_y = C_y r_u b \sin (\pi y/b) + r_u w, \text{ lb/in}$$

$$R = C_R r_u b^2, \text{ lb}$$

Where, C_x, C_y, and C_R are design coefficients for practical aspect ratios which are calculated with reference to Table 6-9 in the UFC-3-340-02 document. Figure 2-5 illustrates assumed distribution of panel edge shear forces as support reactions. The standard guideline for the calculation of design load is explained as follows.

- Case I - curtain wall with linear response

In order to obtain a linear response for curtain wall, the design static load and effective static load are calculated as follows.

$$r_u = r_{eff} = C_r (t/b)^2 \text{ psi}$$

The center deflection of the glass pane is given as,

$$X_u = C_D (b^2/t)$$

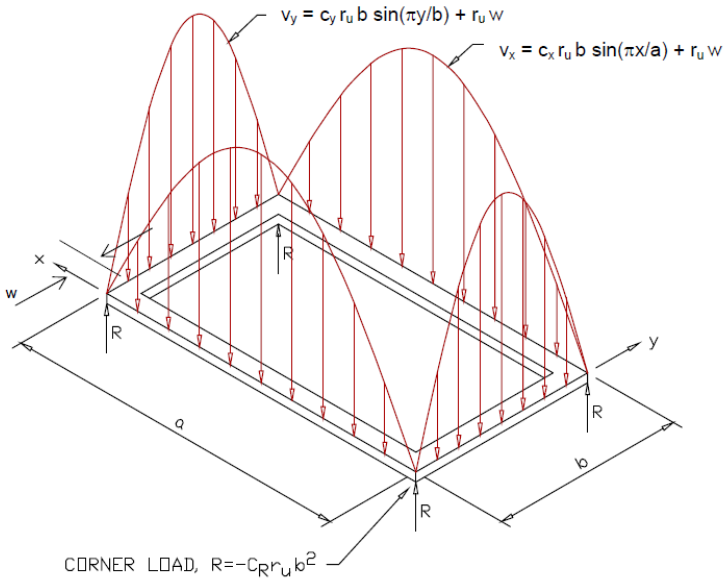

Figure 2 - 5 : Distribution of static design frame loads

Here, C_r and C_D are coefficients for calculating effective resistance and center deflection, given in Table 6-8 of UFC-3-340-02 document. The fundamental period of vibration is given as,

$$T_N = C_T (b^2/t)$$

Where, C_T is the coefficient mentioned in the last column of Table 6-8 of UFC-3-340-02.

- Case II - curtain wall with nonlinear response

When the b/t ratio of the curtain wall glass pane is greater than that specified in column 2 of Table 6-8 in UFC-3-340-02, a non-dimensional design stress is calculated as follows.

$$S_{ND} = 0.0183 (b/t)^2$$

Where, b = shorter dimension of glass pane measured between centerlines of gaskets in inches and, t = actual thickness of glass from Table 6-7 of UFC-3-340-02 in inches (Use a/b = 4 for values of a/b > 4).

Next, determine the non-dimensional load L_{ND} from Figure 6-49 of the UFC document, with the values of S_{ND} and a/b calculated as above. Thus, the static design resistance can be obtained as follows.

$$r_u = 876{,}000 (L_{ND})(t/b)^4 \text{ psi}$$

Thus, the above value of static design resistance can be used in calculating frame design loads. In order to calculate the corresponding non-dimensional deflection, the values of a/b and L_{ND}, can be used from Figure 6-50 of UFC-3-340-02. When the value of X/t exceeds 10, recalculate the value for r_u, using the value of L_{ND} corresponding to X/t value of 10 using Figure 6-49 of the UFC document. Thus, the center of deflection of glass pane is given as,

$$X_u = (X/t)t, \text{ in}$$

Now, the effective elastic static design resistance, which is the equivalent static design load of a plate behaving elastically at the same strain energy as that of nonlinearly responding plate at the design center of deflection X_u, given as,

$$r_{eff} = 0.4\ (r_1 + r_2 + r_3 + r_4 + 0.5\ r_u) \text{ psi}$$

where,

r_1 = resistance at 0.2 X_u

r_2 = resistance at 0.4 X_u

r_3 = resistance at 0.6 X_u

r_4 = resistance at 0.8 X_u

Here, values of r_1 to r_4 are calculated from Figures 6-49 and 6-50 of UFC-3-340-02 document, considering r_u and X_u obtained for nonlinear curtain wall glass pane response.

The effective stiffness is then calculated as follows,

$$K_E = r_{eff}/X_u, \text{ psi/in}$$

Similarly, the time period of the structure is given as,

$$T_N = 2\ \pi\ (K_{LM}\ m\ /\ K_E)^{1/2}, \text{ msec}$$

where:

$K_{LM} = 0.63 + 0.16(a/b - 1),\ 1 \leq a/b \leq 2$

$K_{LM} = 0.79,\ a/b > 2$

and unit mass of the glass, $m = 233t$, lb-ms^2/in^3

After the calculation of static design resistance for elastically and inelastically responding glass panes, the blast overpressure capacity of the glass is obtained as below.

$$B = r_{eff}/DLF$$

DLF is the dynamic load factor obtained from Figure 3-49 of the UFC document, where, T/T_N is the ratio of blast duration to fundamental time period. For $T/T_N > 10$, use DLF = 2 and for $T/T_N < 0.05$, use DLF = 0.3.

2.3.3 Phenomenon of rebound

During the positive phase duration of blast loading, the curtain wall shows inward deflection which may be followed by a rebound phase causing outward deflection of the glass and the curtain wall frame. This outward (negative) deflection can cause the window to fail while the positive blast pressure is still acting on the curtain wall. If the curtain wall weakens due to rebound during positive phase duration, the glass fragments tend to fall inside of the structure, causing a potential threat to the building occupants. However, if the curtain wall fails during the rebound causing negative deflection, the glass fragments fall outside of the structure.

During the negative phase of blast loading, phenomenon of rebound will occur when the effective duration of blast is not greater than one half times of the natural frequency of the curtain wall. Similarly, during the positive phase duration, rebound will occur when the blast duration is not greater than ten times of the natural frequency of the structure. However, considering a conservative approach, the resistance function for the maximum rebound load, r^-, can be found as the design static load, r_u, from the Case I and Case II listed in *Section 2.3.2* and the negative resistance function being the mirror image of the positive resistance function.

2.4 PREVIOUS RESEARCH ON BLAST RESISTANCE OF CURTAIN WALLS

This section presents previous experimental and analytical research performed to study and enhance the response of curtain walls under blast loads. The majority of previous research was in the form of experimental testing and validation of results with numerical analyses. A summary of previous research is presented in the following sections with a view of identifying research gaps.

<u>Saatcioglu, M. Alameer A. and Elnabelsy, G. (2017a and 2017b) and Saatcioglu, M. (2020)</u>

A comprehensive research program was conducted at the Blast Research Laboratory of the University of Ottawa to investigate performance of curtain walls under blast loads. The laboratory is equipped with a pneumatically driven shock tube as a blast simulator. The primary objective of the research program was to analyze and enhance the performance of curtain walls

used by Global Affairs Canada (GAC) in Canadian assets abroad to mitigate blast risk. Figure 2-6 illustrates the geometric details of the curtain wall components tested. Figure 2-7 depicts the cross-sectional geometry of vertical and horizontal mullions.

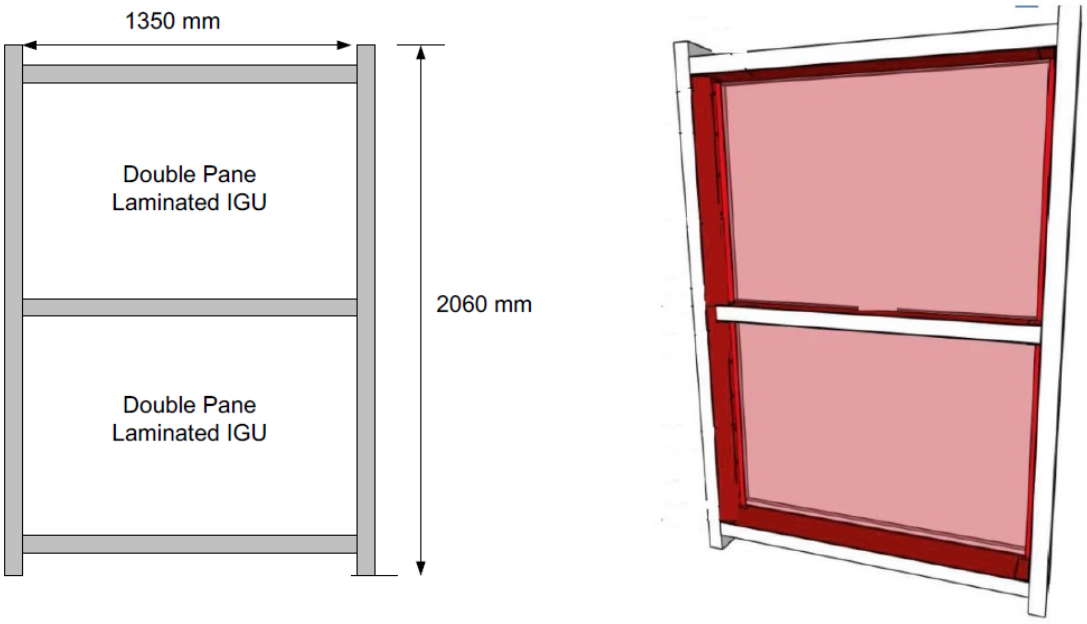

Figure 2 - 6 : Front view of curtain wall (left) and 3-D view of curtain wall (right)

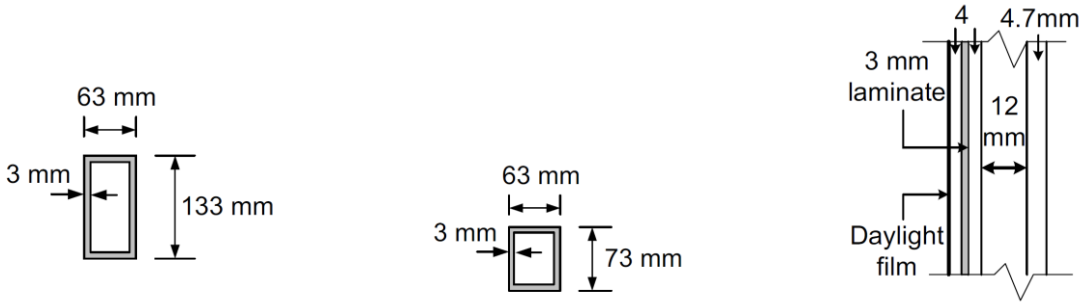

a. Vertical Mullion Section **b. Horizontal Mullion Section** **c. IGU Section**

Figure 2 - 7 : Details of curtain wall components

The mullions were made of rectangular aluminum sections. The focus was placed on double pane insulated glass units (IGU) with vertical and horizontal (transoms) mullions. The glass panels consisted of laminated blast-resistant tempered glass panes separated from other glass panes by an insulating air gap. The IGU consists of 4.7 mm thick tempered glass on the outer pane which was exposed to the blast loads. The inner pane consisted of two 4 mm tempered glass, laminated

by a 3 mm lamination on the protected side of the curtain wall. Figure 2-8 illustrates a typical test specimen considered.

Figure 2 - 8 : Typical curtain wall specimen during installation for testing

Three phases of research were conducted. Phase I consisted of tests of two full size curtain wall specimens to investigate the effectiveness of a catchment system known as “Guardian Coil” for the protection of occupants in a building. Both windows were protected by Guardian Coil, placed at 300 mm away from the curtain walls. Curtain Wall 1 was tested using the test specimen without any retrofit, simulating the on-site conditions on the building. The second specimen was retrofitted by adding an additional ply of mechanically anchored 7 mil protective film. The film was applied to both interior panes. The mechanical anchoring for the top IGU pane was done by anchoring the protective film to top and bottom horizontal mullions (without anchoring to the vertical mullions), promoting one-way action. The bottom interior pane was anchored along four edges (to horizontal and vertical mullions), promoting two-way action. The second curtain wall was further retrofitted by securing the middle horizontal mullion to the two vertical mullions by means of aluminum angles and drill-through bolts.

Both curtain walls were subjected to similar pressure time histories. Curtain Wall 1 was subjected to a maximum reflected pressure-impulse combination of 85.5 kPa and 1334 kPa-msec; and Test 2 was subjected to 85.6 kPa and 1923 kPa-msec. The curtain wall without the retrofit failed through the detachment of horizontal mullion early in response, with the penetration of glass shards towards the witness panel. The glazed curtain wall panes fell into the Shock Tube and the

fragments of unprotected exterior glass penetrated towards the witness panel 3.0 m away from the curtain wall, scoring 5 (High Hazard – No protection) on the standard GSA Rating Scale. The penetrated glass fragments reached the witness panel, weighing 1014 grams. The protected (glazed) windowpanes that fell into the Shock Tube were damaged/cracked but maintained their integrity. The Guardian Coil also maintained its integrity while developing yielding of the coils at the top and bottom where it was attached to the tracks. Some of the hooks connecting the Guardian Coil were detached from the tracks, though the unit as a whole remained in place, catching large curtain wall components but not the entire glass fragments. The coil was found to be partially open after the test. Figure 2-9 illustrates the damage observed during the test, with Figure 2-10 showing the specimen at the end of the test.

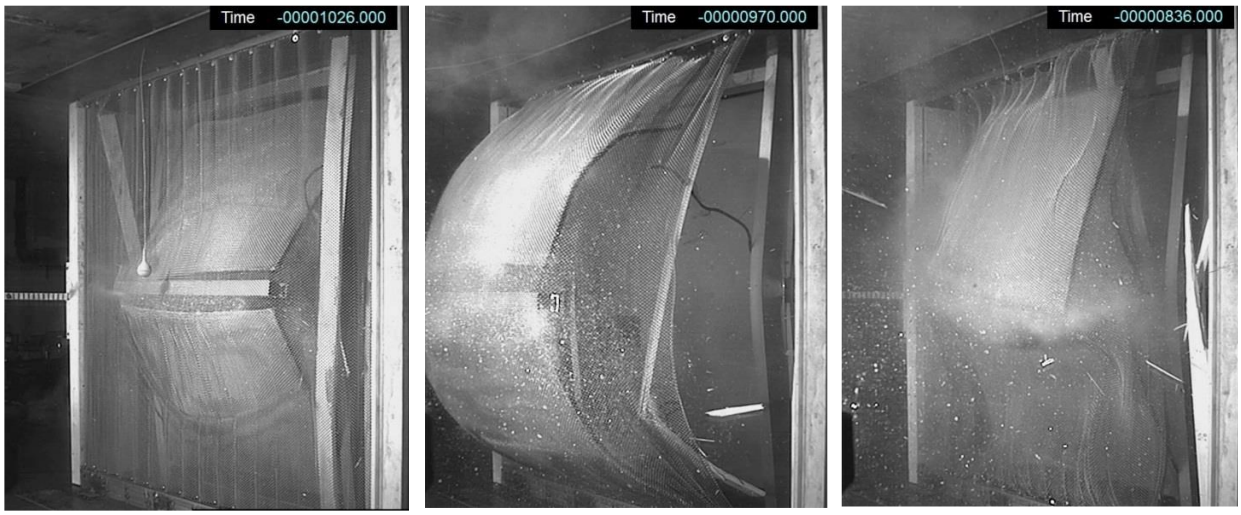

a. **b.** **c.**

Figure 2 - 9 : **Curtain Wall 1 response during blast: a. Detachment of horizontal mullion, b. Catchment by guardian coil, c. Debris fall back in shock tube**

The second (retrofitted) curtain wall (Curtain Wall 2) performed better with significant damage to the vertical mullions. Both vertical mullions fractured in central regions where the horizontal mullion was bolted as part of the retrofit strategy. The glazed windowpanes remained intact and remained attached to the mullions. The unprotected external glass panes failed, and the glass fragments fell into the Shock Tube with some shards flying in through the side opening of damaged curtain wall where the blast pressure vented and carried glass fragments. Only a small amount of glass shards penetrated, weighing 760 grams, which fell within a 300 mm distance in

front of the Shock Tube. The Guardian Coil was able to contain larger fragments and damaged curtain wall components. The overall performance was judged to score 3(a) (low hazard-high protection) on the GSA Ranking Scale. Figure 2-11 shows the test specimen after the test.

Figure 2 - 10 : Curtain Wall 1 after the test

a. Front view at the end of Test 2

b. Side view after moving the drapery to expose the vertical mullion

Figure 2 - 11 : Retrofitted Curtain Wall 2 after testing

Phase II research consisted of tests of two additional curtain walls, having the same properties as those used in Phase I. However, the specimens were not protected by the catchment system, but instead they were retrofitted for improved blast performance. The first test in Phase II (labelled as Curtain Wall 3 test) had a curtain wall that was retrofitted similar to the Curtain Wall 2 tested in Phase I, with some variations. The retrofit consisted of inner panes strengthened by adding an additional ply of mechanically anchored 7-mil protective film. The films were mechanically anchored to vertical mullions only, performing in one-way action. The curtain wall was further retrofitted by enhancing the connection between the middle horizontal mullion and the vertical mullions on both sides by means of aluminum angles, epoxy glued on the mullions. Unlike the Curtain Wall 2, the connection enhancement in Curtain Wall 3 was done without the use of through bolts, which were believed to have weakened the vertical mullion flexural capacity in the critical positive moment region. Furthermore, Curtain Wall 3 was tested under a reduced threat scenario, with a maximum reflected pressure of 80 kPa and a maximum impulse of 448 kPa-msec. This curtain wall performed very well. The unprotected top and bottom outer panes failed, as expected. The inner panes, mechanically glazed, performed very well and survived the blast loads without a crack. The horizontal mullion remained attached to the vertical mullions and the chemically bonded (epoxy glued) angles used to enhance the connections performed well without any sign of detachment. The vertical mullions deflected by 25 mm at their mid-heights (where the horizontal mullion was attached) and the horizontal mullion deflected by 35 mm at mid-length. The curtain wall remained intact without the detachment of any of the inside components. The horizontal aluminum piece on the unprotected blast side was detached on one side and remained attached to the vertical mullion on the other side. The curtain wall was rated as “1” on the standard GSA Rating Scale, indicating “safe” performance with no blast hazard to the curtain wall. Figure 2-12 illustrates the performance of the Curtain Wall 3. It should be noted however, that the test specimen consisted of two double pane IGUs, one above the other, without the side IGUs on both sides of the vertical mullions. Hence the vertical mullions were subjected to loads coming from pressures acting on one side, with the implication that they may be subjected to approximately 50% of the blast loads expected in the prototype building.

a. Prior to testing

b. After the test

Figure 2 - 12 : Test of Curtain Wall 3

The second curtain wall specimen in Phase II (Curtain Wall 4) was tested after implementing an enhanced retrofit strategy, which included strengthening of the mullions. The retrofit for this curtain wall consisted of inner panes strengthened by adding an additional ply of mechanically anchored 7-mil protective film. The films were mechanically anchored only to vertical mullions to perform in one-way action. The curtain wall was further retrofitted by strengthening both vertical mullions and the middle horizontal mullion by epoxy bonding two 3.18 mm aluminum plates on both sides of each mullion. This method of strengthening vertical mullions was intended to increase elastic flexural capacity by a factor of 1.5 (assuming perfect bond between the added plates and the existing mullions). The strength increase was believed to provide additional capacity against higher threats relative to that for Curtain Wall 3, and also account for the fact that in the prototype building the blast pressures would be applied to glass units on both sides of vertical mullions, unlike the test condition. Furthermore, the connections between the middle horizontal mullion and the vertical mullions on both sides were enhanced by means of two aluminum angles at each end, epoxy glued and screwed using three 9.5 mm self-tapping screws to the mullions, one at the top and the other at the bottom of each connection. The curtain wall was subjected to 84 kPa of reflected pressure and 1630 kPa-msec of reflected impulse. This level of pressure-impulse combination corresponds to a very significant increase in the threat level relative to that used to test Curtain Wall 3. Curtain Wall 4 did not perform well. The horizontal

mullion was detached and flew in towards the witness panel along with all four panes of glass. While the vertical mullions remained connected to the Shock Tube frame, three of the four vertical aluminum plates that had been used for strength enhancement were also detached from the mullions. The angles used to connect the horizontal mullion to the vertical mullions failed and were detached at vertical mullion ends, flying in along with the horizontal mullion. The epoxy glue and the screws used to secure the angles sheared off at the ends. The performance of curtain wall was rated as “5 – high hazard – no protection” based on the Standard GSA Test Ranking. Figure 2-13 illustrates the performance of the specimen.

It was decided to extend the experimental findings of Phase I and Phase II analytically to other curtain wall scenarios in Phase III. Furthermore, pressure impulse (P-I) diagrams were needed to assess the effects of different threat levels on curtain walls. The analytical assessment of curtain walls in Phase III involved the use of a manual single degree of freedom (SDOF) non-linear dynamic analysis method outlined in the US Unified Facilities Criteria (UFC) of the US Department of Defence (UFC 3-340-02) and the RC-Blast Software developed at the University of Ottawa. The emphasis was placed on the analysis of Curtain Wall 3, without the vertical mullion retrofit, and Curtain Wall 4 with the strengthened mullions. Displacement time histories were generated for each case for simply supported and fully fixed vertical mullions. In addition, P-I diagrams were developed for each case. The analysis was extended to include analytical models subjected to the same blast loads but resisted by a single mullion.

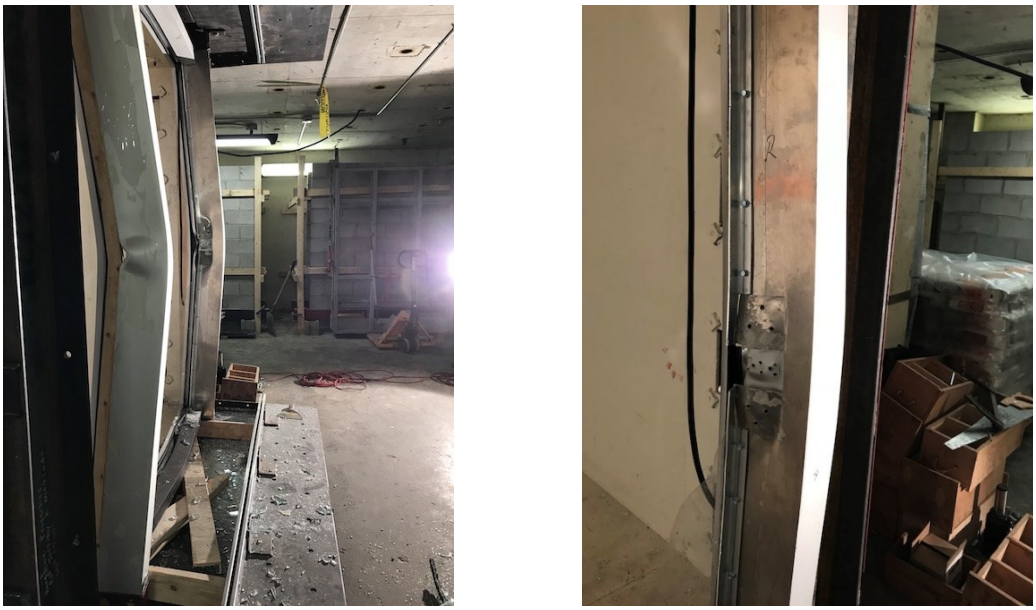

Figure 2 - 13 : Damage to vertical mullions (left) and failure of the mullion connection (right)

The analytical results showed that excellent correlations exist between the charted-solution presented in the UFC document and those generated by software RC-Blast, as well as experimental observations and the results generated by the software. It was found that the retrofit strategy developed on the basis of test data was not adequate if a single mullion were to resist the same blast loads. Hence, an enhancement was proposed to the hardening procedure suggested earlier, involving the replacement of the aluminum plates with two L-shaped aluminum angles overlapping over the mullion flange. This hardening technique, coupled with securing the connections between the horizontal and vertical mullions and increasing the safety of glass panels by mechanically anchored protective films would provide sufficient risk mitigation strategy for the threat level considered, by limiting inelasticity in the vertical mullions.

Further analysis of a selected prototype building was conducted using the actual floor height of 3.1 m in the building, as opposed to the analytical models that replicated the scaled experimental models. These analyses were conducted under the increased threat level of 176.8 kPa reflected pressure and 627.2 kPa-ms reflected impulse, with an equivalent duration of 7.1 ms based on an idealized triangular pressure-time distribution. The increased threat level and the increased storey height relative to the earlier cases considered, necessitated further hardening of the mullions using steel sections. A retrofit strategy, consisting of the use of matching 63 X 63 mm X 6.3 mm HSS section (2.5 in X 2.5 in X ¼ in) and two steel side plates of 6.3 mm (1/4 in) thickness, was considered. The results indicated satisfactory performance if fully composite behaviour between the existing mullion and the added steel sections was attained.

Kennedy, B.T., Weggel D.C., and Keanini, R.G. (2013)

Kennedy et al. (2013) performed tests of curtain walls, validated by an analytical study. The test program included a conventional curtain wall and two other specimens in which one had annealed glass panes with conventional compression gaskets and the other had annealed glass panes with structural silicone sealant for glazing. Effects of these two modifications on the laminated glass and the mullions were studied with respect to nonlinear behavior, failure resistance and global energy absorption of the system. The study also demonstrated the application of an equivalent SDOF model to complex nonlinear MDOF response. Figure 2-14 shows the test of a wet glazed test specimen.

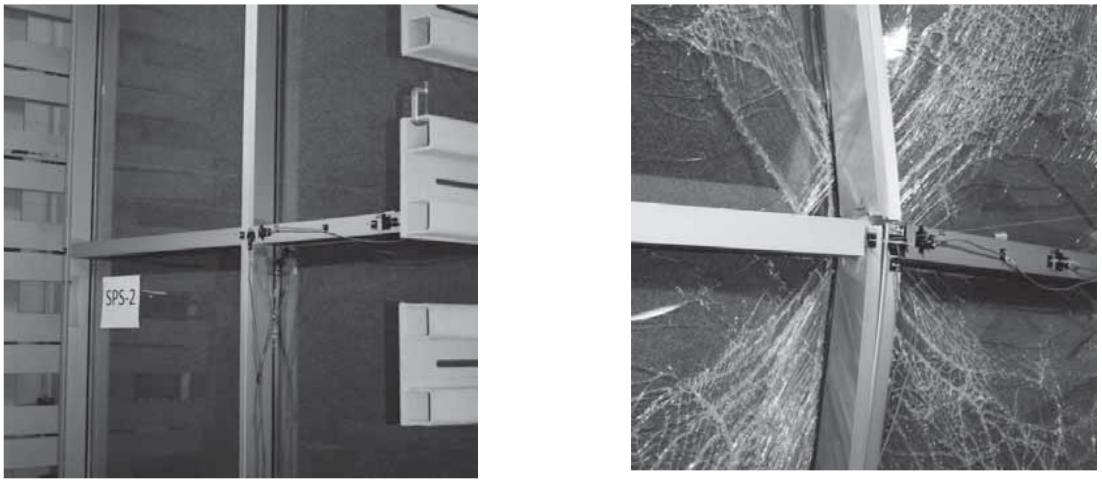

Figure 2 - 14 : Wet glazed specimen before loading (left) and Wet glazed specimen after loading (right)

A combined resistance function was developed for each quadrant of the curtain wall on the basis of the local deformations recorded at different nodes of the curtain wall using interpolation functions. Integration of the resistance curve represented energy absorbed by that particular quadrant up to its ultimate failure. The ultimate energy absorbed by wet glazing was greater by 31% than that of dry glazing. This resulted in end rotations and mid height deflection of wet-glazed wall to be greater than those for the dry-glazed wall.

Dynamic analyses were performed by the researchers with an approximate linear elastic and perfectly plastic bilinear resistance functions. The slope of linear elastic region, maximum elastic resistance and the deflection at ultimate failure were used as the parameters of the bilinear resistance function for the wet glazed curtain wall, which had the maximum energy absorption capacity. After computing and comparing the ultimate energy from the resistance functions obtained from experimental and numerical investigation, analytical resistance functions were found to have 6.8% higher energy than the experimental resistance functions. The results also indicated that the structural silicone sealant resulted in the detachment of the glass pane from the mullion, while the laminated glass was able to transfer in-plane tensile stresses associated with membrane action.

Ralston, A. D., Weggel D. C., and Wheelan, M. J. (2015)

The aim of this study was to develop a finite element model and validate it using the experiments conducted on actual curtain walls. Ralston et al. (2015) performed blast tests on conventional curtain walls to check their efficacy in safeguarding the building against blast loads. Three specimens with silicone sealant were used instead of the conventional compression gaskets. The tests were performed in an open arena of the Infrastructure Security and Emergency Responder Research and Training (ISERRT) facility in Gastonia, NC. The blast resistance of the curtain walls was also studied with the help of a simple nonlinear single degree of freedom expression (NSDOF). During the experiments, each specimen was tested under incremental loading, which resulted in the failure of the curtain walls as shown in Figure 2-15. The specimen with the maximum load resulted in the tearing out of the glass due a combined action of shear and torsion on the silicone bead. As there was no catastrophic failure, a medium level of protection was established as per UFC 4-010-01.

A finite element model was generated using commercial code LS-DYNA. The laminated glass was modelled as a shell element with a defined failure strain rate such that, once the critical strain rate was reached the shell element would not contribute to the stiffness of the frame. A typical test curtain wall is shown in Figure 2-15. The corresponding finite element mode is depicted in Figure 2-16.

Figure 2 - 15 : Curtain wall specimen before testing (left) and after testing (right)

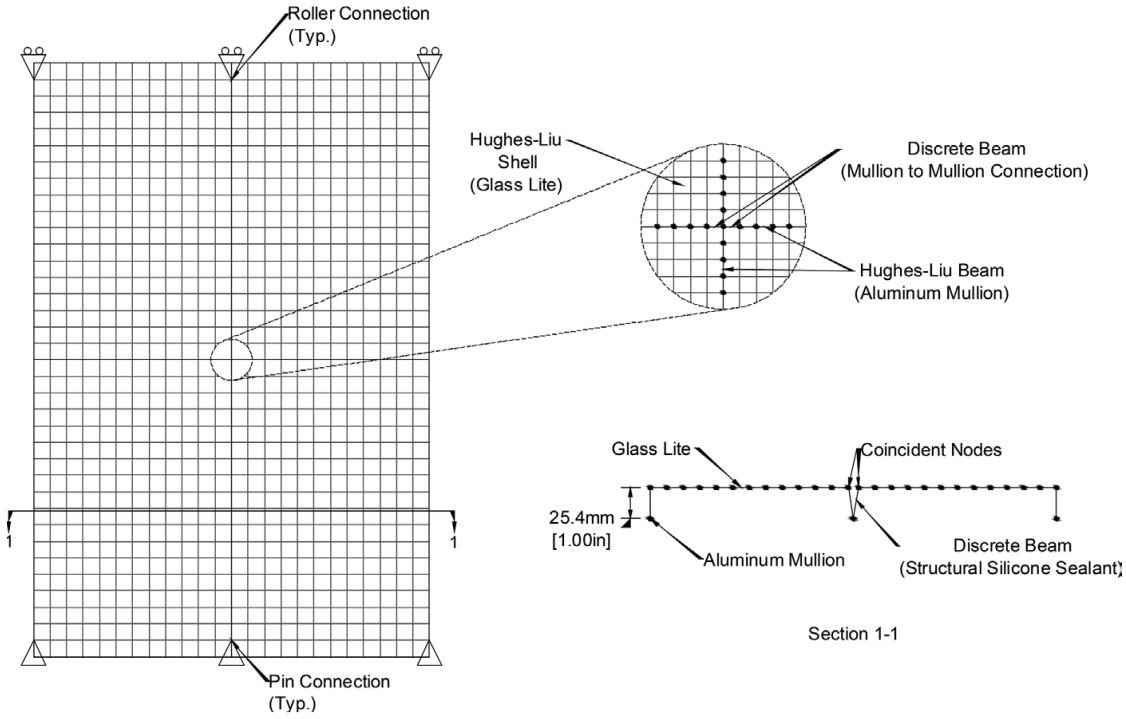

Figure 2 - 16 : Curtain wall finite element model

The blast load parameters recorded by the transducer in physical testing were applied to the FE model in the form of idealized blast wave forms, considering the effect of fluid structure interaction (FSI). After computing the fundamental period of the system, the damping effect was calculated considering structural, aerodynamic and FSI effects. Aerodynamic and FSI effects were considered as the curtain walls were lightweight and flexible. The program simulation resulted in identical response of the FE model in terms of deflection time histories of glass and mullions.

Based on the experimental and FE analysis it was concluded that, most of the specimens failed because of the extensive mid height deflection of the vertical mullions and the remaining failed due to the large tear out length of the glass. It was also learnt that the accuracy of the results is governed by the high strain rates of the glass and damping of the system.

Weggel, D. C., Zapata, B. J., and Keifer, M. J. (2007)

The research paper aims to study the properties and dynamic behavior of glass curtain walls equipped with split screw spline mullions. The two differences made to the conventional curtain wall were, i) instead of monolithic glass, laminated glass was used with silicone sealant in place of compression gaskets and ii) the split screw spline vertical mullions were employed, as illustrated in Figure 2-17. Static and free vibration tests were performed on curtain wall

specimens using an air bag apparatus and pluck tests, respectively. Based on the loading of pluck tests, it was observed that the horizontal mullions exhibited a low rotational stiffness for out of plane rotations relative to the centerline of the vertical mullion. The damping of the system was calculated by using half-power point method for each mode of vibration. The observations made were validated with the analytical research program.

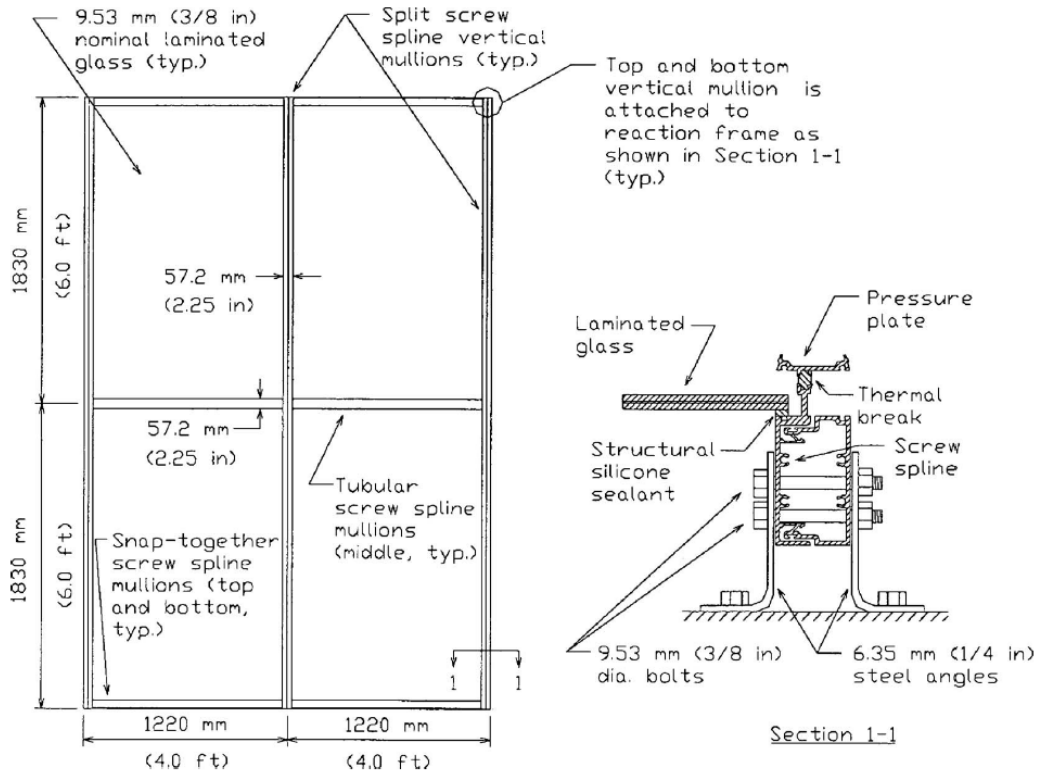

Figure 2 - 17 : Elevation and section of split screw spline curtain wall specimen

ANSYS structural analysis program was used to model the curtain walls. Glass lites were modelled as shell elements which represented the overall stiffness of the system. It was found that the static and experimental deflections calculated had a difference of 8%. This calibrated model was used for finite element modal analysis. It was observed in the modal analysis that the mode shapes for the first, second and fourth modes represented symmetrical mode shapes along vertical and horizontal axes. There was little difference observed between prominent analytical modal frequencies and experimental frequencies. This may have happened due to the half-power point method used for computation of damping.

Overall, it was concluded that the incorporation of split screw spline mullions in the curtain wall assembly was viable. The system showed less differences between static finite element analysis

and experimental values with respect to laminated glass thickness, mullion flexural rigidity, connection stiffnesses (both mullions to mullion and mullion to structural backup) and the performance of the silicone sealant used. The paper thus showed reliability and serviceability performance of the split screw mullions in curtain walls.

Brewer, T. R., Morrill, K. B., and Crawford, J.E. (2015)

Brewer et al. (2015) developed a different form of curtain wall for the US Government overseas infrastructure which included use of steel tubes in place of aluminum mullions anchored between the floors identifying them as Steel Stud Curtain Walls (SSCW). Experimental research was conducted on the system. The test specimen was in the form of a three-story curtain wall subjected to consecutive blast load impulse of over 2000 kPa-msec. The steel tubes were first fitted to the test reaction structure and then blast resistant windows were placed in in the wall at the second floor level. The first and ground floor had granite cladding and forced entry / ballistic resistant (FE/BR) windows. Glazing thickness was reduced in subsequent floors from 65 mm at the ground floor to 51 mm at subsequent floors above. The blast loads were observed to be transferred from the curtain wall panels to the vertical mullions, and then to the support beams and the framing system of the building. Figure 2-18 illustrates the curtain wall befor and after the test. It was observed that the granite cladding was fragmented after the detonation. The blast-proof windows were cracked, and the spandrel was destroyed completely. In the interior of the building, the cracked pieces of lamination were found along with the debris created by failure of the FE/BR wall.

The experimental results were validated with modelling and analysis of the structure using a CFD software. It was observed that the analytical and experimental results had a little difference due to the under prediction of blast load at some areas by 15%. Overall, it was concluded that the curtain wall developed was strong enough to resist the applied blast loads with a minimum damage in the interior of the building.

Figure 2 - 18 : SSCW before (left) & after blast detonation (right)

Marchand, K., Davis, C., Sammarco, E., Bui, J., and Casper, J. (2016)

Marchand et al. (2016) investigated the response of conventional curtain walls designed for gravity and wind loads, against blast loads. Tests were conducted using a shock tube, and the results were validated with a FE model using LS-DYNA. Five tests with two shots per test were performed on eight identical specimens to study the response of IGU and mullions from no damage to complete failure. The curtain walls had two IGU, and the glass panes were attached to the supporting frame with silicone sealant. In the FE modelling, the aluminum mullions were represented as Timoshenko type beam element and mullion connections as ideal pinned supports. IGU glass panes, interlayer material and spacers were modelled as shell elements and the connections to curtain walls were modelled as idealized single point kinematic constraints.

The test results showed deflections, which were captured with digital image correlation (DIC), indicating progression from elastic to plastic behavior as the blast intensity increased from the first to fifth test. Significant yielding of the mullions was observed during Test 4 and 5, and the mullions developed permanent deformations. Figure 2-19 illustrates the behavior of the test specimens. The IGU also suffered significant damage, developing in-plane tension and stretching as it approached the failure point. All the analysis results agreed well with experimental data, representing acceptable precision of the performed analysis. Figure 2-20 shows the FE model used in the analyses.

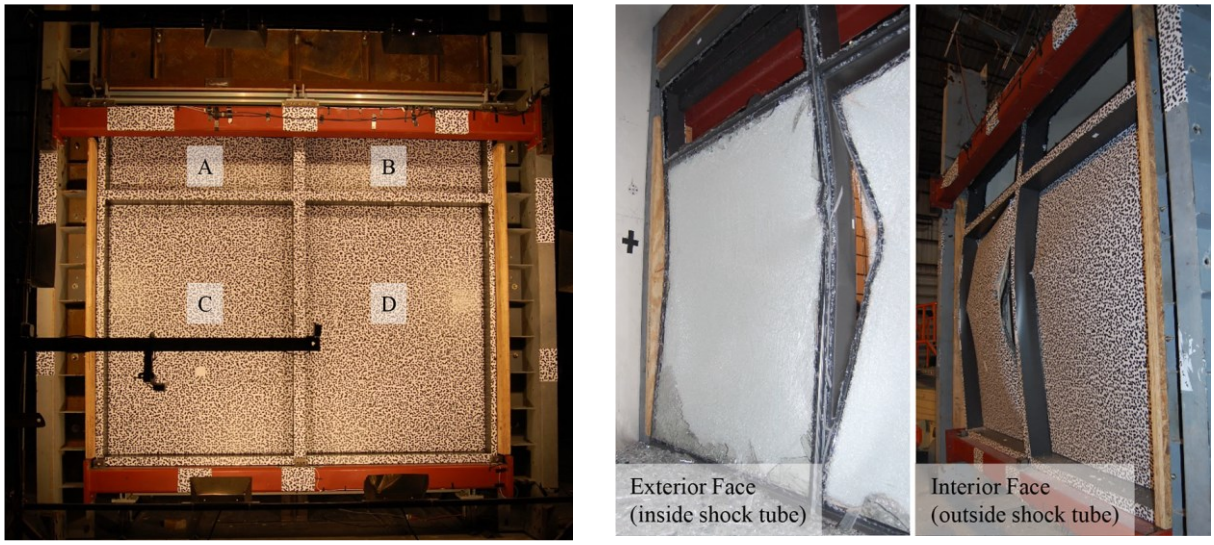

Figure 2 - 19 : Curtain wall specimen before (left) and after blast loading (right)

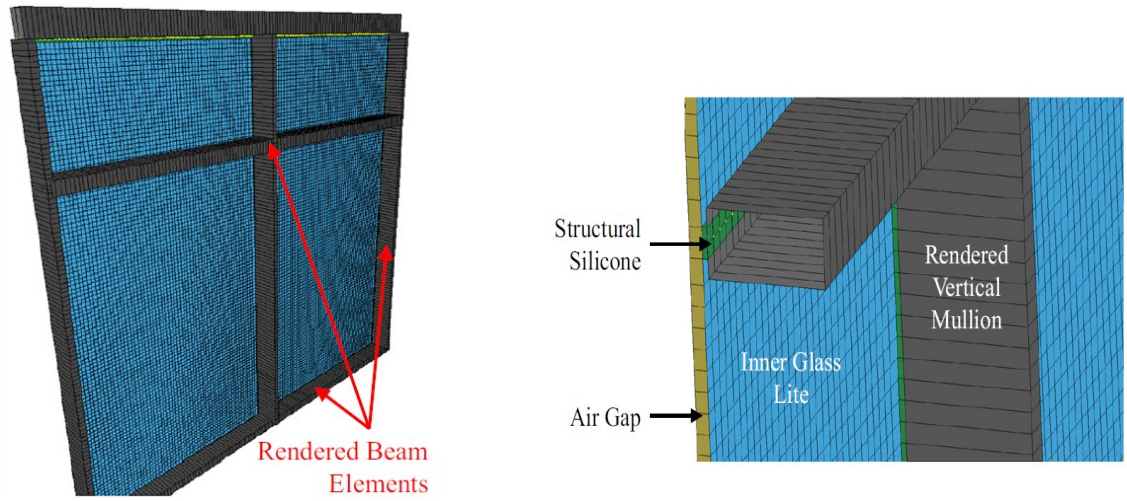

Figure 2 - 20 : Curtain wall FE model rendered view (left) and vertical c/s details (right)

Nawar, M., Salim, H., Lusk, B., and Kiger, S. (2014)

Nawar et al. (2014) investigated the behavior of curtain walls with conventional and retrofitted mullions and annealed glass assembly under blast loads. Figures 2-21 and 2-22 represent the fabrication of the conventional and retrofitted curtain wall specimens. The retrofitted curtain wall assembly consisted of a conventional curtain wall assembly supported by an additional laminated glass pane backed up by an additional mullion assembly as described in Figure 2-22. The curtain wall specimens were subjected to 42 kPa-320 kPa-msec and 45 kPa-284 kPa-msec pressure impulse combinations using a shock tube facility for conventional and retrofitted specimens, respectively. The test results for conventional curtain walls revealed significant

damage due the cracking of the annealed and laminated glass, however no damage was experienced by the supporting mullions. Large deformations were observed at the connection angles between the header and the sill. The results for retrofitted curtain walls indicated satisfactory performance with the outer part of the curtain wall with annealed glass developing failure, but the inner assembly with the laminated glass supported by an additional mullions did not suffer any damage.

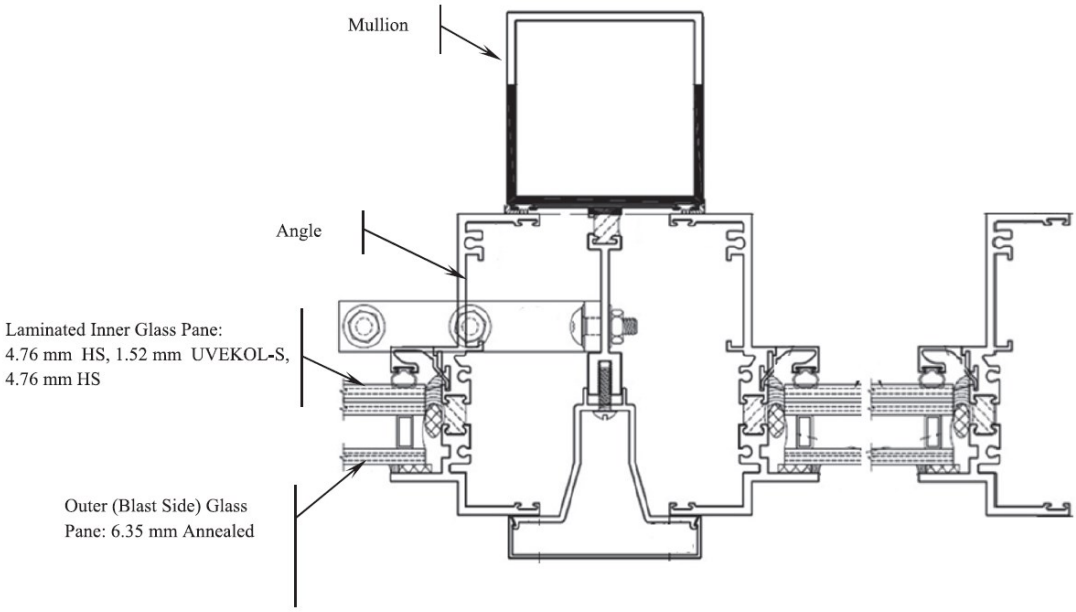

Figure 2 - 21 : Ordinary curtain wall specimen

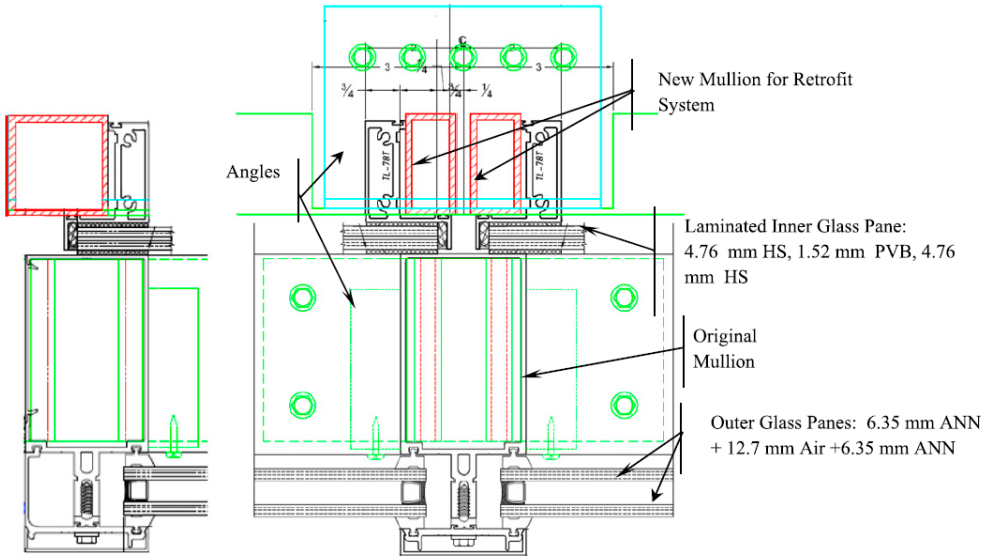

Figure 2 - 22 : Blast resistant curtain wall mullion

The test specimens were analyzed numerically using LS-DYNA. The glass panes were modelled using shell elements. The interlayer polymer material was assumed to behave plastically till failure. The numerical simulation generated similar results as those obtained experimentally. However, in some cases, at the reflected peak pressure, the numerical evaluation indicated failure, whereas no failure was observed during the actual physical testing. Overall, the retrofitted mullions showed improved performance in resisting blast loads.

Deng, Rong-Bing and Jin, Xiang-Long (2010)

Deng and Jin (2010) conducted analytical investigation of curtain walls. Arbitrary Lagrangian-Eulerian (ALE) method was adopted for the analysis with the help of FEA tool in LS-DYNA. ALE method is a combination of purely Lagrangian method and purely Eulerian method, which overcomes the mesh distortion limitation of purely Lagrangian method, and instability of solutions for the purely Eulerian. As a result, a smooth parallel algorithm for contact interface between the Lagrangian and ALE elements was implemented. The curtain wall specimens were analyzed under a blast shock waves generated by 50 kg TNT at a standoff distance of 12.5 m and 0.5 m above the ground. The curtain wall specimen is described in Figure 2-23. The glass unit was modelled as a linear elastic entity, the inter glass connecting polymer as linear viscoelastic material, the supporting aluminum frame as plastic kinematic model, a linear polynomial state equation for the surrounding atmosphere and fixed boundary conditions for the frame. The pressure time history and the peak overpressure were obtained by the exponential function given by Friedlander equation and the Henrych equation, respectively. The propagation of shockwave represented the efficiency of ALE technique. Figure 2-24 shows the behavior of the curtain wall for the blast load in which the cracking of inner glass layer of each glass pair was observed. However, no significant damage was observed to the aluminum frame. The results of this numerical analysis agreed well with pre-executed experimental results concluding an accurate behavior of the ALE implemented FE model.

Bedon, C. and Amadiao, C. (2017)

Bedon and Amadiao (2007) conducted a FEA study on blast performance enhancement of curtain walls using energy dissipation devices. The model employed is illustrated in Figure 2-25. The devices considered were, visco-elastic (VE) dampers and elasto-plastic dampers (ADAS), shown in Figure 2-26 and 2-27, respectively. When VE devices were used, stresses in glass panes, silicon joints and mullions were reduced considerably as maximum reactions were transferred to the supporting backup. Brittle failure of the structure was prevented as these devices induced inherent deformation capacity to the structure. The FEA also proved to be effective as the structure was able to take additional dynamic loads in addition to the blast loading. The efficacy of the dissipator was largely dependent on the VE compound and hence its design should be carefully executed to avoid larger strains that may result in failure.

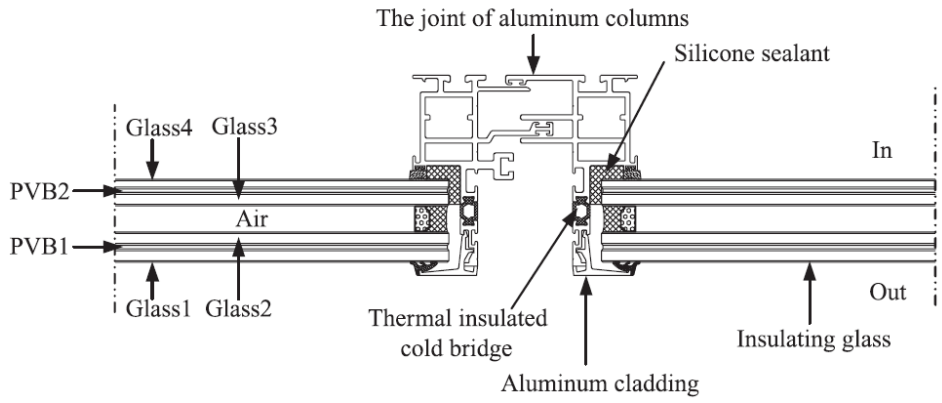

Figure 2 - 23 : Curtain wall specimen cross section

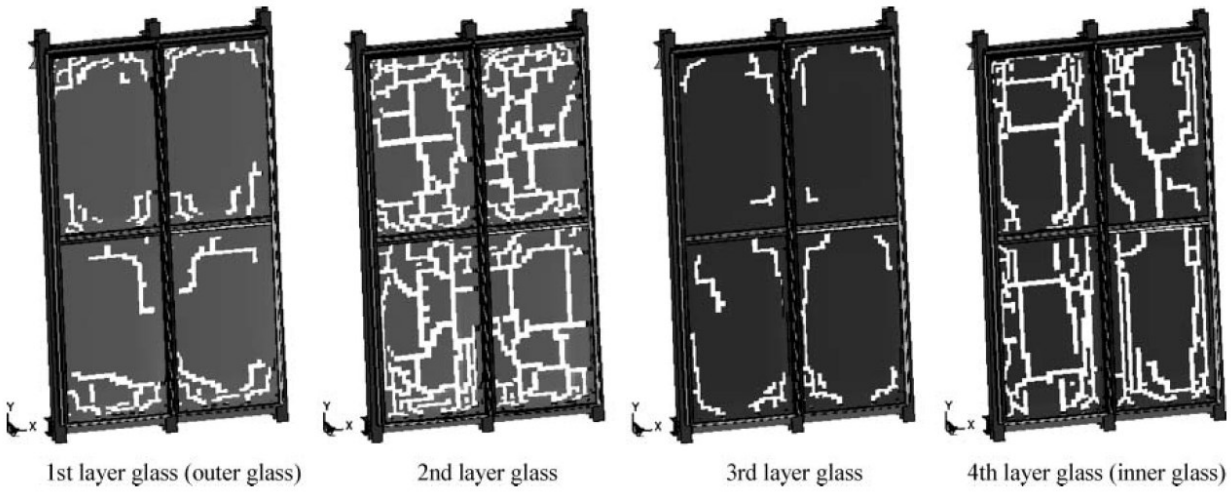

Figure 2 - 24 : Curtain wall behavior under blast loads

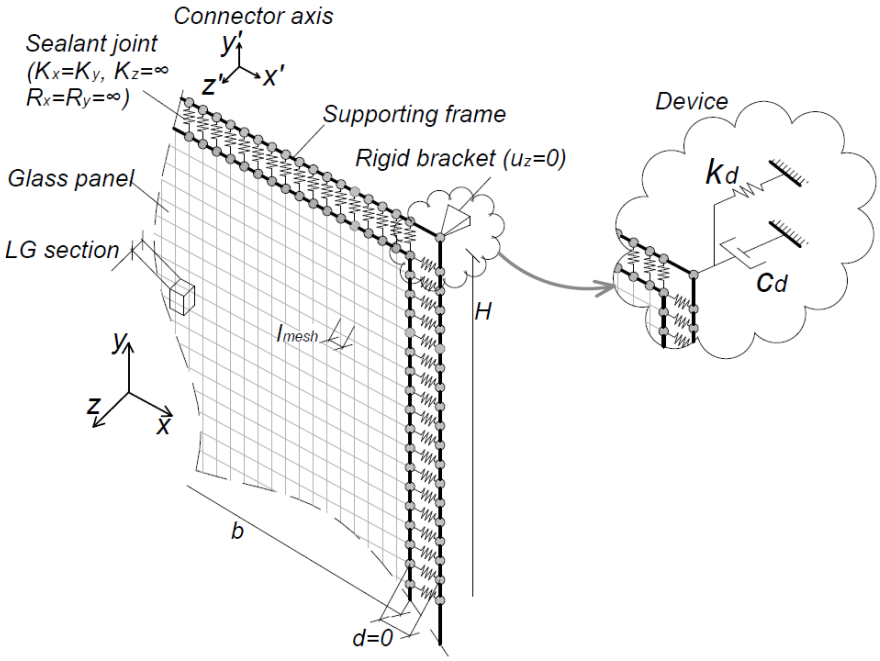

Figure 2 - 25 : Schematic representation of FEA model

ADAS device proved to be more mechanically stable than the VE dampers. The researchers suggested that the elastic stiffness and shear resistance of ADAS must be designed properly to provide better stiffness and strength at the supports. They act as rigid supports to curtain walls until the blast loads exceed the elasto-plastic shear resistance. Therefore, it was concluded that VE and ADAS devices can provide the desired level of strength and stiffness to curtain wall frames when designed properly with due consideration given the above points.

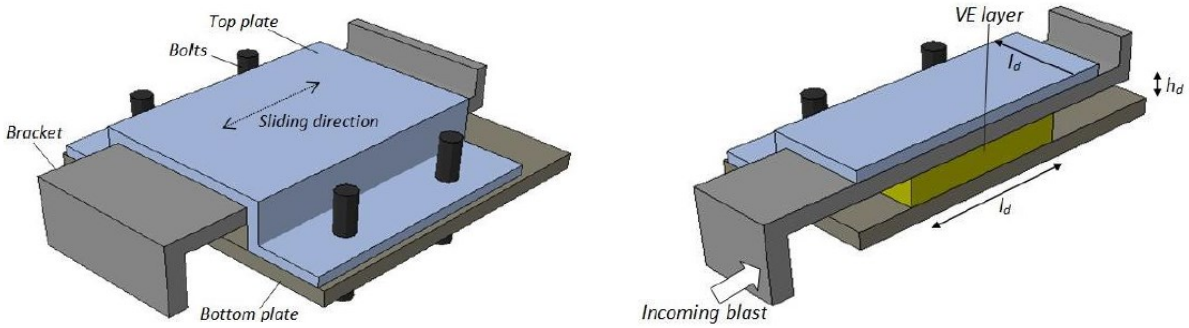

Figure 2 - 26 : VE device assembly (left) and cross section (right)

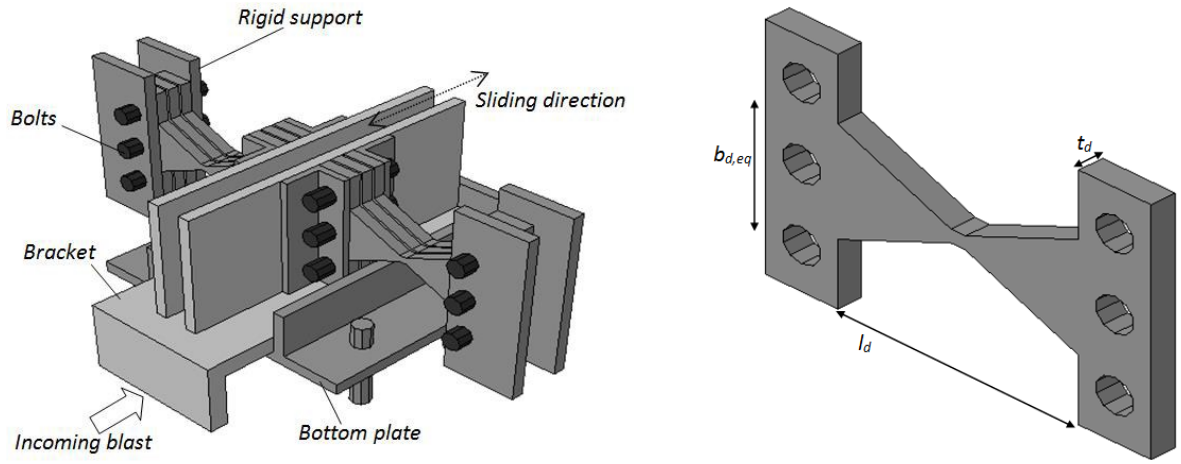

Figure 2 - 27 : ADAS device assembly (left) and X shaped steel components (right)

2.5 SUMMARY OF LITERATURE REVIEW AND RESEARCH NEEDS/GAPS

The key findings and the limitations observed in previous research are summarized in this section and tabulated in Table 2-1. The section also identifies the needs for current research.

- Different authors and research groups conducted experimental and/or numerical research on behavior and retrofit of blast-resistant curtain walls. A number of projects involved new developments for improved curtain wall performance. The previous investigations focused on the behavior of mullions, mullion connections and laminated panes. The majority of research concentrated on conventional curtain walls with little modification to safeguard them against blast loads.
- Most of the previous research concentrated on performance enhancement of laminated glass and its connection to aluminum frames (mullions).
- Few researchers included strengthening of curtain wall mullions by adding reinforcement or glass panes by adding additional laminated glass.
- The use of shock dissipating devices improved blast resistance and ductility of mullions.
- Some of the hardening techniques employed focused on increasing strength and stiffness of mullions against blast loads. However, these techniques proved to be uneconomical, sometimes resulting in unnecessary increase in strength.
- The overall assessment of the above literature survey indicated that practical, architecturally pleasant and structurally sound hardening techniques are needed for curtain wall mullions.

Table 2 - 1 : Summary of literature review representing techniques for blast resistance of CW, analysis method and subsequent results

Author	Blast Resistance Mechanism	Analysis Method
M. Saatcioglu (Phase-I, 2017a)	Horizontal and vertical mullion connection strengthening by aluminum angles with the use of bolting, mechanical glazing to IGU and IGU to frame connection with square aluminum section along the circumference.	Shock tube testing.
Result	Vertical mullion weakening due to bolting of connection and no significant damage to the IGU after blast loading.	
M. Saatcioglu (Phase-II, 2017b)	Horizontal and vertical mullion connection strengthening by aluminum angles with the use of epoxy glue and bolting, mechanical glazing to IGU, IGU to frame connection with square aluminum section creating a one-way action and hardening of mullions with aluminum plates on both the sides.	Shock tube testing.
Result	Heavy damage to the mullions with a poor performance of cold welding and destruction of IGU panes.	
B. T. Kennedy (2013)	Structural silicone sealant used to attach glass pane to the mullions. However, no significant strengthening given to the mullions	Air bag loading apparatus and numerical analysis using LS-DYNA.
Result	Inelastic deformation of mullions resulting in the ripping off the sealant from the frame. Transferring of the tensile loads to the frame due to membrane action of the laminated glass causing significant energy absorption.	
A.D. Ralston (2015)	Structural silicone sealant used to attach glass pane to the mullions. However, no significant strengthening given to the mullions	Open arena blast loading and numerical analysis using LS-DYNA considering FSI, aerodynamic and damping effects of the frame.
Result	Extensive mid height deflection of the vertical mullions and tearing out of glass due to high strain rates and damping.	
D. C. Weggel (2007)	Use of laminated glass and structural silicon sealant for glass to frame connection. However, no significant strengthening to the mullions.	Air bag loading apparatus, pluck test and numerical analysis using ANSYS code.
Result	Low rotational stiffness of horizontal mullions resulted in its out of plane rotations relative to vertical mullion.	

Author	Blast Resistance Mechanism	Analysis Method
T.R. Brewer (2015)	Use of steel tubular sections instead of the aluminum sections. Use of blast resistant windows and FE/BR windows. Reduction of glazing thickness based upon the anticipated blast intensity experienced by the different floor.	Open arena blast loading with its validation from advanced CFD code.
Result	The developed heavy-duty curtain wall was strong enough to resist the blast loading resulting in no damage to the mullions and cracking of glass panes and destruction of some secondary structural elements.	
K. Marchand (2016)	Structural silicone sealant used to attach glass pane to the mullions. However, no significant strengthening given to the mullions	Shock tube testing with the use of DIC technique and its validation with LS-DYNA code using Timoshenko beam concept.
Result	Plastic deformation causing the yielding of the mullion and near failure cracking resulting of IGU.	
M. Nawar (2014)	Strengthening of the curtain wall using additional laminated inner glass pane and mullion retrofitting assembly. Reliable connections developed between the two assemblies.	Shock tube testing with its validation using LS-DYNA code.
Result	Satisfactory results with the outer curtain wall assembly suffering considerable damage resulting in the safeguarding of the inner laminated glass and additional mullions.	
R. B. Deng (2010)	Structural silicone sealant used to attach glass pane to the mullions. However, no significant strengthening given to the mullions	Numerical simulation using LS-DYNA code with the incorporation of ALE modelling method.
Result	Systematic modelling efforts led accurate analysis resulting in cracking of laminated glass panes and surprisingly no damage occurred to the mullion assembly of the curtain wall.	
C. Amadio (2017)	Use of visco-elastic dampers and elasto-plastc devices to support the curtain wall faming at the designated locations. However, no direct strengthening of the mullion assembly.	Numerical analysis using the ABAQUS FEA software.
Result	Proper dissipation of the reactions avoiding the brittle failure with increased resistance to the other dynamic loads. Cracking of the glass panes was observed with no significant damage to the mullion assembly.	

CHAPTER 3. EXPERIMENTAL RESEARCH

3.1 GENERAL

This chapter presents experimental phase of current research. The test program forms part of an overall research program with wider scope, focusing on shock tube tests of curtain walls and curtain wall elements at the University of Ottawa. It forms Phase IV of the research program, involving tests of individual aluminum mullions hardened with steel plates and plate assemblies.

3.2 DETAILS OF TEST SPECIMENS

The test specimens consisted of 3 full-scale aluminum mullions and 3 companions retrofitted (hardened) mullions that utilized steel plates and/or steel section assemblies. The reference mullions (unretrofitted) were named as Mullions 1 to 3, representing as built conditions in existing curtain walls. The retrofitted mullions were labelled as Mullion 1H to 3H, depending on the desired level of hardening and the type of steel sections used for hardening. The following retrofit scenarios were considered in the experimental program.

- Steel L shaped sections covering both sides of web and the tension flange (Mullion 1H).
- Steel side plates covering both sides of web (Mullion 2H).
- Hollow steel sections (HSS) with a square geometry attached on the tension flange with the help of steel side plates (Mullion 3H).

All the above-mentioned sections were connected to the aluminum section with the help of self-tapping screws. The details of the assembly of specimens are described in the proceeding sections.

3.2.1 Description of test specimens

3.2.1.1 Mullions 1 & 1H

The first pair of mullions tested included rectangular aluminum sections with section dimensions of 152 mm x 51 mm x 3 mm. Mullion 1 was as built aluminum specimen and Mullion 1H was a companion specimen with identical geometry but hardened with two L shaped steel sections. The steel sections had a thickness of 3 mm, covering the two faces of the web and the tension flange. The back flange of the rectangular section was assumed to have the glass, and hence was not accessible for hardening. Table 3-1 provides the cross-sectional details of the two mullions. The L shaped steel sections were attached to the aluminum rectangular section with the help of

self-tapping screws having 5.5 mm diameter and 32 mm length. Figure 3-1 shows the arrangement and spacing of screw pattern for Mullion 1H. Centre-to-centre spacing of 100 mm was used with a clear distance of 25 mm between the side edge of the mullion and the bolting assembly.

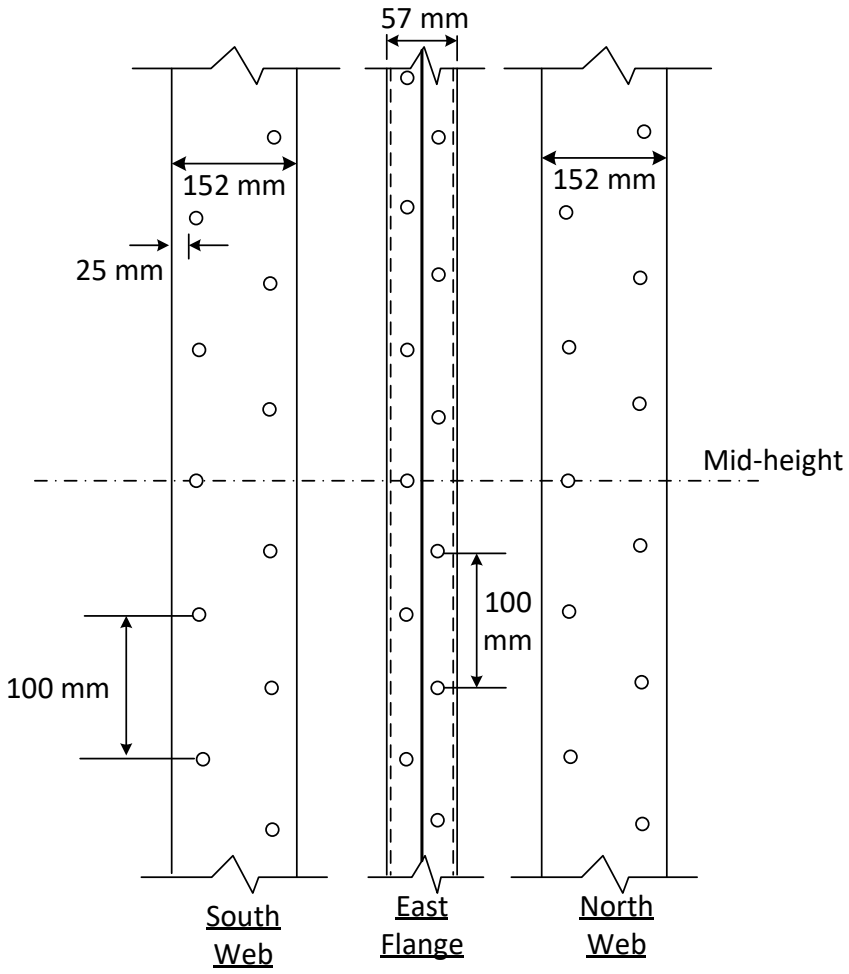

Figure 3 - 1 : Bolted screw pattern for L shaped steel sections used for mullion hardening

Table 3 - 1 : Test-I Summary of specimens

Test Specimen	Section Details	Retrofitting Assembly	Detailed Cross-Section
Mullion 1	152 mm x 51 mm x 3 mm (6 in x 2 in x 1/8 in)	Specimen to be tested in as built conditions	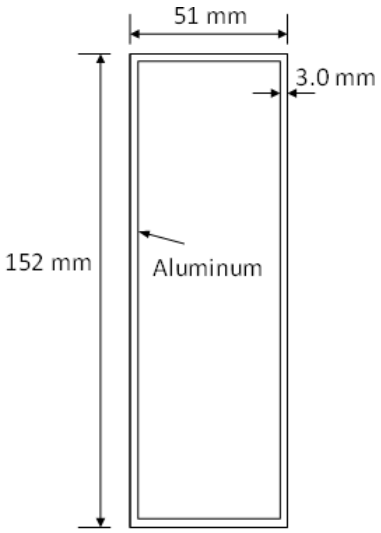 Mullion 1
Mullion 1H	152 mm x 51 mm x 3 mm (6 in x 2 in x 1/8 in)	Two L shaped steel sections with 3 mm thickness, bolted 100 mm c/c along the north and south web face and East flange with self-tapping screws of 5.5 mm dia., 32 mm long.	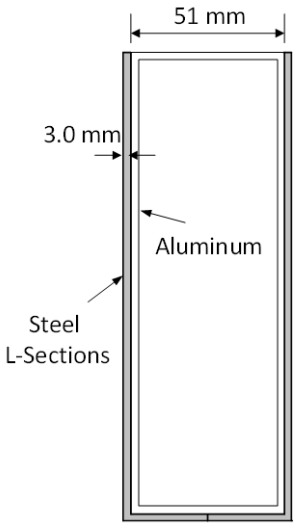 Mullion 1H

3.2.1.2 Mullion 2 & 2H

The second set of tests involved aluminum mullions with the same outside dimensions of 152 mm x 51 mm as the first set, but with slightly thicker sections having 4.8 mm wall thickness. The retrofit scheme in this case involved 3 mm thick steel plates secured on both sides of the web, without the strengthening of the flange. Table 3-2 shows the details of the mullions. The steel plates were attached to the aluminum section with the help of self-tapping screws having 5.5 mm diameter and a length of 32 mm. Mullion 2H was the first retrofitted mullion that was tested in the experimental program. The spacing provided between the screws was 200 mm c/c. After the first shot, it was felt that this spacing resulted in some tendency of the plates to bend between the screws. Hence the spacing was subsequently reduced to 100 mm. Figure 3-2 illustrates the screw pattern used. A clear edge distance of 25 mm was maintained between the screws and the side edges of the mullion.

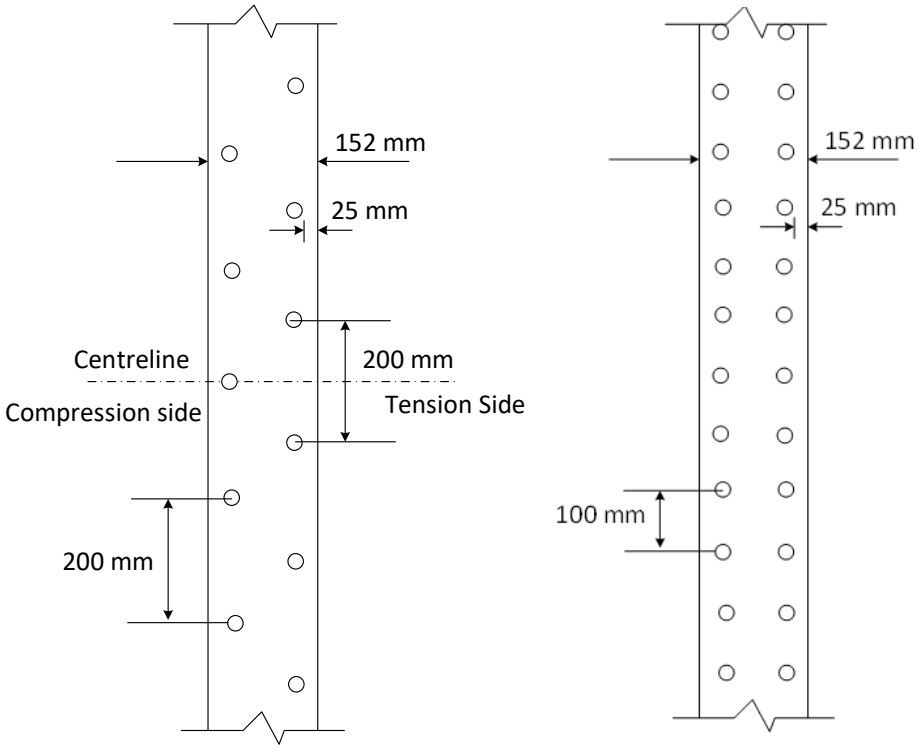

Figure 3 - 2 : Bolted screw pattern for steel plate sections with spacing of 200 mm c/c (left) and 100 mm c/c (right) used for mullion hardening

Table 3 - 2 : Test-II Summary of specimens

Test Specimen	Section Details	Retrofitting Assembly	Detailed Cross-Section
Mullion 2	152 mm x 51 mm x 4.8 mm (6 in x 2 in x 3/16 in)	Specimen to be tested in as built conditions.	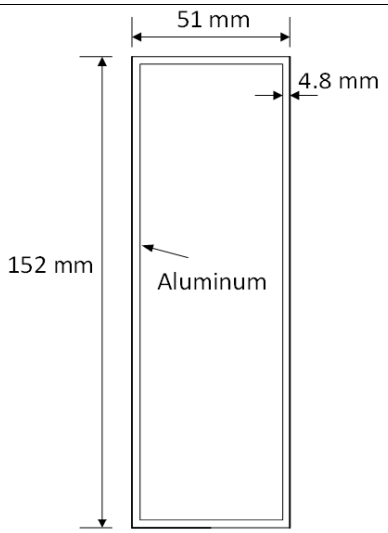 Mullion 2
Mullion 2H	152 mm x 51 mm x 4.8 mm (6 in x 2 in x 3/16 in)	Two steel plate sections with 3 mm thickness, bolted 100 mm c/c along the north and south web face with self-tapping screws of 5.5 mm dia., 32 mm long.	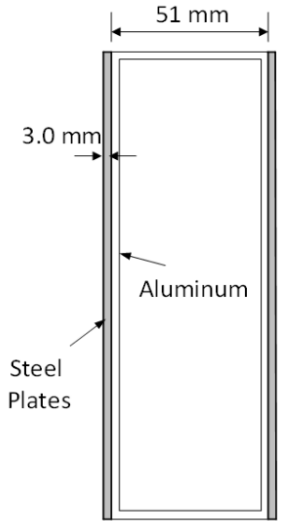 Mullion 2H

3.2.1.3 Mullion 3 & 3H

The third set of mullions tested included the smallest size mullions with 127 mm x 51 mm x 3 mm cross-sectional geometry. Mullion 3H was hardened with a 51 mm square hallow steel section (HSS) with a 3 mm wall thickness, placed on the tension flange side of the aluminum mullion with two steel plates of 3 mm thickness along both sides of the web as illustrated in Figure 3-3. The same self-tapping screws as before were used with a spacing of 100 c/c with a clear distance of 25 mm to the edge of the mullion. The square HSS section was first placed on the tension flange, followed by the two side plates, which were attached to the aluminum mullion by means of 5.5 mm diameter screws. Table 3-3 shows the geometric details of the mullions.

Figure 3 - 3 : Mullion 3H - HSS section on tension flange (left) & side plate bolting (right)

Table 3 - 3: Test-III Summary of specimens

Test Specimen	Section Details	Retrofitting Assembly	Detailed Cross-Section
Mullion 3	127 mm x 51 mm x 3 mm (5 in x 2 in x 1/8 in)	Specimen to be tested in as built conditions.	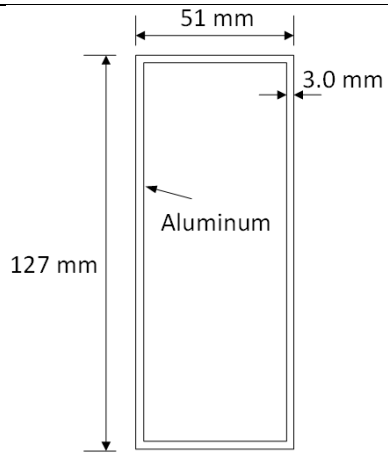 Mullion 3
Mullion 3H	127 mm x 51 mm x 3 mm (5 in x 2 in x 1/8 in)	51 mm square HSS section, 3 mm thick, attached to the tension flange. Two steel plate sections with 3 mm thickness, bolted 100 mm c/c along the north and south web face with self-tapping screws of 5.5 mm dia., 32 mm long.	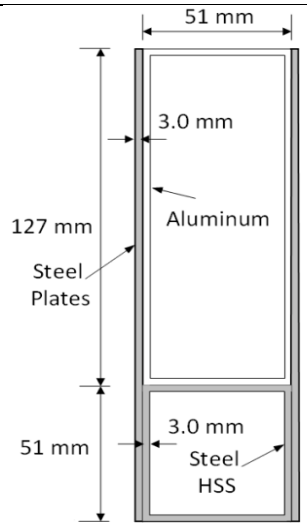 Mullion 3H

3.3 TEST SETUP & DATA ACQUISITION

3.3.1 Shock tube details and description

The blast load testing of mullions was conducted at the Shock Tube Facility of the University of Ottawa's Blast Research Laboratory. The pneumatically operated shock tube simulates the effect of detonation without the need of actual explosives. Figure 3-3 depict the Shock Tube. It consists of three main components described as follows.

i. Driver section

The blast wave energy is generated in the driver section. The driver section has six steel pipe sections with 6.35 mm thickness, each with an inner diameter of 597 mm. Two sections have length of 1525 mm, one with 915 mm length, the other one with 610 mm length and the last two with 305 mm length. The driver length can be adjusted from 305 mm to 5185 mm with increments of 305 mm in order to control the reflected pressure and impulse. The two consecutive pipe sections are bolted with 12 number of 31.75 mm bolts with a synthetic gasket in between in order to ensure proper sealing when pressurized. One end of the driver section is sealed off with 38.1 mm thick steel plate and the other end is connected to the spool section. The entire driver section assembly is supported by an inverted C-section tray.

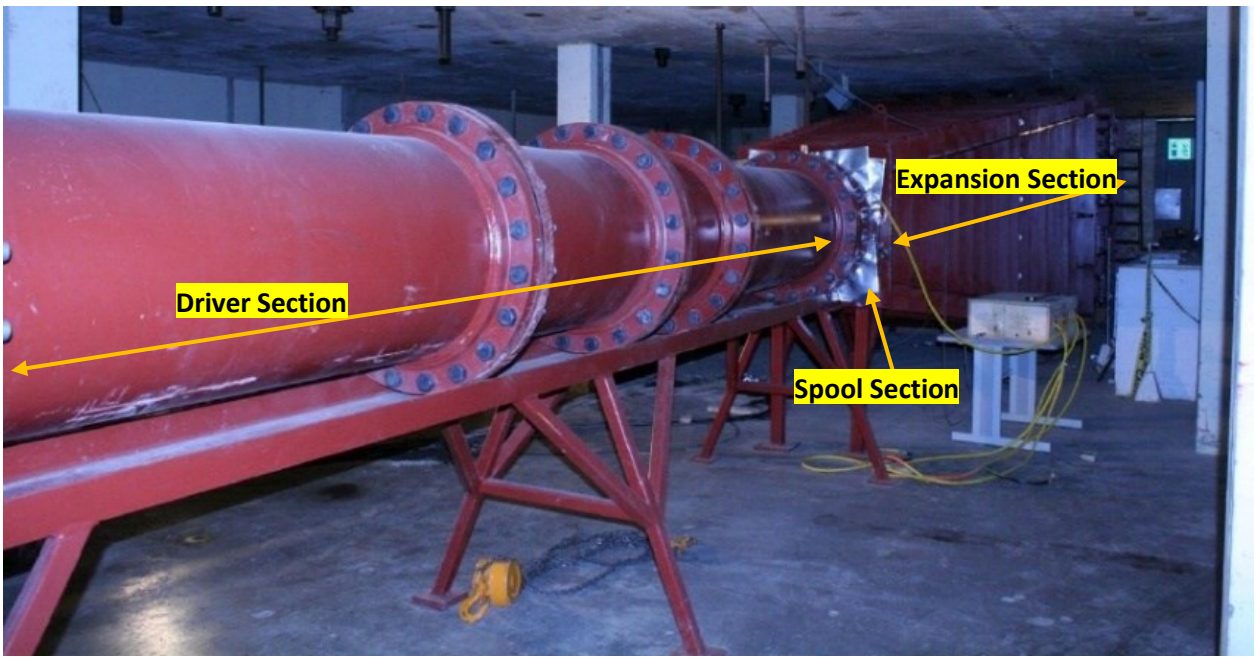

Figure 3 - 4 : Shock tube assembly

ii. Spool section

The firing of the blast energy generated in the driver section is controlled through this spool section. The length of the spool section is 90 mm and is bolted in between the driver and the expansion sections. The spool section consists of two aluminum diaphragms which are connected between the driver-spool section and spool-expansion section. The combinations of Grade 1100 aluminum diaphragms are selected such that their specified rupture strength is greater than the varying pressure gradient across the driver-spool-expansion section assembly. This mechanism ensures safe and accurate control of the blast wave firing and it is called as 'double diaphragm firing system'.

iii. Expansion section

The expansion section is the part of shock tube where the blast wave detonated in the spool section propagates and hits the specimen attached to the other end. The length of expansion section is 6096 mm with one end attached to the spool section with a circular opening of 597 mm diameter and the other end square opening of 2032 mm x 2032 mm connected to the testing frame. The testing frame is fitted along the perimeter of this opening with the dimensions of 203 mm wide and 12.5 mm thick. The testing frame also has twenty 19 mm diameter bolts so that the specimen can be attached to the shock tube.

Figure 3 - 5 : Shock tube expansion section opening / vents

The control station for the shock tube is present on the main floor of the structure lab above the blast laboratory. The static pressure gauges that monitor the pressurization of the driver and spool sections ensures that the differential pressure across these sections is less than the rupture strength of both diaphragms. The shock tube firing is initiated when the pressure in the spool section is released after the targeted pressure is achieved. This causes the rupture of driver-spool diaphragm, followed by the spool-expansion diaphragm. Thus, a shock wave is caused by the pressurized air in driver section which travels through the expansion section to equalize with the atmospheric pressure. Thus, the shock tube can effectively simulate the first positive pressure wave caused by the explosive material detonation. The high explosive blasts can also cause negative pressures, but the shock tube is not designed to develop those negative pressures. Table 3-4 shows the combination of maximum reflected pressure-reflected impulse that can be achieved with the driver lengths available.

Table 3 - 4 : Maximum shock tube pressure ranges that can be attained with the University of Ottawa Shock Tube (Lloyd, 2009)

			Approximate Equivalent TNT (Hemispherical-Reflected)		
Driver Length	Reflected Pressure	Reflected Impulse	Mass	Standoff	Scaled Distance
(mm)	(kPa)	(kPa-ms)	(kg)	(m)	($m/kg^{1/3}$)
305	78	217	8	12	6.0
915	92	410	42	18	5.2
1830	100	840	290	33	5.0
3355	103	1760	2500	67	4.9
4880	104	2690	10000	106	4.9

3.3.2 Data acquisition and instrumentation

The data acquisition of the entire experiment was done with the help of advanced instrumentation setup which included devices such as Data Acquisition system (DAS), pressure sensors, Linear Variable Displacement Transducers (LVDTs), two high speed cameras and the camera tracking software. The pressure sensors installed on the sides of the shock tube expansion sections are activated by the shock wave which triggers the DAS. In response, the DAS captures the signal and triggers the camera. Thus, the camera captures the recording, which is stored in a laptop for further analysis. Simultaneously, the reflected pressure measured by the

pressure sensors and the displacement measured by LVDTs are sent to DAS for further analysis. The details of the individual instruments are described as follows.

i. Data Acquisition System (DAS)

DAS is the main program which receives input from various instruments synchronized with it. The magnitude of reflected pressures is received from the pressure gauges on the shock tube, mid-height deflection is received from the LVDTs, and the strains from the strain gauges. The data received is captured at a rate of 1000 kilo-samples per second (kS/s).

ii. Pressure sensors

The pressure sensors are attached along the perimeter of the opening of the expansion section of the shock tube. The reflected pressure measured by these gauges is then transferred to the DAS. However, it is a common case of variable pressure measurement by the pressure gauges due to which the larger value measured is considered for further analysis. Sometimes it happens that extremely large pressure intensities are measured by the bottom sensor due to the flying debris falling on it; but such values are ignored for further analysis.

iii. Linear Variable Displacement Transducers (LVDTs)

LVDTs are the displacement measuring devices at the designated locations for a particular section. For the present mullion study, the LVDTs were placed at at mid-height of the mullion height. In order to maintain the position of the LVDT, it was fixed to a post by a nut-bolt assembly. In the event the LVDT fails to record the displacement data, high speed camera images provide backup data.

iv. High speed video cameras

The high-speed cameras with frame capturing rate of 2000 fps were used to record the response of the unhardened and hardened mullions against blast loading. These camera video recordings are of great help in measuring displacements when LVDTs fail to measure displacements, as was the case for testing Mullion 2H. Figure 3-6 illustrates a flow chart for the instrumentation used.

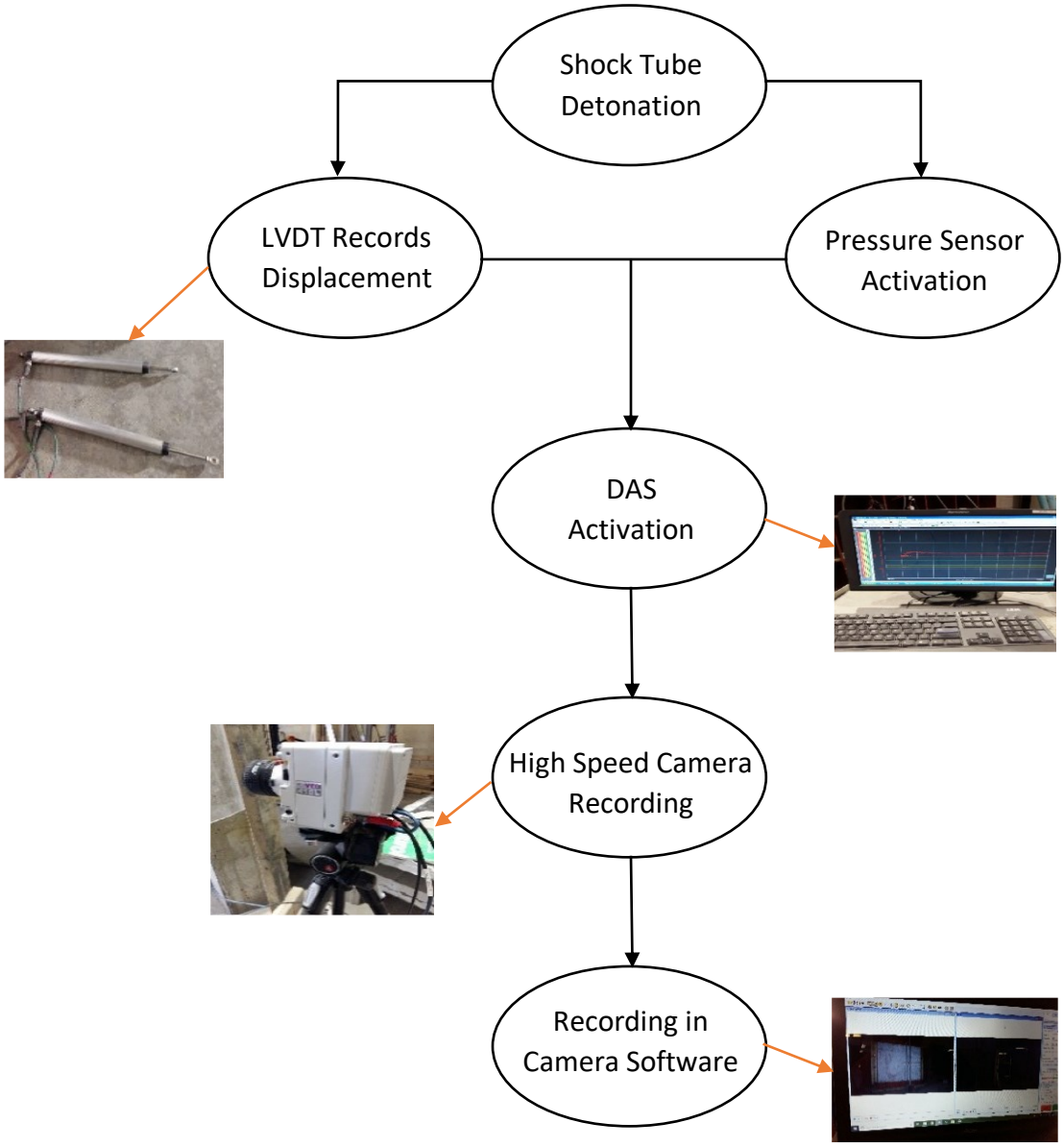

Figure 3 - 6 : Blast test instrumentation functions flow chart

3.4 MATERIAL PROPERTIES

All the test specimens comprised of two main materials i.e., aluminum and steel. The tubular aluminum sections and the steel sections, which were purchased from local suppliers, were commonly used metals in the construction industry. The material properties were provided by the suppliers. The stress-strain characteristics of the aluminum was verified by coupon tests in the earlier phase of the research program (Saatcioglu, M. 2020). Table 3-5 provides the basic properties of the materials, which were also used in the analytical component of the current research project.

Table 3 - 5 : Material properties

Material	Steel	Aluminum
Yield Stress (MPa)	350	210
Density of Material (kg/m^3)	7850	2700
Modulus of Elasticity (N/mm2)	200000	70000
Shear Modulus (N/mm^2)	77000	25800
Poisson's ratio	0.3	0.33

3.5 TEST PROCEDURE

The main focus of current research was on individual response of aluminum mullions to blast loading, with or without the steel hardening elements. Therefore, it was felt that testing individual mullions, rather than the entire curtain wall assembly would permit larger number of tests. The glass panes that would collect and transfer the applied blast pressure to vertical mullions were simulated by a load application device, which would collect the applied pressure and transfer the resulting load as uniformly distributed blast loading on the mullions. The details and geometry of the load application device are described in the following section.

3.5.1 Load application device

A single mullion was placed in front of the shock tube for each test, positioned in a central location of the Shock Tube expansion section, which had a 2 m by 2 m test area. The load application device consisted of a 0.51 mm 24 Gauge steel sheet with 8 - 76 mm square HSS sections with a wall thickness of 4.8 mm placed horizontally to apply point loads on the mullion. Figure 3-7 illustrates the load application device used. The blast load was taken by the steel sheet, transferred to the vertical mullion in the form of uniformly distributed load by the horizontal HSS

sections without providing any resistance because of the flexibility of the thin steel sheet. The load application device assembly was fixed to the top and bottom of the Shock Tube and it was free to move along the sides.

The load application device did not offer any resistance to the blast load, because of the free movement with sufficient flexibility of the thin steel sheet assembly. The mass of the load application device was 107 kg, which was equal to the mass of a double pane glazed IGU unit and a horizontal aluminum mullion representing a curtain wall assembly.

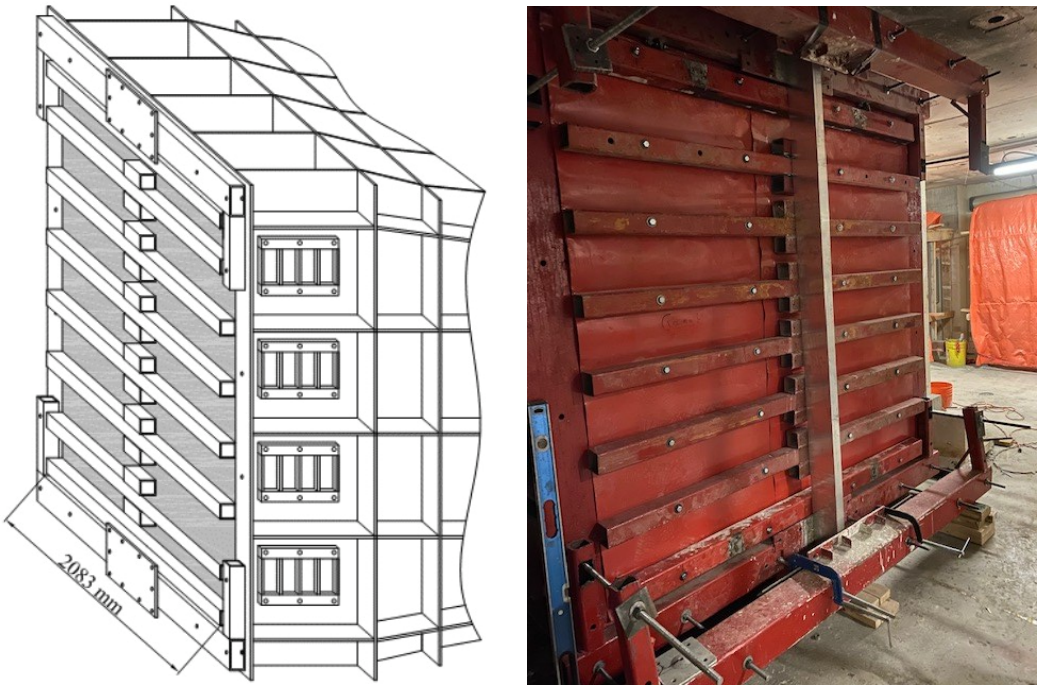

Figure 3 - 7 : Schematic diagram of load application device (left) and actual mullion test (right)

The test specimens were then subjected to a sequence of blast loads at different intensities until the specimens either failed or underwent a considerable residual displacement. The magnitude of pressure-impulse combinations and mid-height deflections were recorded with the help of the instrumentation set up described in the previous section.

3.5.2 Boundary conditions

The development of the boundary conditions was one of the most important tasks as the accuracy of the entire experiment is affected by it. In order to create a worst-case scenario in terms of the positive bending moment resistance, and also as representative of the majority of mullions in practice, simple supports were incorporated in all tests. Thus, the ends of the mullions

were free to rotate as there were no rotational constraints given to them. The simply supported ends represented the assembly of the mullions connected to floor slabs, as often is the case in actual practice. However, in some cases, the mullion assembly may be continuous over the slabs generating continuous supports, which were represented by the support conditions used in the tests. The assembly of the simple support condition is illustrated in Figure 3-8.

Figure 3 - 8 : Test mullion with simple support assembly

3.6 TEST RESULTS

The behavior of mullions with respect to their mid-height deflections and the failure patterns are discussed in this section. The details of the blast loading intensity and the number of blast shots applied to each specimen are also indicated. The comparison of the behavior of unhardened and hardened mullion sections is presented in a graphical format in order to obtain a clear understanding of the significance of the harderning technique employed. The following sections describe in detail the performance of erach mullion tested.

3.6.1 Test results & comparison – Mullion 1 & Mullion 1H

3.6.1.1 Test results - Mullion 1

Mullion 1 had section dimensions of 152 mm x 51 mm with a wall thickness of 3 mm, without any hardening. This mullion was subjected to only one blast shot with a pressure-impulse

combination of 27 kPa – 191 kPa-msec. The blast shot left a considerable damage to the mullion due to which this mullion was not subjected to further blast shots. Local buckling of the compression region at the mid-height portion of the mullion was observed. Maximum deflection of 45.7 mm was recorded during the test, and the section had a residual displacement of 24 mm. Figure 3-9 describes the condition of Mullion 1 prior to testing. Figure 3-10 shows the time histories of reflected pressure applied and the mid-height deflection recorded.

Figure 3 - 9 : Mullion 1 prior to blast test

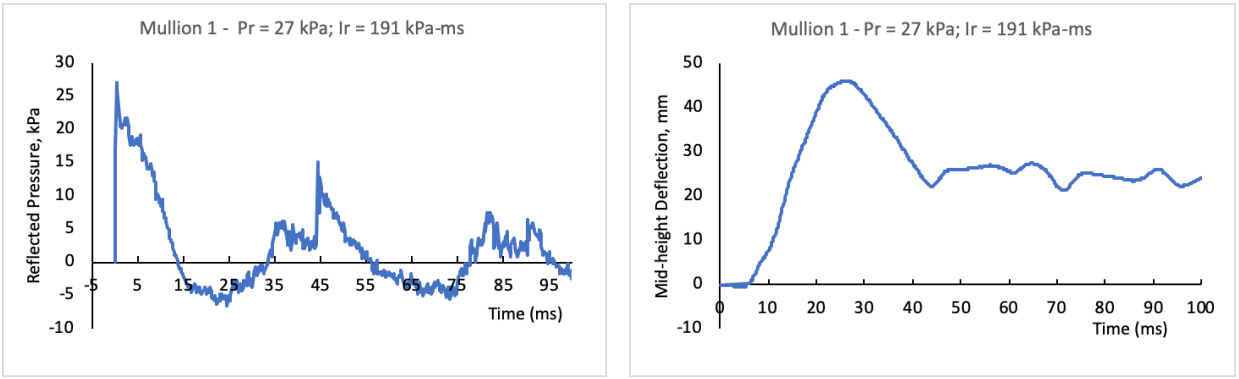

Figure 3 - 10 : Mullion 1 pressure-time history (left) & deflection-time history (right)

Figure 3-11 illustrates the condition of the mullion after the test. Web buckling was observed on the compression side, and the mullion reached its inelastic capacity. Therefore, no further load was applied on this specimen.

a.

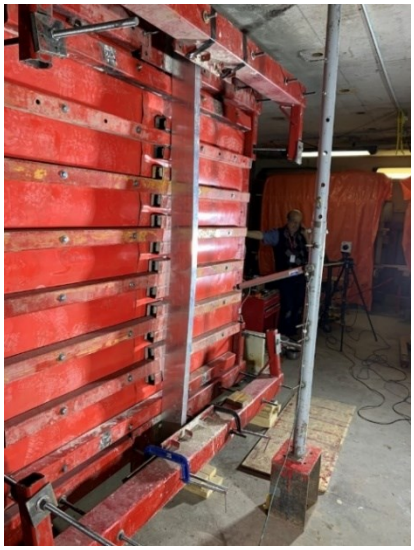

b.

c.

d.

Figure 3 - 11 : Mullion 1 at the end of test

3.6.1.2 Test results - Mullion 1H

Mullion 1H was companion to Mullion 1 with the same core aluminum section but hardened with externally applied steel sections. The hardening technique used involved two L shaped steel

angles attached to the aluminum section with the help of self-tapping screws. The hardened mullion prior to testing can be seen in Figure 3-12.

Figure 3 - 12 : Mullion 1H prior to blast test

Mullion 1H was subjected to the same level of blast shot that was applied to Mullion 1, which generated significant damage. The pressure-impulse combination of this shot was 27 kPa – 210 kPa-msec. Maximum deflection of 28 mm and a residual deflection of 10 mm was recorded. However, no significant damage was observed in the mullion at this level of loading. Thus, the mullion was subjected to a second shot at a higher intensity. Figures 3-13 and 3-14 show the pressure time and mid-height deflection time histories recorded during the first and second shots, respectively.

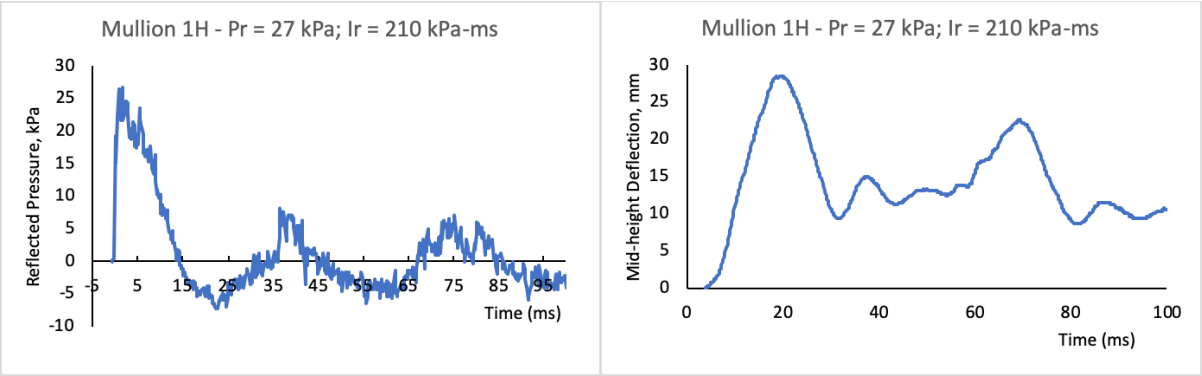

Figure 3 - 13 : Mullion 1H first shot pressure-time history (left) & deflection-time history (right)

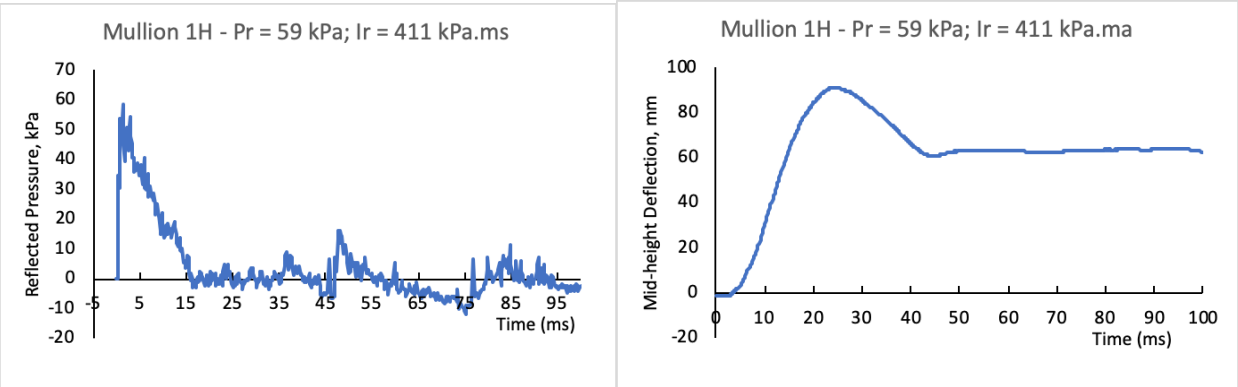

Figure 3 - 14 : Mullion 1H second shot pressure-time history (left) & deflection-time history (right)

The second blast shot had an intensity of more than twice as that of the first blast shot. The pressure-impulse combination of 59 kPa – 411 kPa-msec was recorded. The second shot resulted in considerable damage to the hardened mullion section causing a maximum displacement of 91 mm and a residual displacement of 60 mm. An excessive amount of web buckling of compression fibers at the mid-height segment of the steel angles was observed. Until the web buckling, a composite action was observed between the aluminum section and the steel angles. Figure 3-15 illustrates the damage observed in the Mullion after the second shot.

Figure 3 - 15 : Mullion 1H steel angle web buckling after the second shot

3.6.1.3 Comparison of results – Mullion 1 & Mullion 1H

The peculiar differences and unique responses observed in the behaviors of Mullion 1 and Mullion 1H are described below:

- The maximum displacement of Mullion 1H during the first blast shot was about half as much as that observed in Mullion 1 under the same level of blast load.
- Mullion 1 developed significant web buckling at mid-height at the end of the first blast shot. In comparison, the hardened Mullion 1H did not experience any damage under the same level of blast loading and remained essentially elastic.
- The blast load capacity of Mullion 1H was thus observed to increase by a factor of 2.2 as compared to mullion 1 response. Figure 3-16 shows the comparison of the two mullions, illustrating the improved behavior of the hardened mullion.

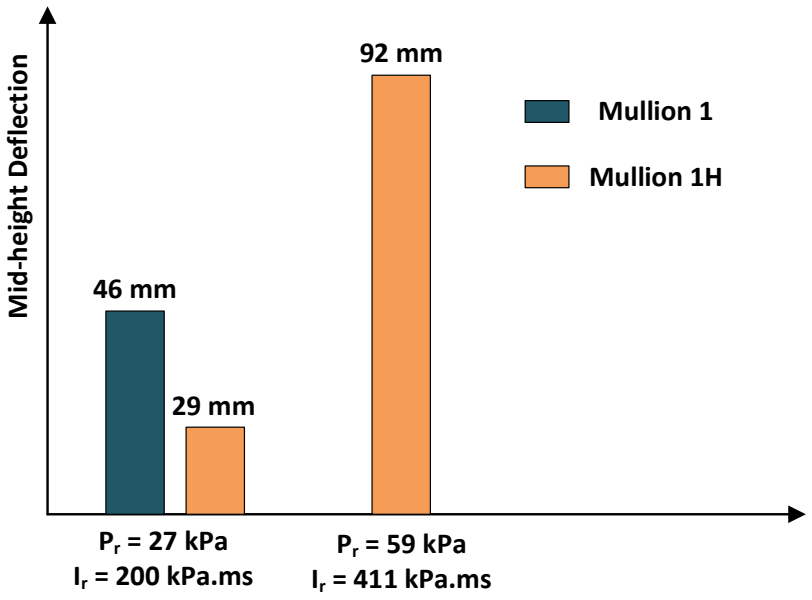

Figure 3 - 16 : Comparison of Mullion 1 & Mullion 1H

3.6.2 Test results & comparison – Mullion 2 & Mullion 2H

3.6.2.1 Test results - Mullion 2

Mullion 2 had the same section dimensions as those of Mullion 1; 152 mm length and 51 mm width, except for the wall thickness, which was 4.8 mm as opposed to 3.0mm. The pressure-impulse combination applied for the first blast shot was 30 kPa – 225 kPa-msec. The maximum mid-height deflection recorded was 37 mm with a negligible residual displacement. The mullion

behavior was essentially in the elastic range of deformations. Figure 3-17 shows the blast test data for the first shot. It can be observed in Figure 3-18 that, no considerable damage was imparted on the mullion after the first blast shot, with residual displacement of about 5 mm.

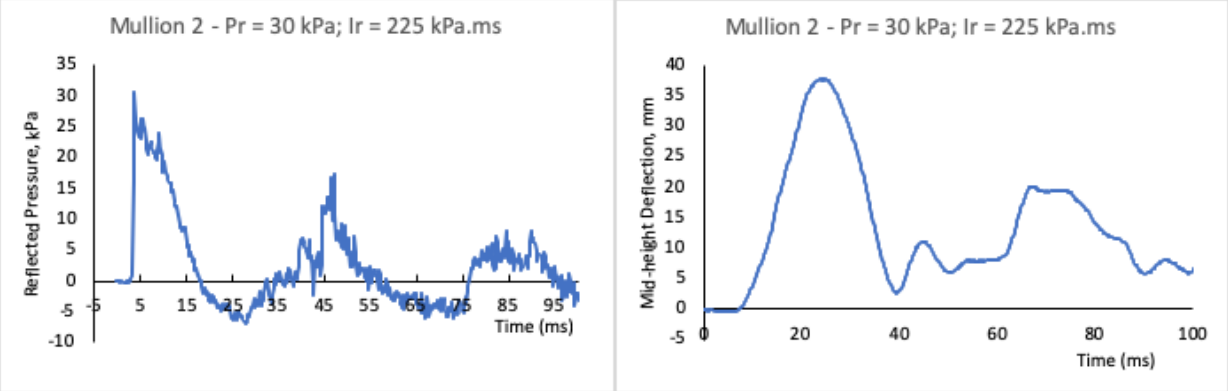

Figure 3 - 17 : Mullion 2 first shot pressure-time history (left) & deflection-time history (right)

Figure 3 - 18 : Mullion 2 after first shot

The mullion was then subjected to second blast shot. The pressure-impulse combination for the second shot was 38 kPa – 270 kPa-msec. The maximum displacement recorded at mid-height was 54 mm with a residual displacement of 20 mm. The mullion remained essentially elastic with limited inelasticity. The blast test data for the second shot is illustrated in Figure 3-19.

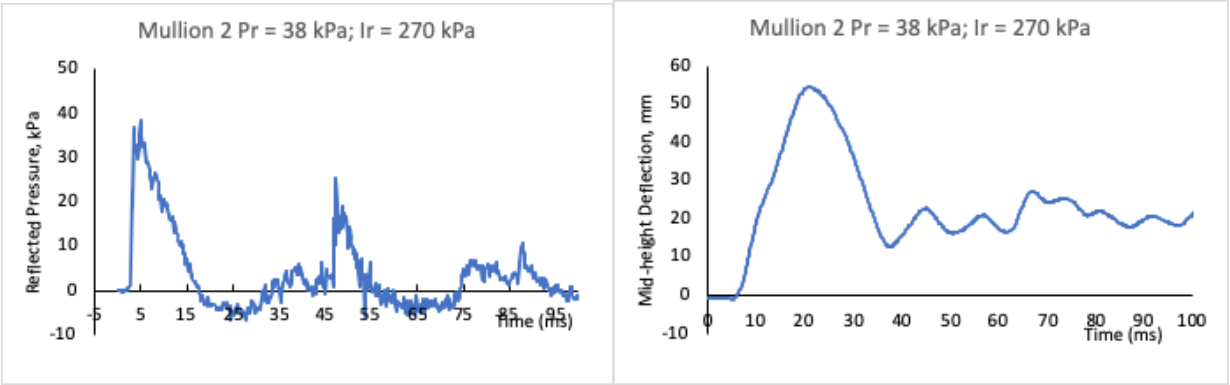

Figure 3 - 19 : Mullion 2 second shot pressure-time history (left) & deflection-time history (right)

Because of the limited inelasticity observed after the second shot, the mullion was subjected to third blast shot with a reflected pressure-impulse combination of 44 kPa – 337 kPa-msec. This level of loading resulted in increased plastic deformations with a maximum deflection of 61 mm and a permanent deflection approaching 30 mm. Figure 3-20 shows the test data recorded for the third blast shot. Figure 3-21 depicts inelastic deformations observed in Mullion 2.

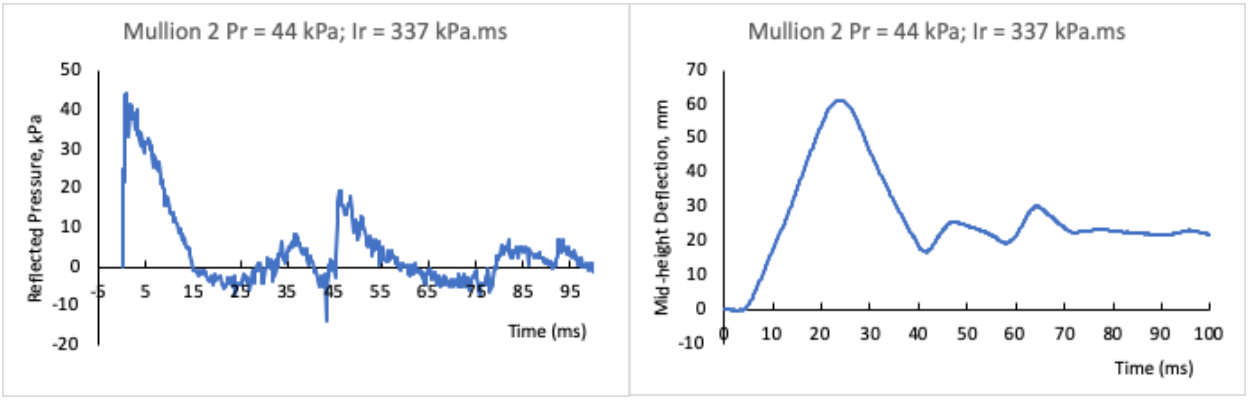

Figure 3 - 20 : Mullion 2 third shot pressure-time history (left) & deflection-time history (right)

3.6.2.2 Test results - Mullion 2H

Mullion 2H was companion to Mullion 2. The core of Mullion 2H was same as that of Mullion 2. The hardening technique used to reinforce the mullion consisted of two steel plates with a thickness of 3 mm, attached to both sides of the web with self-tapping screws. Initially the screws were placed with 200 mm spacing. This is illustrated in Figure 3-22. The first shot had a pressure-impulse combination of 41 kPa; 332 kPa-msec. Maximum displacement of 53.5 mm was recorded with a residual displacement of 25 mm. The test data recorded are presented in Figure 3-23.

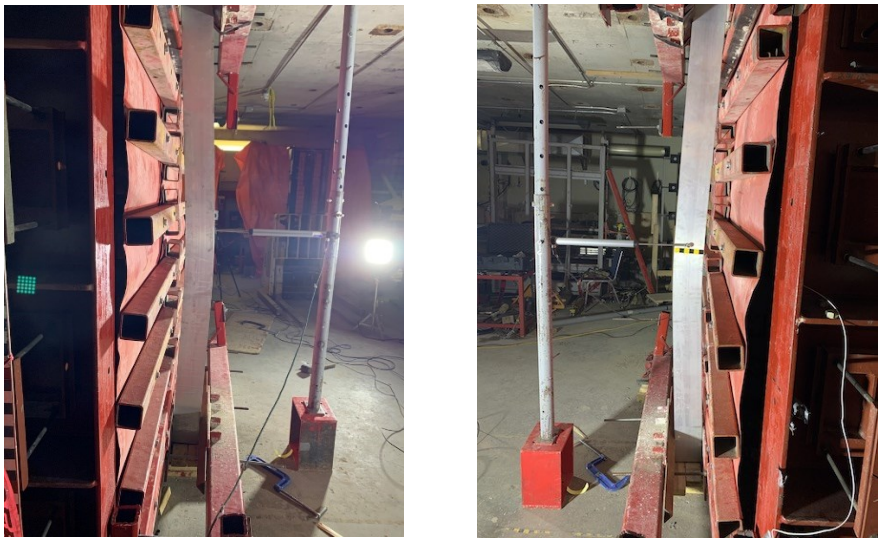

Figure 3 - 21 : Mullion 2 after the third shot

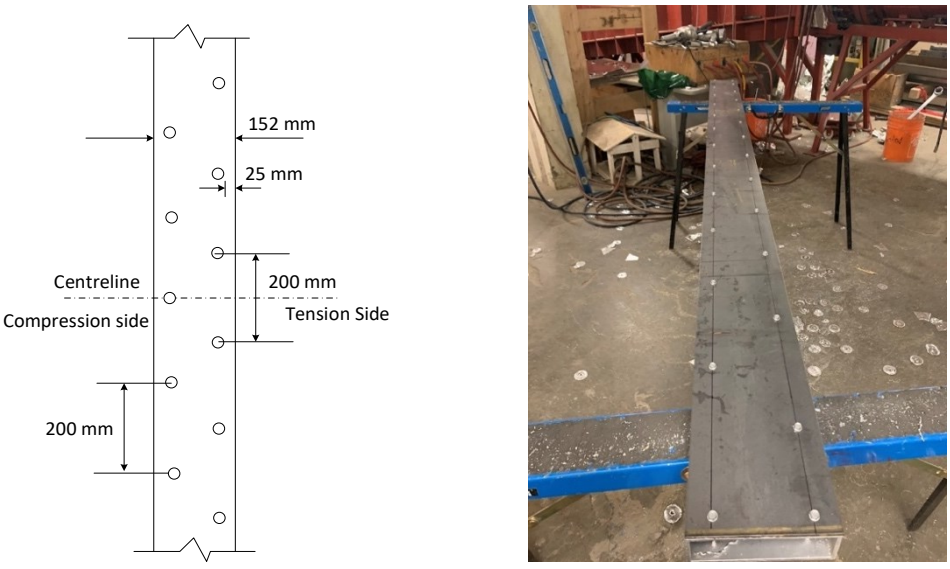

Figure 3 - 22 : Mullion 2H under preparation with initial bolt spacing of 200 mm c/c

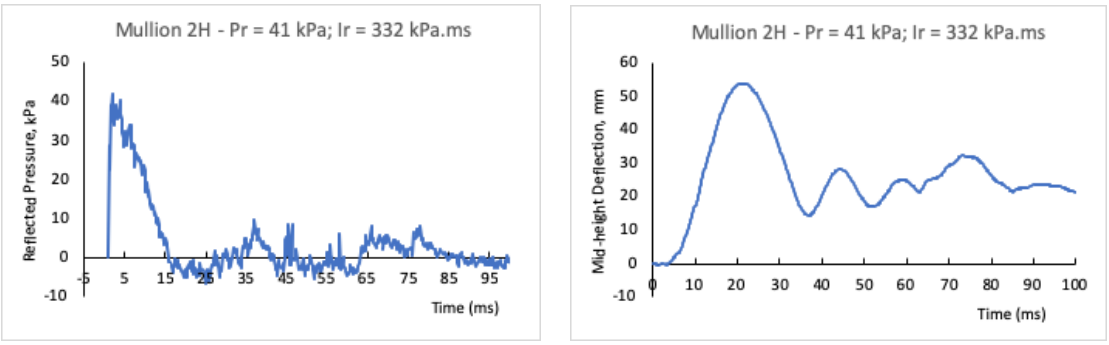

Figure 3 - 23: Mullion 2H first shot pressure-time history (left) & deflection-time history (right)

After the first shot, it was observed that the steel plates between the bolts were bent. Figure 3-24 clearly depicts the bending of the steel plates in between consecutive screws. Mullion 2H was the first retrofitted specimen tested and the maximum buckling length to ensure full composite behavior was uncertain prior to testing. Additional screws were placed after the first shot to reduce the spacing to 100 mm c/c prior to applying the second shot. The pressure-impulse combination for the second test was 65 kPa – 487 kPa-msec. The maximum mid-height displacement recorded was 88 mm. Figure 3-25 illustrates test data after the second shot. However, no permanent damage was observed after this test and the specimen was further subjected to an increased blast load as the third shot.

Figure 3 - 24 : Mullion 2H with bolt spacing 200 mm c/c after the first shot

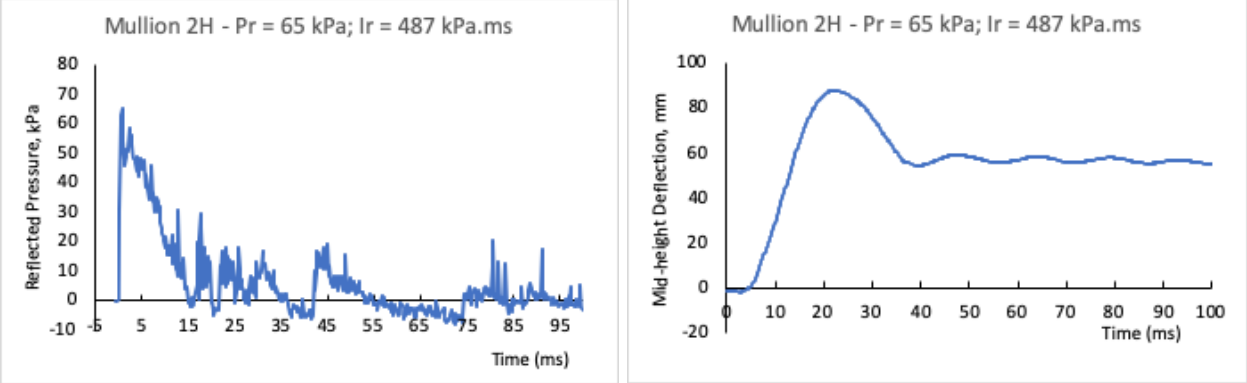

Figure 3 - 25 : Mullion 2H second shot pressure-time history (left) & deflection-time history (right)

The third blast shot was more intense with a pressure-impulse combination of 82 kPa – 645 kPa-msec. During the third shot due to the problems with instrumentation, the pressure sensors for to measuring reflected pressure and the LVDT for measuring mid-height displacements were not able to capture the data. However, the reflected pressure was estimated based on the recorded driver pressure and the mid-height displacement was estimated from the digital image correlation after processing the high-speed video. The maximum displacement recorded at mid-height was 149 mm with a residual displacement of 78 mm.

Post blast observations indicated that the steel plates experienced web buckling on both sides of the web, near the compression fibers. Also, the aluminum core section suffered web buckling to such an extent that it was ruptured near the maximum compression zone. Figures 3-26 and 3-27 depict the failure pattern of Mullion 2H after the third shot.

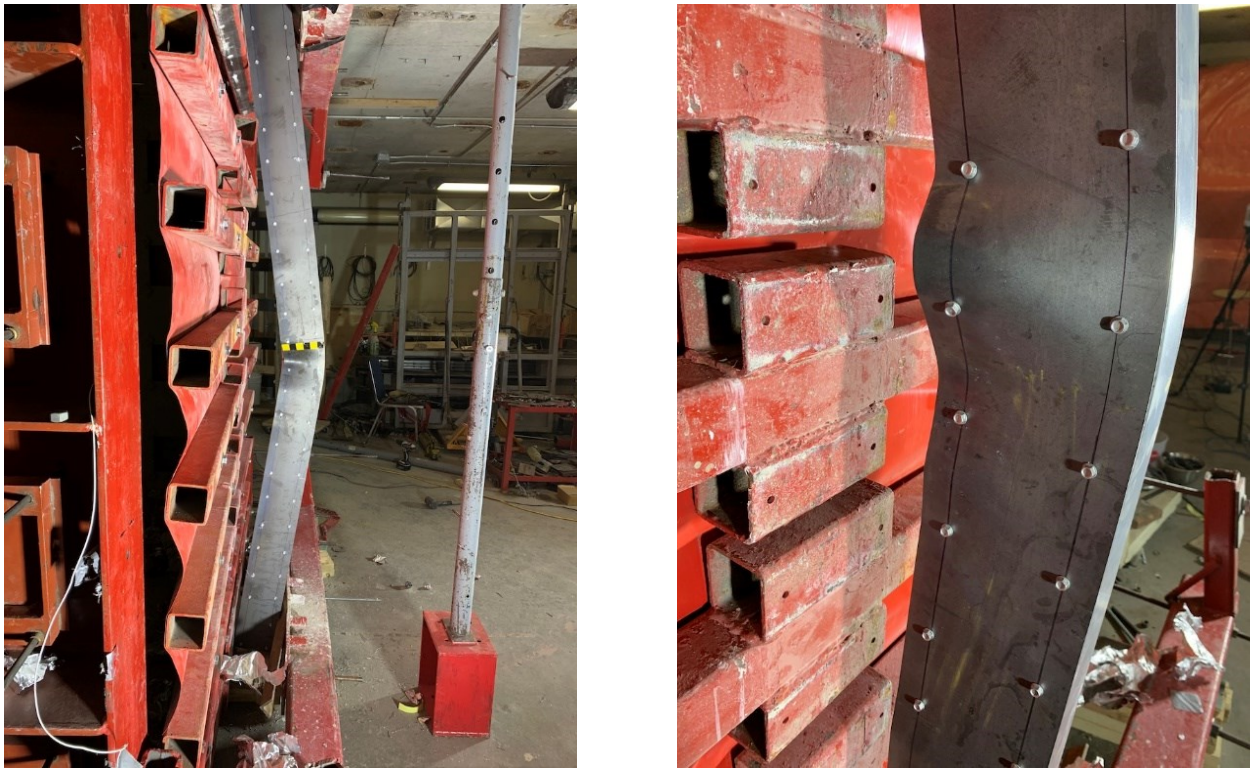

Figure 3 - 26 : Mullion 2H after the third shot

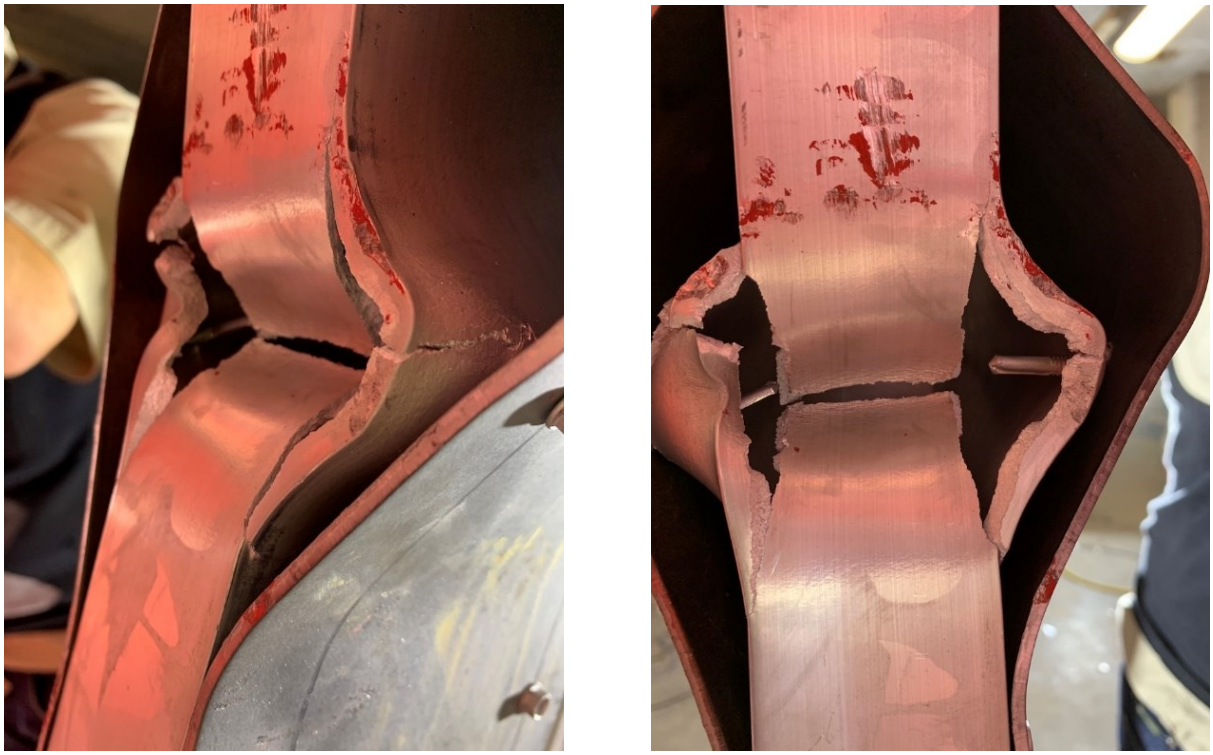

Figure 3 - 27 : Close up view of Mullion 2H after the third shot

3.6.2.3 Comparison of results – Mullion 2 & Mullion 2H

The comparison of Mullion 2 and 2H behavior is shown in Figure 3-28. The following provides a summary of observations made during the tests with the following comparisons of their performances:

- The hardening technique adopted in Mullion 2H was the simplest of all the options considered in the experimental program with only two rectangular plates attached on the existing aluminum mullion. This resulted in equally higher load resistance as the L-shaped steel angles used in Mullion 1H. The load carrying capacity was approximately doubled relative to that of the unretrofitted mullion.
- The addition of the steel plates improved the deformability and support rotation of the mullion, resulting in 2.4 times the maximum deflection recorded for the unretrofitted mullion.
- It was experimentally observed that reducing the centre-centre spacing of self-tapping screws from 200 mm to 100 mm resulted in better performance and near full composite

behavior between the aluminum and the steel until after significant inelasticity developed in the mullion.

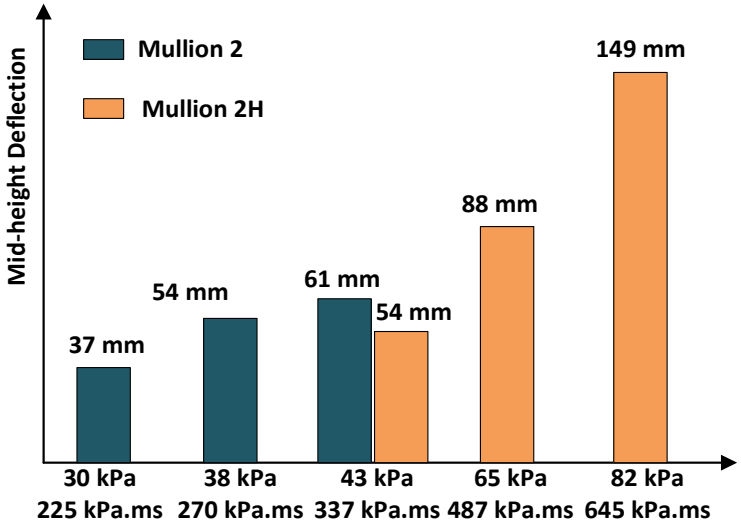

Figure 3 - 28 : Comparison of Mullion 2 & Mullion 2H

3.6.3 Test results & comparison – Mullion 3 & Mullion 3H

3.6.3.1 Test results - Mullion 3

Mullion 3 was the weakest among the three sets of mullions considered in the experimental program, but it was hardened with the strongest assembly, consisting of steel plates along the web and an HSS section on the tension flange (Mullion 3H) as discussed in. the next section. The aluminum section had dimensions of 127 mm x 51 mm x 3 mm.

Mullion 3 was subjected to a single shot of blast load with a pressure-impulse combination of 25 kPa – 208 kPa-msec. This level of blast load was damaged the section, generating a maximum inelastic deflection of 71 mm and a residual deflection of 42 mm. The deflection values recorded were highest amongst all the mullions tested under this particular blast load. The pressure-time history and displacement-time history recorded during the experiment can be seen in Figure 3-29. Figures 3-30 shows Mullion 3 before and after the test. The deflections observed were indicative of failure and the specimen was no longer subjected to further blast loads.

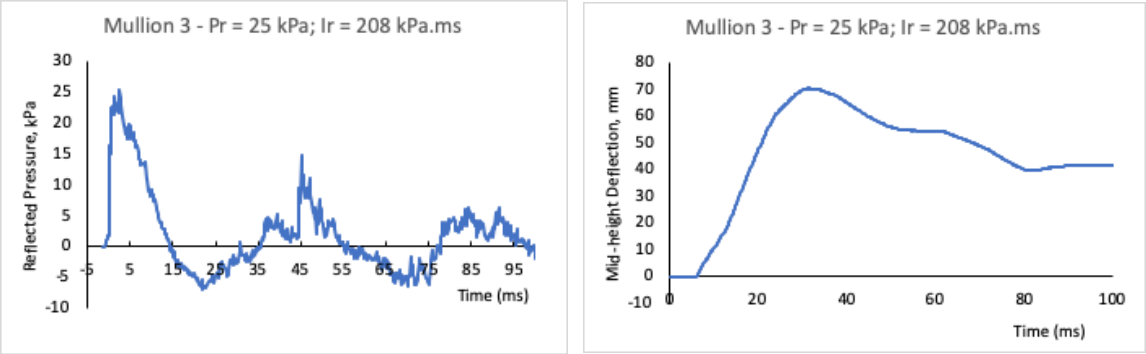

Figure 3 - 29 : Mullion 3 first shot pressure-time history (left) & deflection-time history (right)

Figure 3 - 30 : Mullion 3 prior to first shot (left) and after first shot (right)

3.6.3.2 Test results - Mullion 3H

The interior core of Mullion 3H was same as that of Mullion 3 as described in *Section 3.2.1.3*. A The hardening involved the use of 51 mm square steel HSS section with a wall thickness of 3 mm on the tension flange, connected together with 3 mm thick steel plates screwed on both sides of the web. The screw configuration is presented the *Section 3.2.1.3,* and had a c/c spacing of 100 mm.

The first blast shot applied had a pressure-impulse combination of 26 kPa – 207 kPa-msec. The maximum displacement recorded at mid-height was 26 mm with a permanent displacement of 15 mm. The data recorded is shown in Figure 3-31. This level of load resulted in limited inelasticity, as illustrated in Figure 3-32 with reserve capacity for further loading.

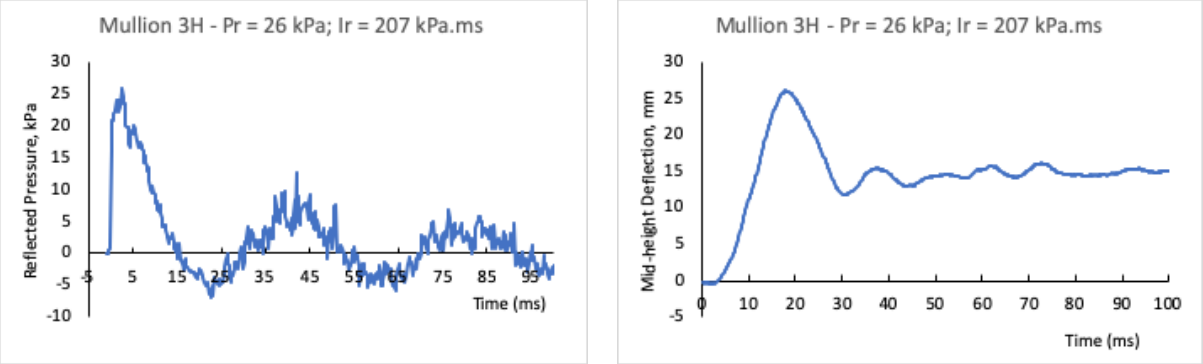

Figure 3 - 31 : Mullion 3H first shot pressure-time history (left) & deflection-time history (right)

Figure 3 - 32 : Mullion 3H before (left) and after (right) the first shot

The second shot applied to Mullion 3H had a pressure-impulse combination of 51 kPa – 428 kPa-msec. The maximum deflection captured at mid-height was 98 mm. The second shot left a heavy damage to the member, resulting in web buckling of the aluminum section. However, the steel HSS section attached to the tension flange did not experience any damage. The test data of

second shot is described in Figure 3-33. The web buckling can be seen in Figure 3-34 with the rupture of the compression flange.

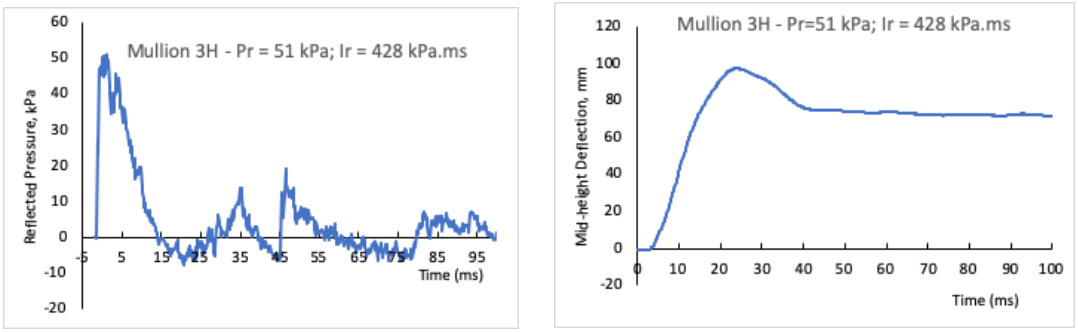

Figure 3 - 33 : Mullion 3H second shot pressure-time history (left) & deflection-time history (right)

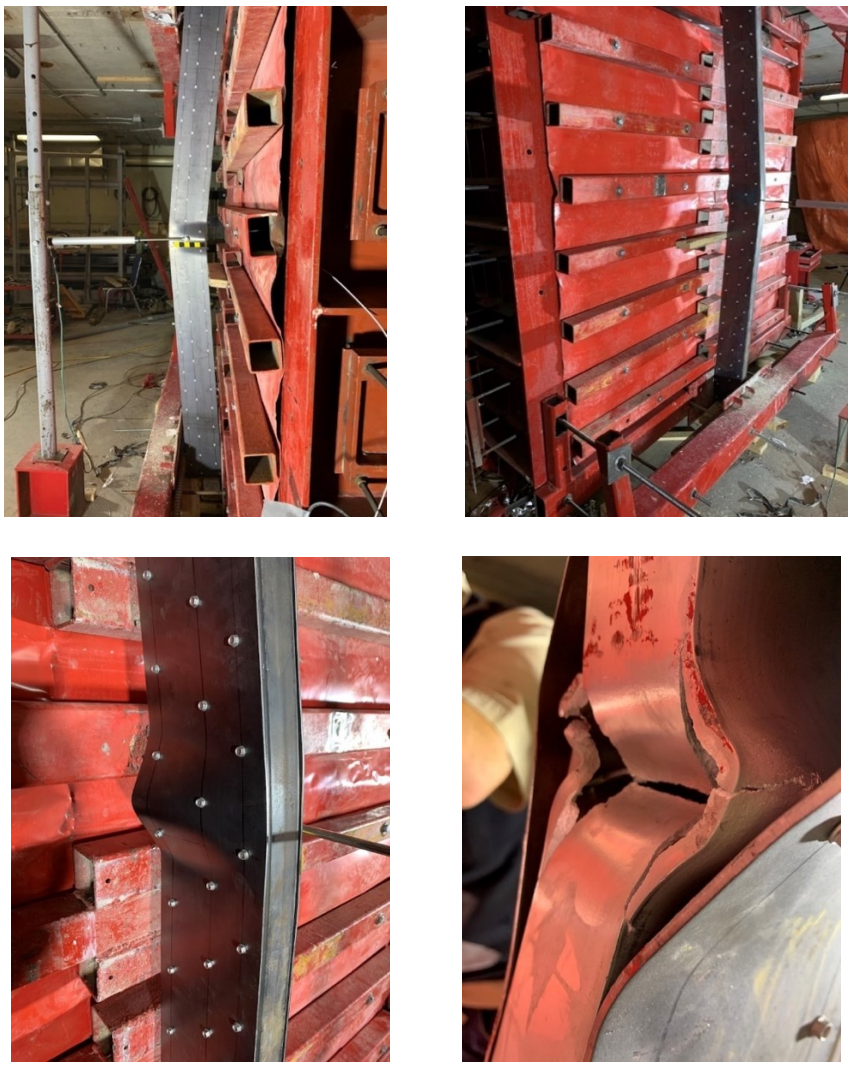

Figure 3 - 34 : Mullion 3H web buckling after second shot

As the web buckling at mid-height portion severely damaged the section, it could not provide further resistance and no further load was applied. Figure 3-34 indicates full composite action of the core aluminum section, steel plates and the HSS section as there was no bending of steel plates between the consecutive screws.

3.6.3.3 Comparison of results – Mullion 3 & Mullion 3H

Comparisons of Mullion 3 and 3H are shown in Figure 3-35 in terms of the intensity of blast loads and the maximum mid-height deflections measured. The following observations provide information on the effectiveness of the hardening technique employed:

- Mullion 3H developed 30% less deflection under the same blast load prior to failure because of its increased stiffness. The load bearing capacity of Mullion 3H increased by a factor of 2.0 as compared to Mullion 3.
- The spacing of 100 mm used to fasten steel to aluminum was found to be adequate to maintain full composite action between the aluminum core and the steel enclosure.
- Even though Mullion 3 was the weakest among the ones considered, hardening it with the strongest assembly resulted in significant improvements, with the highest displacement (2.6 times) relative to the companion unretrofitted specimen (Mullion 3). However, it is noteworthy that the failure was governed by the failure of unhardened compression side of the mullion, implying that this could be the governing mode of failure, limiting the requirements for further strengthening of the tension side.

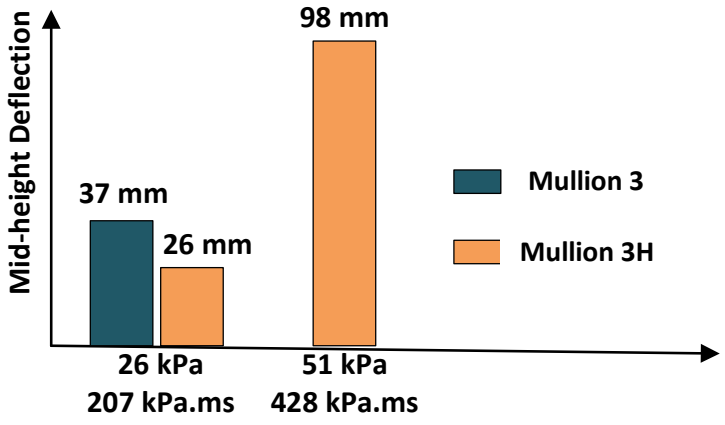

Figure 3 - 35 : Comparison of Mullion 3 & Mullion 3H

3.7 TEST RESULTS DISCUSSION & REVIEW

The test results indicate the beneficial response of the hardened mullions with the use of steel plates or steel plate-HSS assembly. The following specific observations were made during testing.

- The unhardened sections used in conventional building construction may be vulnerable against blast loads.
- The three main hardening techniques used to improve the response of aluminum mullion sections consist of, i) L-shaped steel plates, ii) rectangular steel plates, and iii) HSS section in combination with steel side plates, all attached to the existing aluminum mullions by means of self-tapping screws.
- The use of self-tapping screws to connect externally provided steel sections to existing aluminum mullions provide sufficient composite action when the spacing between the screws is limited to 100 mm.
- The blast load capacity of Mullion 1H was almost increased by a factor of 2.0 as compared to the unhardened companion Mullion 1. Also, the mid-height deflections for the tests on these mullions with same blast load intensities resulted in less deformation of Mullion 1H which was approximately half of the deflection recorded for Mullion 1.
- Mullion 2H incorporated steel plates attached to its web outer faces in order to provide additional strength and stiffness. This resulted in an increased blast capacity by a factor of 1.9. During this set of tests, the spacing of screws was also investigated as a parameter and it was concluded that a maximum screw spacing of 100 mm ensured fully composite behavior between the two materials.
- Mullion 3 was the weakest section of all of the unhardened tested mullions. This mullion represented the presence of weak and slender sections in existing curtain walls with potentials for catastrophic failures when subjected to blast loads.
- Mullion 3H had a square HSS section along the tension flange and additional two steel plates attached on the web side faces with a 100 mm c/c screw spacing. This assembly increased both strength and stiffness significantly.
- Mullion 3H resulted in a decrease of 30% in mid-height deflections and an increase of strength by a factor of 2.0 relative to the unhardened companion mullion.

- The support conditions for all test specimens consisted of a knife-edge type of simple support provided on one side. However, the other side of the mullions bared against the shock tube frame, developing significant restraint against rotation.

The overall review and test sequence of experimental research is given in Table 3-6.

Table 3 - 6 : Summary and sequence of experimental tests

Test Specimen	Blast Shot Sequence	Blast Shot Details		Recorded Mid-height Displacement (mm)	Final Residual Displacement (mm)	Failure Description
		Reflected Pressure (kPa)	Reflected Impulse (kPa-msec)			
Mullion 1	Shot 1	27	191	45.7	24	Web buckling at mid-height along compression fibers.
Mullion 1H	Shot 1	27	210	28	60	Composite section web buckling at mid-height along compression fibers.
	Shot 2	59	411	91		
Mullion 2	Shot 1	30	225	37	30	Inelastic bending of the section along the mid span.
	Shot 2	38	270	54		
	Shot 3	44	337	61		
Mullion 2H	Shot 1	41	332	53.5	78	Steel plates suffered web buckling and rupture of the compression flange of aluminum section.
	Shot 2	65	487	88		
	Shot 3	82	645	149		
Mullion 3	Shot 1	25	208	71	42	Inelastic bending of the section along the mid span.
Mullion 3H	Shot 1	26	207	26	70	Steel plates suffered web buckling and rupture of the compression flange of aluminum section.
	Shot 2	51	428	98		

CHAPTER 4. ANALYTICAL RESEARCH

4.1 INTRODUCTION

The hardened and unhardened mullions tested in the experimental phase of research were analyzed to gain better understanding of the mullion behavior while validating the results. The analysis consisted of nonlinear single degree of freedom (SDOF) dynamic analysis. The analysis was conducted both by using computer software RC-Blast, developed earlier at the University of Ottawa (Jacques 2014), and by using the charts developed by the US Army (Uniform Facilities Criteria - UFC 2008). The software was also used to generate pressure impulse (PI) diagrams for the mullions to show ductility demands in the entire range of reflected pressure-impulse combinations. The overview of the chapter is outlined below.

- Section 4.2: Analysis tools.
- Section 4.3: Development of resistance functions.
- Section 4.4: Validation procedures.
- Section 4.5: Pressure impulse diagrams.
- Section 4.6: Analytical study summary and discussion.

4.2 ANALYSIS TOOLS

4.2.1 Unified Facilities Criteria (UFC) - Charted Solution

The Unified Facilities Criteria (UFC) of the United States Department of Defense (UFC 3-30-02) includes a manual method for inelastic SDOF response for systems subjected to blast loading. The UFC approach uilizes the ratio of blast duration (t_d) to fundamental period of structure (T); and the ratio of maximum resistance offered by the structure (R_m) to static blast force applied (pressure times the tributary area) to the structure (F_1) to estimate the ductility demand for the structure (in terms of displacement ductility ratio, μ). The ductility ratio is the ratio of maximum inelastic displacement (u_m) to yield displacement (u_y) of the structure. The fundamental period of the structure is calculated with the following formula.

$$T = 2\pi\sqrt{\frac{K_{LM}m}{k}}$$

In the above expression, K_{LM} is load mass factor, which converts the distributed mass (m) and uniformly distributed load to lumped mass and concentrated force, respectively. Figure 4-1 shows a sample set of charts for determining ductility demands for an element that show perfectly elasto-plasic behavior.

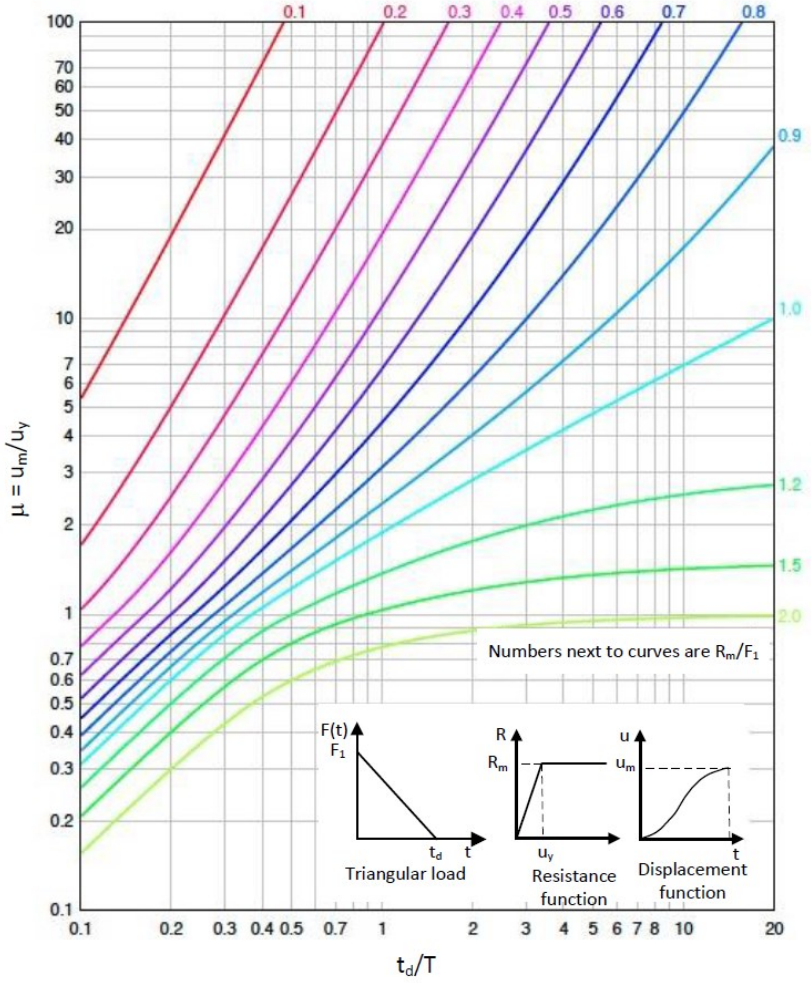

Figure 4 - 1 : UFC Chart for establishing ductility demand of elements under triangular blast loadings

The first step in dynamic analysis involves the computation of resistance function in the form of force-deflection relationship. This defines the elastic stiffness (slope of the initial ascending branch) and the yield resistance (R_m). The resistance function for a simply supported mullion is bi-linear with the first line segment representing elastic stiffness up to the yield, followed by the second line segment representing post-yield stiffness. A typical resistance function for a simply-

supported mullion with a single potential yield region at mid-height is shown in Figures 4-2. Figure 4-3 shows a typical resistance function for mullions with continuous support/support rotational restrained. The latter support condition permits progressive yielding of the member and moment redistribution between the high-moment regions, resulting in a tri-linear resistance function. This type of resistance function can be idealized as bi-linear relationship, typically by setting the area lost to area gained for the application of the UFC charts. Further discussion of resistance functions, with numerical values for each mullion is provided in Section 4.3.

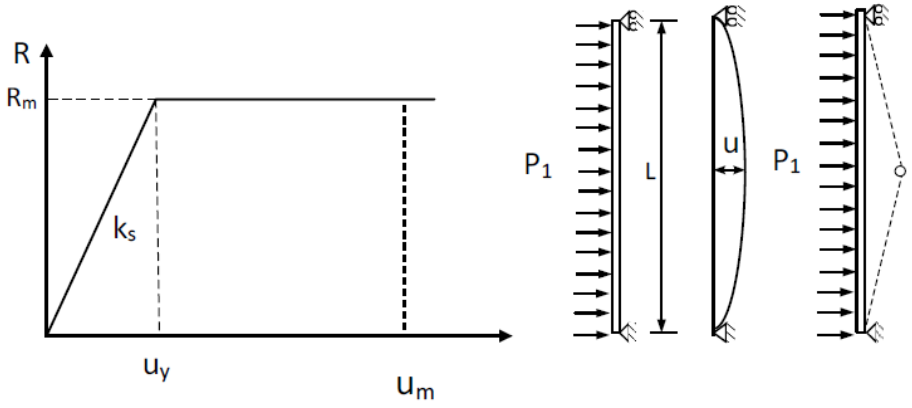

Figure 4 - 2 : Bilinear resistance function for a simply supported mullion

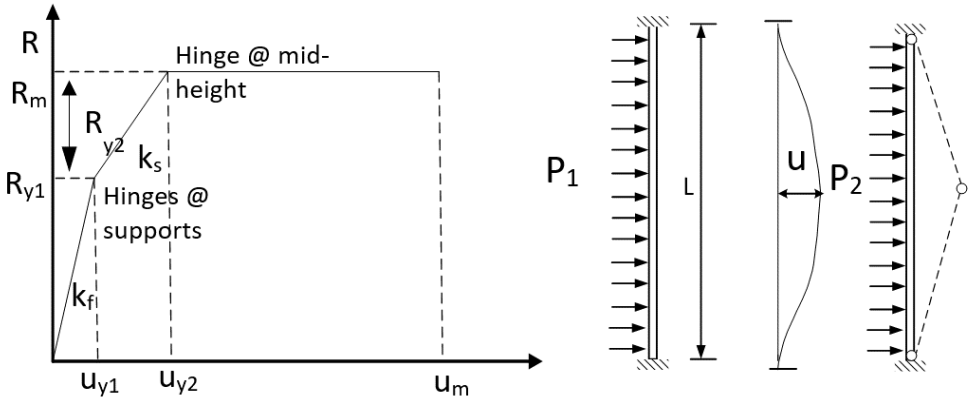

Figure 4 - 3 : Trilinear resistance function for a mullion with support fixity

The UFC charted solution is an easy and a quick way to predict the SDOF response of a structure. However, this method does not consider damping of the structure. The purpose for using the UFC charts in this analytical study is to check the precision/accuracy of the RC-Blast software which is used to analyze the behavior of the unhardened and retrofitted mullions in order to develop the design pressure-impulse diagrams.

4.2.2 RC-Blast blast analysis software

RC-Blast software is an analytical tool developed by Eric Jacques (2014) at the University of Ottawa to study the SDOF response of a structure subjected to blast loading. The software provides displacement time history of a structure under a specified impulsive forcing function, as well as the pressure impulse diagrams to compute ductility demands in a wide range of reflected pressure-impulse combinations. The following steps are followed for the application of this analysis tool.

- Step 1: Input of structural properties

In this step, the numerical values for the lumped mass of the system, tributary area on which the blast load is applied, and the damping coefficient for the structure are entered as input to the software. The input window for structural data entry is shown in Figure 4-4.

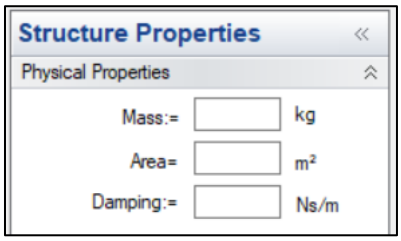

Figure 4 - 4 : Physical properties

- Step 2: Entry of resistance function

The resistance function and the corresponding load mass factor are entered for each flag point, i.e., at points of significant change in stiffness. There may be as many points as needed specified to describe the resistance function. The resistance function for simply supported elements, and for elements that have other support conditions can be effectively defined in this data entry window, which is illustrated in Figure 4-5. Also, the software has a built-in resistance function option for reinforced concrete elements, which provides the results of sectional and member analysis based on the data specified for the reinforced concrete element.

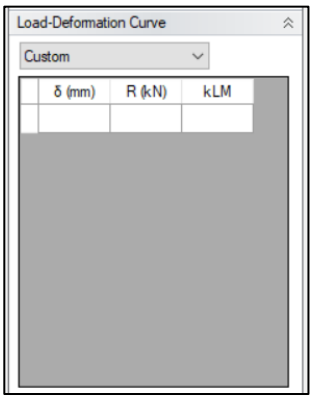

Figure 4 - 5 : Load-deformation resistance function

- Step 3: Hysteretic model

Inbound and rebound yield displacements with unloading stiffnesses are defined in a separate input window. Because of the difference in hysteretic behavior of different materials (steel or concrete), with elasto-plastic or stiffness degrading hysteretic response, the type of hysteretic model is specified. Figure 4-6 shows the input items required for this window.

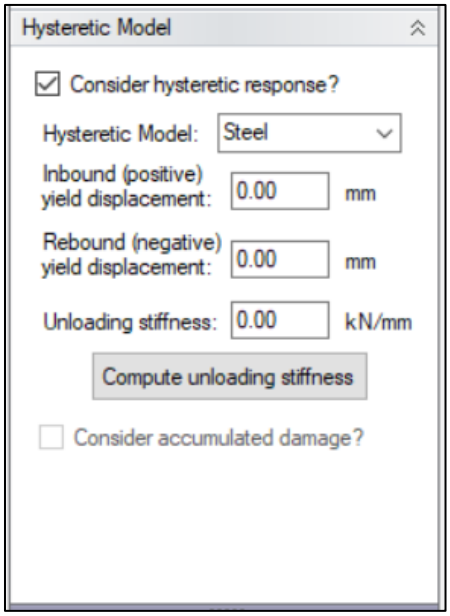

Figure 4 - 6 : Hysteretic Model

- Step 4: Data input for applied pressure

The blast load parameters are defined using a separate window, as illustrated in Figure 4-7. Blast load is either specified in terms peak positive and negative pressure and respective durations, or in terms of charge weight and standoff distance.

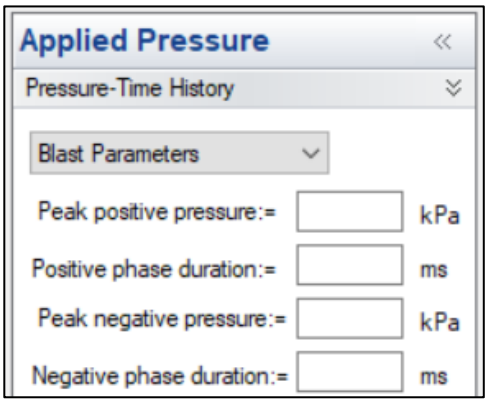

Figure 4 - 7 : Pressure-time history

- Step 5: SDOF analysis options

In this step, the required parameters for SDOF analysis are specified. They include the duration of each time step for numerical integration, maximum analysis time and initial boundary conditions. The input items are shown in Figure 4-8.

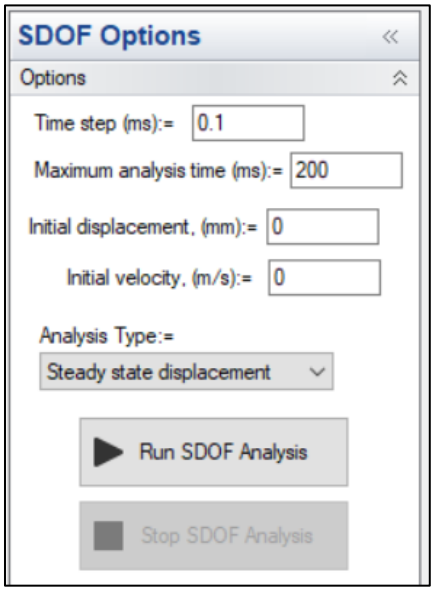

Figure 4 - 8 : SDOF options

- Step 6: P-I diagram specification

This is the final step in data entry. It consists of P-I diagram specification for maximum displacements. The user specifies maximum displacements for which P-I diagrams are calculated, as shown in Figure 4-9.

Once the dynamic analysis is executed, the software outputs eco printout of essential input information, as well as the displacement time history. A sample output is illustrated in Figure 4-10.

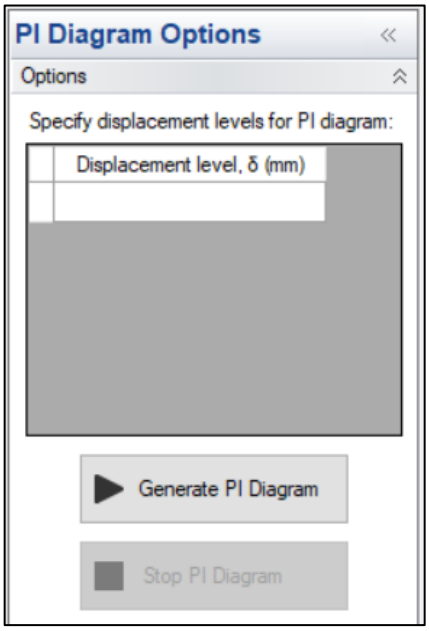

Figure 4 - 9 : P-I diagram options

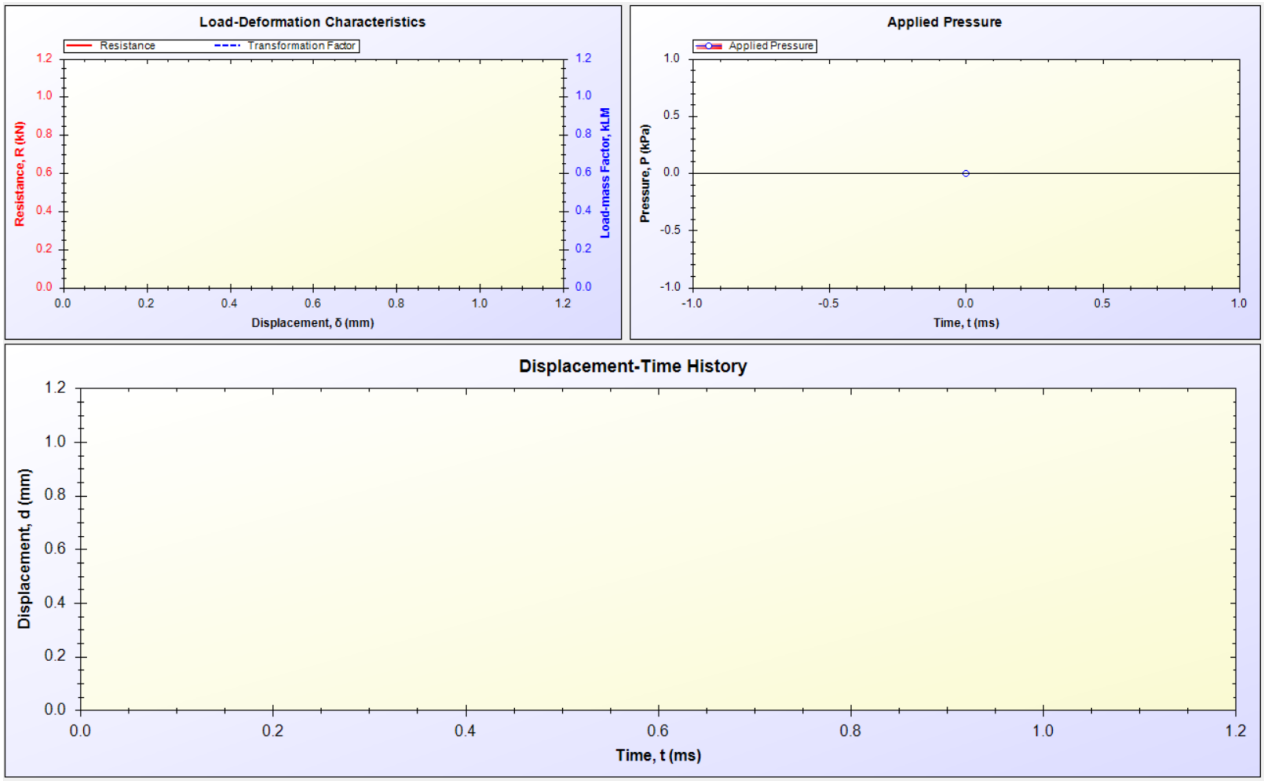

Figure 4 - 10 : Analysis output window

4.3 DEVELOPMENT OF RESISTANCE FUNCTIONS

The first step for nonlinear SDOF analysis is the computation of resistance functions. This involves the use of sectional rigidity (EI) for the aluminum and steel plates (in the case of hardened mullions) and the elastic stiffness as the slope of the initial descending branch. The initial branch continues up to the specified yield strength. Zero post-yield stiffness is assumed beyond the yield point, simulating perfectly elasto-plastic response, as typically observed for aluminum and steel. The descending branch, simulating unloading is assumed to be parallel to the initial elastic stiffness. Details of resistance function are provided in Sections 4.2.1 and 4.2.2. In this section, the resistance functions developed for all six test specimens are shown. The resistance functions were developed for both simply supported and fixed end conditions. The rationale for considering both support conditions is demonstrated subsequently, as the intended simple supports during the tests resulted in some fixity at the ends. The computational details are given in Appendix A. The SDOF that utilized the resistance functions provided inelastic displacement time histories, as well as the P-I diagrams for selected inelastic displacement (ductility) levels.

4.3.1 Resistance functions for Mullion 1

4.3.1.1 Resistance function for simple supports

The details of the resistance function developed for Mullion 1 with simply supported end conditions are given in Figure 4-11 and Table 4-1. The details of calculations are provided in *Appendix A.1.1.*

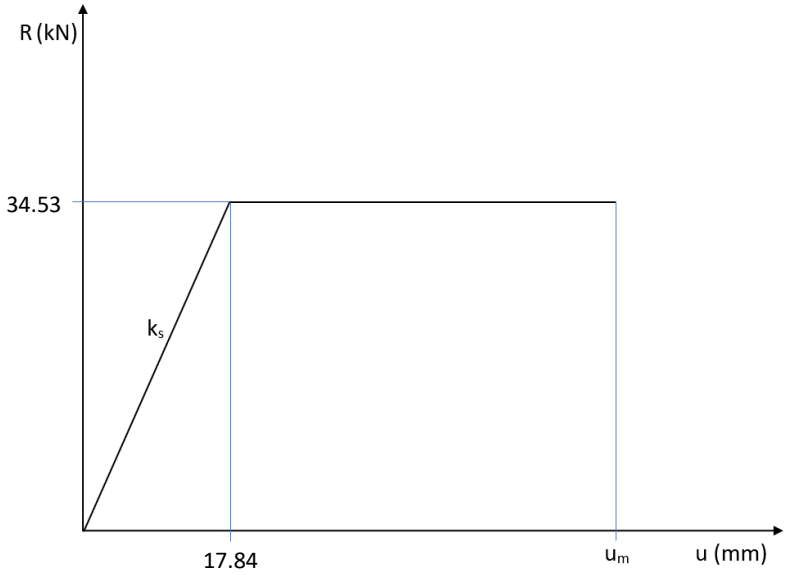

Figure 4 - 11 : Resistance function for Mullion 1 – simply supported

Table 4 - 1 : Values for simply supported Mullion 1 resistance function

Elastic yield resistance	-	R_m	=	34.53	kN
Yield displacement	-	u_y	=	17.84	mm
Stiffness	-	k_s	=	1.935	kN/mm

4.3.1.2 Resistance function for fixed supports

The details of the resistance function developed for Mullion 1 with fixed supports are given in Figure 4-12 and Table 4-2. The details of calculations are provided in *Appendix A.1.2.*

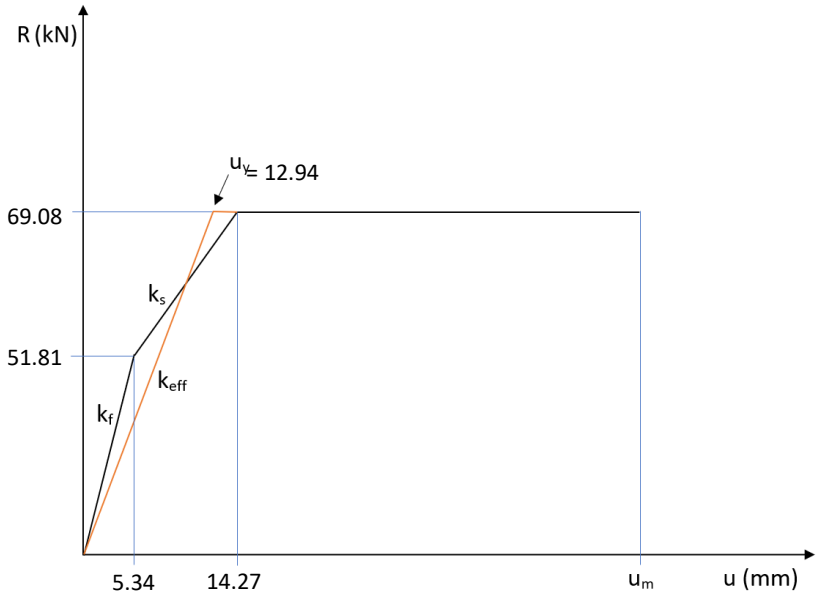

Figure 4 - 12 : Resistance function for Mullion 1 – fixed supports

Table 4 - 2 : Values for Mullion 1 resistance function for fixed support condition

Initial yield resistance	-	R_{y1}	=	51.81	kN
Initial yield displacement	-	u_{y1}	=	5.36	mm
Fixed support stiffness	-	k_f	=	9.68	kN/mm
Final yield resistance	-	R_{y2}	=	17.27	kN
Final yield displacement	-	u_{y2}	=	14.27	mm
Simple support stiffness	-	k_s	=	1.935	kN/mm
Elastic yield resistance	-	R_m	=	69.08	kN
Equivalent yield resistance	-	u_y	=	12.94	mm
Equivalent stiffness	-	K_{eff}	=	5.34	kN/mm

4.3.2 Resistance functions for Mullion 1H

4.3.2.1 Resistance function for simple supports

The details of the resistance function developed for Mullion 1H with simply supported end conditions are given in Figure 4-13 and Table 4-3. The details of calculations are provided in *Appendix A.2.1.*

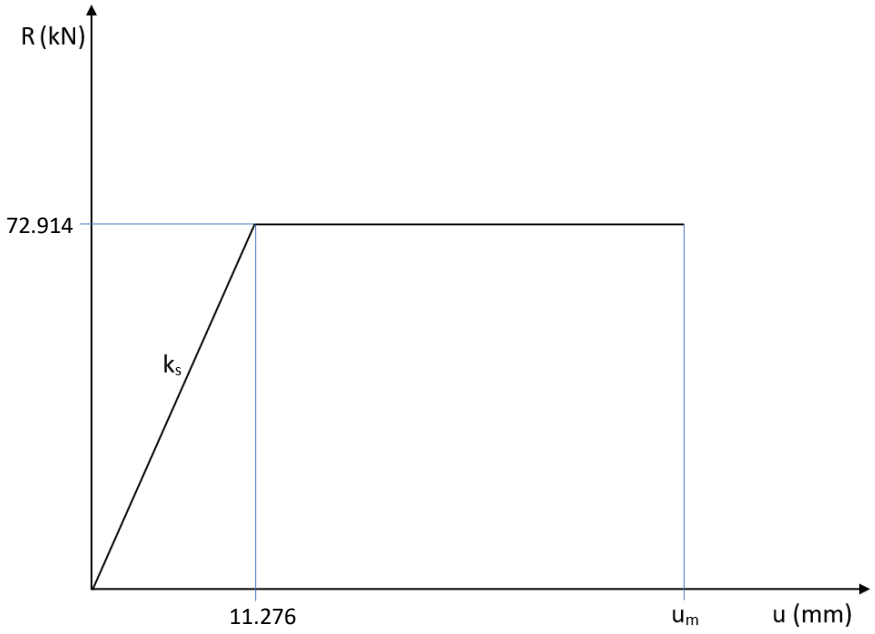

Figure 4 - 13 : Resistance function for Mullion 1H – simply supported

Table 4 - 3 : Values for simply supported Mullion 1H resistance function

Elastic yield resistance	-	R_m	=	72.914	kN
Yield displacement	-	u_y	=	11.276	mm
Stiffness	-	k_s	=	6.47	kN/mm

4.3.2.2 Resistance function for fixed supports

The details of the resistance function developed for Mullion 1H with fixed supports are given in Figure 4-14 and Table 4-4. The details of calculations are provided in *Appendix A.2.2.*

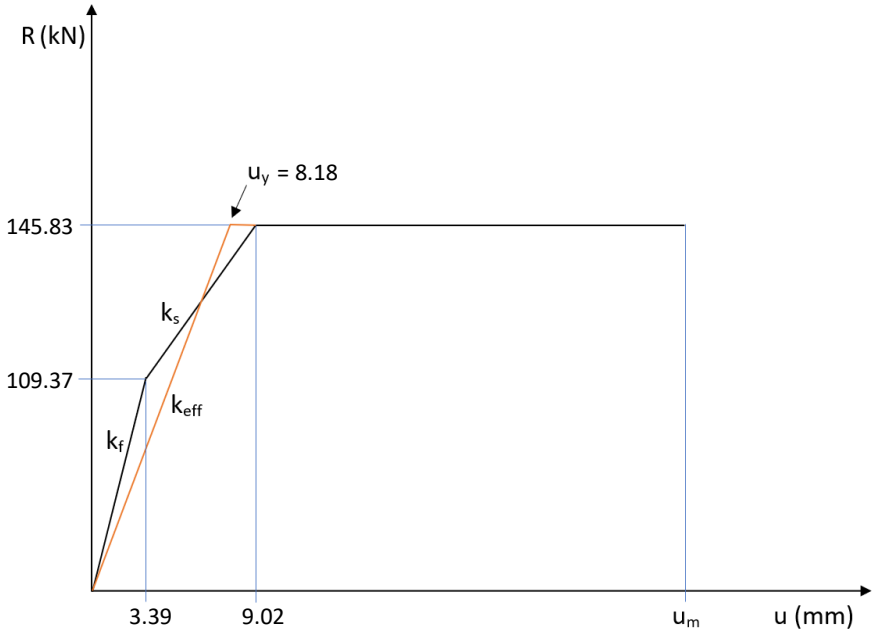

Figure 4 - 14 : Resistance function for Mullion 1H – fixed supported

Table 4 - 4 : Values for Mullion 1H resistance function for fixed end condition

Initial yield resistance	-	R_{y1}	=	109.37	kN
Initial yield displacement	-	u_{y1}	=	3.39	mm
Fixed support stiffness	-	k_f	=	32.33	kN/mm
Final yield resistance	-	R_{y2}	=	36.45	kN
Final yield displacement	-	u_{y2}	=	9.02	mm
Simple support stiffness	-	k_s	=	6.47	kN/mm
Elastic yield resistance	-	R_m	=	145.83	kN
Equivalent yield resistance	-	u_y	=	8.18	mm
Equivalent stiffness	-	K_{eff}	=	17.839	kN/mm

4.3.3 esistance functions for Mullion 2

4.3.3.1 Resistance function for simple supports

The details of the resistance function developed for Mullion 2 with simply supported end conditions are given in Figure 4-15 and Table 4-5. The details of calculations are provided in *Appendix A.3.1.*

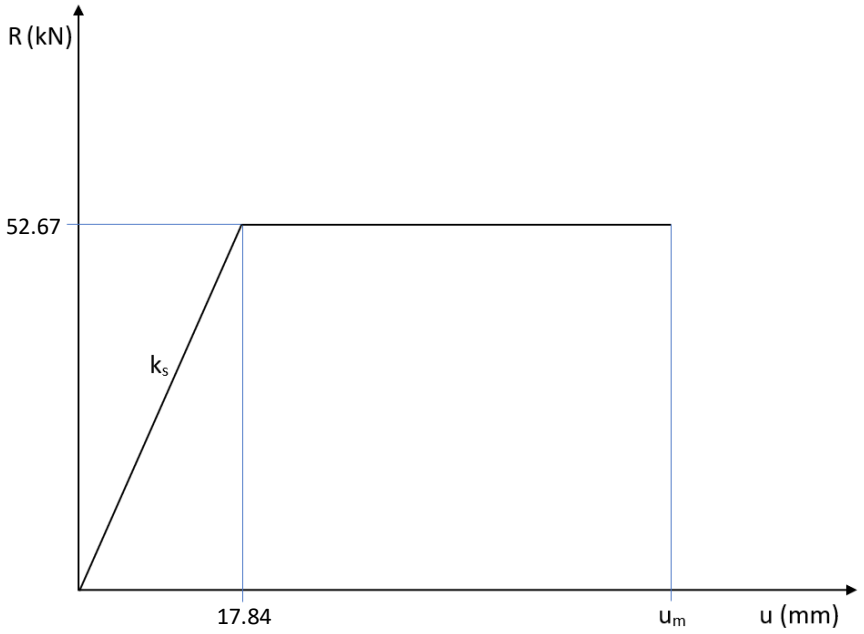

Figure 4 - 15 : Resistance function for Mullion 2 – simply supported

Table 4 - 5 : Values for simply supported Mullion 2 resistance function

Elastic yield resistance	-	R_m	=	52.67	kN
Yield displacement	-	u_y	=	17.84	mm
Stiffness	-	k_s	=	2.952	kN/mm

4.3.3.2 Resistance function for fixed supports

The details of the resistance function developed for Mullion 2 with fixed supports are given in Figure 4-15 and Table 4-5. The details of calculations are provided in *Appendix A.3.2.*

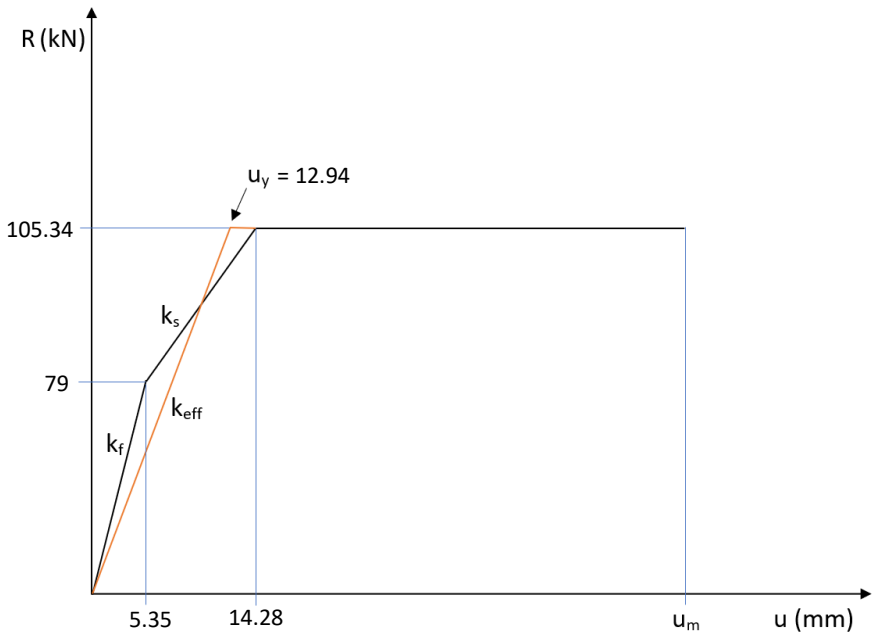

Figure 4 - 16 : Resistance function for Mullion 2 – fixed supported

Table 4 - 6 : Values for Mullion 2 resistance function for fixed support condition

Initial yield resistance	-	R_{y1}	=	79	kN
Initial yield displacement	-	u_{y1}	=	5.35	mm
Fixed support stiffness	-	k_f	=	14.761	kN/mm
Final yield resistance	-	R_{y2}	=	26.335	kN
Final yield displacement	-	u_{y2}	=	14.28	mm
Simple support stiffness	-	k_s	=	2.952	kN/mm
Elastic yield resistance	-	R_m	=	105.34	kN
Equivalent yield resistance	-	u_y	=	12.94	mm
Equivalent stiffness	-	K_{eff}	=	8.144	kN/mm

4.3.4 Resistance functions for Mullion 2H

4.3.4.1 Resistance function for simple supports

The details of the resistance function developed for Mullion 2H with simply supported end conditions are given in Figure 4-17 and Table 4-7. The details of calculations are provided in *Appendix A.4.1.*

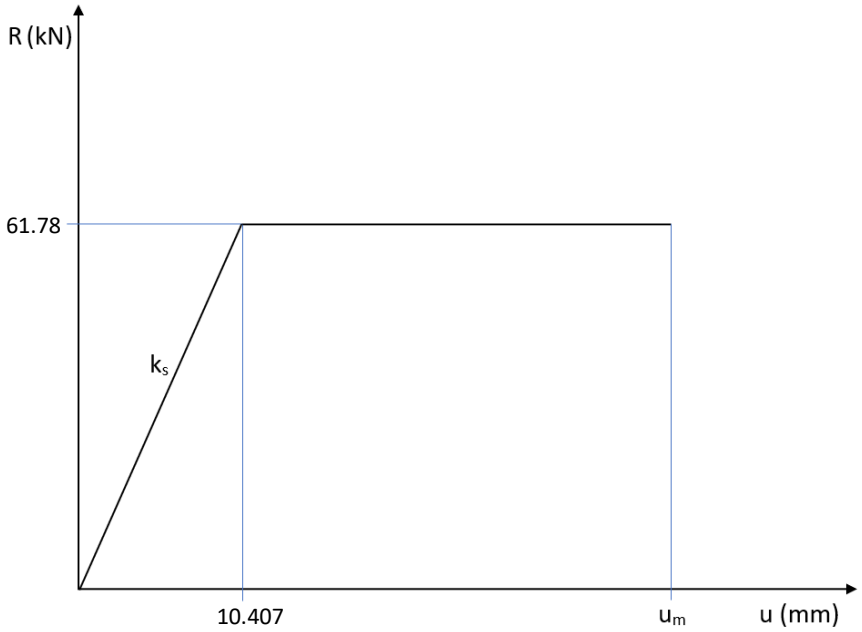

Figure 4 - 17 : Resistance function for Mullion 2H – simply supported

Table 4 - 7 : Values for simply supported Mullion 2H resistance function

Elastic yield resistance	-	R_m	=	61.78	kN
Yield displacement	-	u_y	=	10.407	mm
Stiffness	-	k_s	=	5.937	kN/mm

4.3.4.2 Resistance function for fixed supports

The details of the resistance function developed for Mullion 2H with fixed supports are given in Figure 4-18 and Table 4-8. The details of calculations are provided in *Appendix A.4.2.*

4.3.5 Resistance functions for Mullion 3

4.3.5.1 Resistance function for simple supports

The details of the resistance function developed for Mullion 3 with simply supported end conditions are given in Figure 4-18 and Table 4-8. The details of calculations are provided in *Appendix A.5.1.*

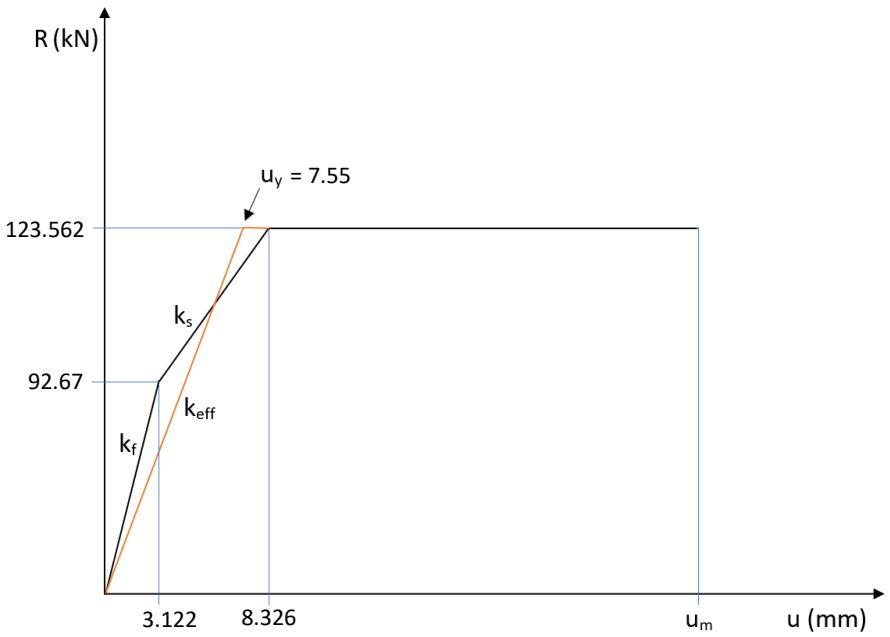

Figure 4 - 18 : Resistance function for Mullion 2H – fixed supported

Table 4 - 8 : Values for Mullion 2H resistance function for fixed support condition

Initial yield resistance	-	R_{y1}	=	92.67	kN
Initial yield displacement	-	u_{y1}	=	3.122	mm
Fixed support stiffness	-	k_f	=	29.682	kN/mm
Final yield resistance	-	R_{y2}	=	30.89	kN
Final yield displacement	-	u_{y2}	=	8.326	mm
Simple support stiffness	-	k_s	=	5.937	kN/mm
Elastic yield resistance	-	R_m	=	123.562	kN
Equivalent yield resistance	-	u_y	=	7.55	mm
Equivalent stiffness	-	K_{eff}	=	16.376	kN/mm

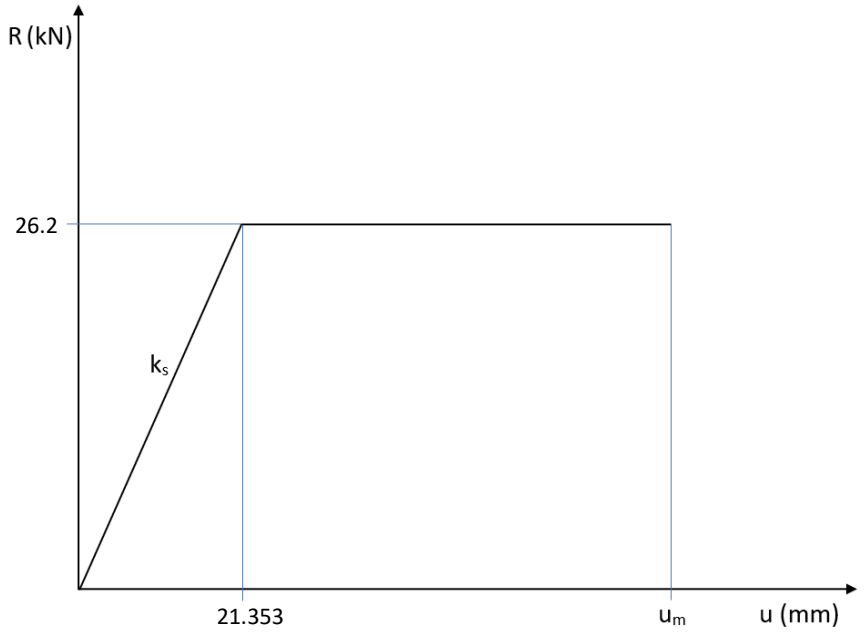

Figure 4 - 19 : Resistance function for Mullion 3 – simply supported

Table 4 - 9 : Values for simply supported Mullion 3 resistance function

Elastic yield resistance	-	R_m	=	26.2	kN
Yield displacement	-	u_y	=	21.353	mm
Stiffness	-	k_s	=	1.226	kN/mm

4.3.5.2 Resistance function for fixed supports

The details of the resistance function developed for Mullion 3 with fixed supports are given in Figure 4-20 and Table 4-10. The details of calculations are provided in *Appendix A.5.2.*

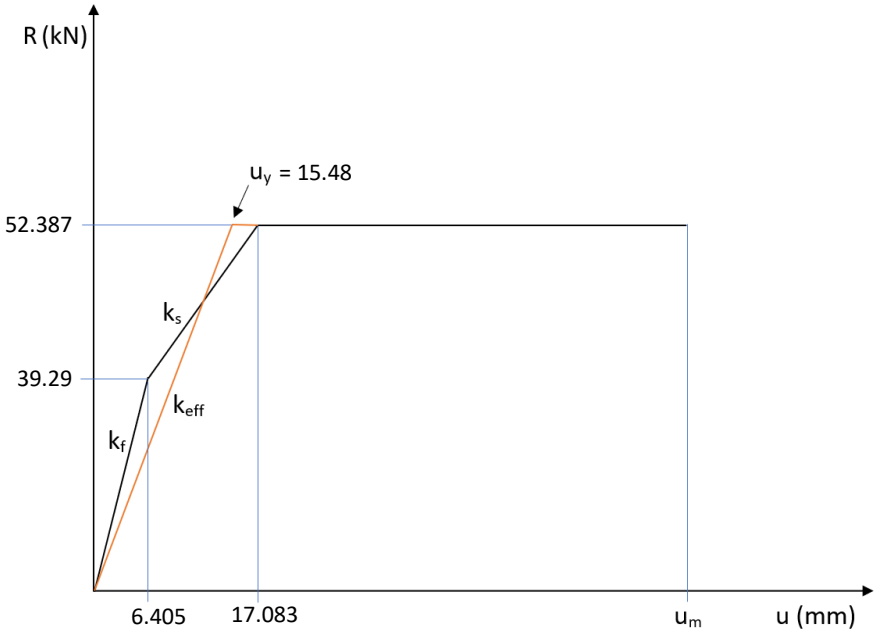

Figure 4 - 20 : Resistance function for Mullion 3 – fixed supported

Table 4 - 10 : Values for Mullion 3 resistance function for fixed support condition

Initial yield resistance	-	R_{y1}	=	39.29	kN
Initial yield displacement	-	u_{y1}	=	6.405	mm
Fixed support stiffness	-	k_f	=	6.133	kN/mm
Final yield resistance	-	R_{y2}	=	13.097	kN
Final yield displacement	-	u_{y2}	=	17.083	mm
Simple support stiffness	-	k_s	=	1.226	kN/mm
Elastic yield resistance	-	R_m	=	52.387	kN
Equivalent yield resistance	-	u_y	=	15.48	mm
Equivalent stiffness	-	K_{eff}	=	3.383	kN/mm

4.3.6 Resistance functions for Mullion 3H

4.3.6.1 Resistance function for simple supports

The details of the resistance function developed for Mullion 3H with simply supported end conditions are given in Figure 4-21 and Table 4-11. The details of calculations are provided in *Appendix A.6.1.*

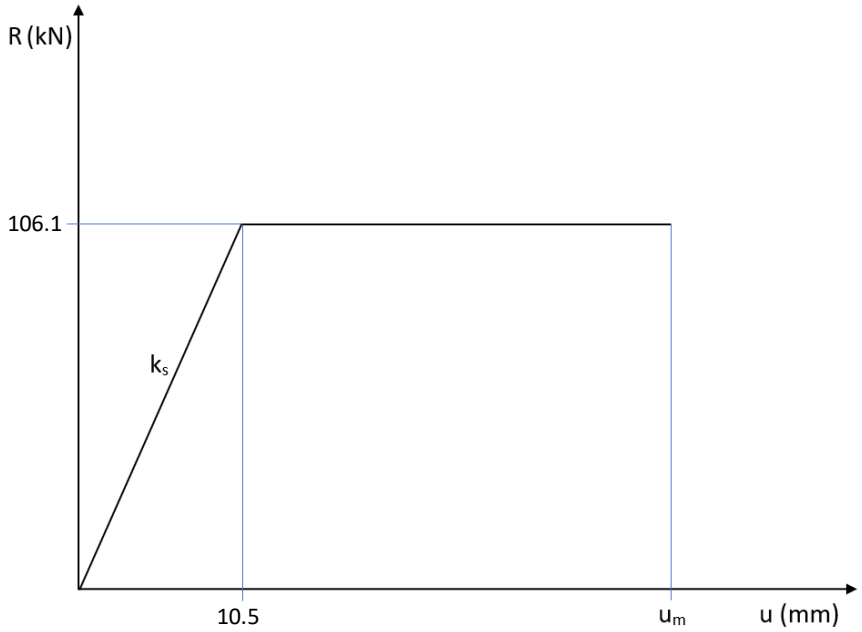

Figure 4 - 21 : Resistance function for Mullion 3H – simply supported

Table 4 - 11 : Values for simply supported Mullion 3H resistance function

Elastic yield resistance	-	R_m	=	106.1	kN
Yield displacement	-	u_y	=	10.5	mm
Stiffness	-	k_s	=	10.109	kN/mm

4.3.6.2 Resistance function for fixed supports

The details of the resistance function developed for Mullion 3H with fixed supports are given in Figure 4-22 and Table 4-12. The details of calculations are provided in *Appendix A.6.2.*

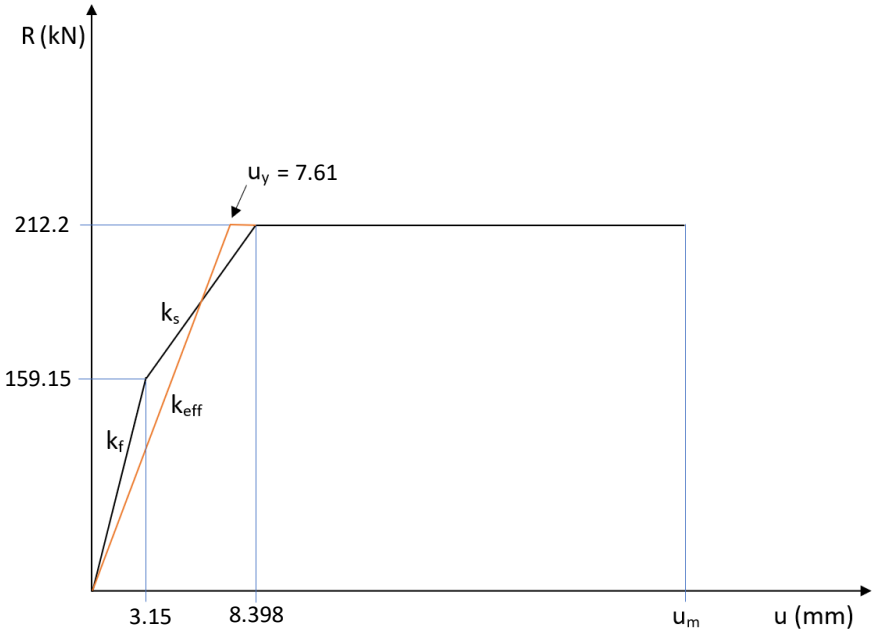

Figure 4 - 22 : Resistance function for Mullion 3H – fixed supported

Table 4 - 12 : Values for Mullion 3H resistance function for fixed support condition

Initial yield resistance	-	R_{y1}	=	159.15	kN
Initial yield displacement	-	u_{y1}	=	3.15	mm
Fixed support stiffness	-	k_f	=	50.541	kN/mm
Final yield resistance	-	R_{y2}	=	53.05	kN
Final yield displacement	-	u_{y2}	=	8.398	mm
Simple support stiffness	-	k_s	=	10.109	kN/mm
Elastic yield resistance	-	R_m	=	212.2	kN
Equivalent yield resistance	-	u_y	=	7.61	mm
Equivalent stiffness	-	K_{eff}	=	27.85	kN/mm

4.4 VALIDATION PROCEDURES

4.4.1 Correlation of UFC charted solution and RC-Blast software

Nonlinear dynamic response of Mullion 1 and Mullion 1H were computed using the UFC charts and RC-Blast software to assess the accuracy and the reliability of the analytical tools. The analyses were conducted twice for each mullion, with simple and fixed supports. Although the experimental tests were intended for simple support conditions, the knife edge support provided on one side of the support was not sufficient to eliminate rotational restraint at the ends. Hence, the mullions were prevented to rotate fully at the supports as they bared against the shock tube frame under high deformations, developing significant restraint against rotation. This is illustrated in Figure 4-23. Therefore, the comparison of these two analytical tools was made for both support conditions, i.e., simple supports and fully fixed supports.

Figure 4 - 23 : Support conditions at the ends during all the mullion tests

Custom built resistance functions were defined in RC-Blast software for SDOF response history analysis of Mullion 1 and Mullion 1H as described in *Sections 4.3.1* and *4.3.2*, respectively. The calculations for the computation of maximum displacements using the UFC Charts are given in *Appendix B.* The results are compared in Figures 4-24 to 4-27 under the same blast shots that

were applied to the mullions during the experimental phase. Mullion 1 results for simple support condition shows excellent agreement between the maximum displacements obtained from the SDOF analysis and the UFC charted solution, both indicating 116 mm of maximum mid-height displacement under the first blast shot. The same mullion shows very good correlation of maximum displacements under the fixed support conditions, with SDOF analysis indicating 39 mm and the UFC charted solution indicating 41 mm. The minor difference between the two results indicates inaccuracies introduced during the process of idealizing the tri-linear resistance function as bilinear relationship for the UFC solution, which provides charts for only bilinear resistance functions. Similarly, good correlations were obtained from the analysis of hardened Mullion 1H. The correlation under simple support condition when subjected to Shot 2 with significant yielding of the mullions and steel plates was 275mm for SDOF analysis versus 282 mm for the UFC charted solution. The same comparison under fixed support condition was 84 mm versus 86 mm, obtained from the SDOF analysis and UFC Charts, respectively. A contributing factor for any potential inaccuracy in results for the retrofitted mullions may be attributed to less than perfect composite action between the inner aluminum mullions and outer steel plates during response, while perfect bond is assumed in the analyses. The comparison of analyses results indicates high level of confidence in the SDOF analysis tool and the computation of resistance functions before the SDOF dynamic analysis is used to validate test data and further used to generate P-I diagrams as design aids for use under different combinations of reflected pressures and impulses as blast load threats.

4.4.2 Validation of RC-Blast software and experimental tests

This section provides the validation of the results obtained from RC-Blast analysis against those recorded during the test. The validation process is carried out for Mullion 1 and Mullion 1H for both simple support and fixed end conditions. Damping was considered in the analysis and was taken equal to 2% of critical damping. The resistance functions calculated in *Section 4.3.1* and *Section 4.3.2,* were used with corresponding physical properties. Although, the experiments intended for simple support conditions, there was fixity developed during the tests, as described earlier in Section 4.4.1 and illustrated in Figure 4-23. Indeed, the analysis results agreed well with test data when fixed support conditions were considered in the analysis, though the

experimental response indicated somewhat less than full fixity at the supports, which is expected. Figures 4-28 to 4-31 show the comparison of SDOF analysis and experimentally recorded plastic (residual) deflections.

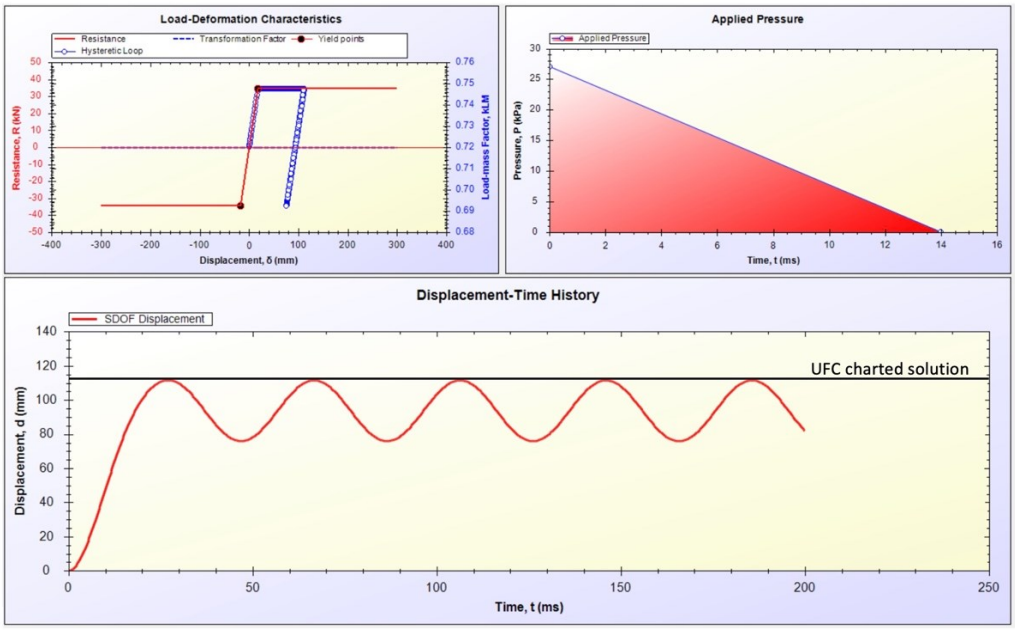

Figure 4 - 24 : Validation of UFC charted solution and RC-Blast software – Mullion 1 – simple supports

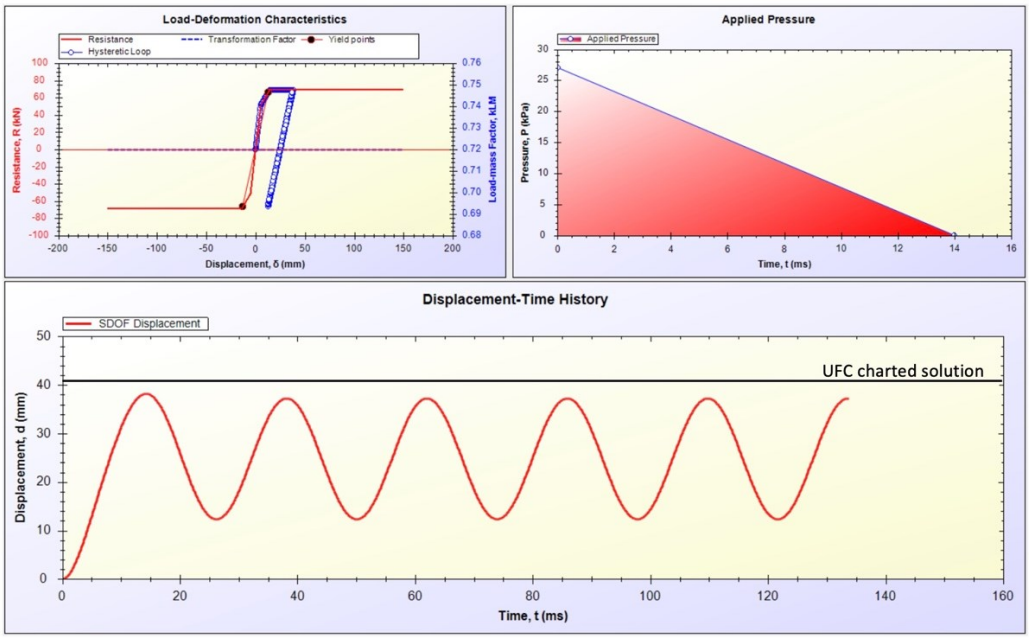

Figure 4 - 25 : Validation of UFC charted solution and RC-Blast software – Mullion 1 – fixed supports

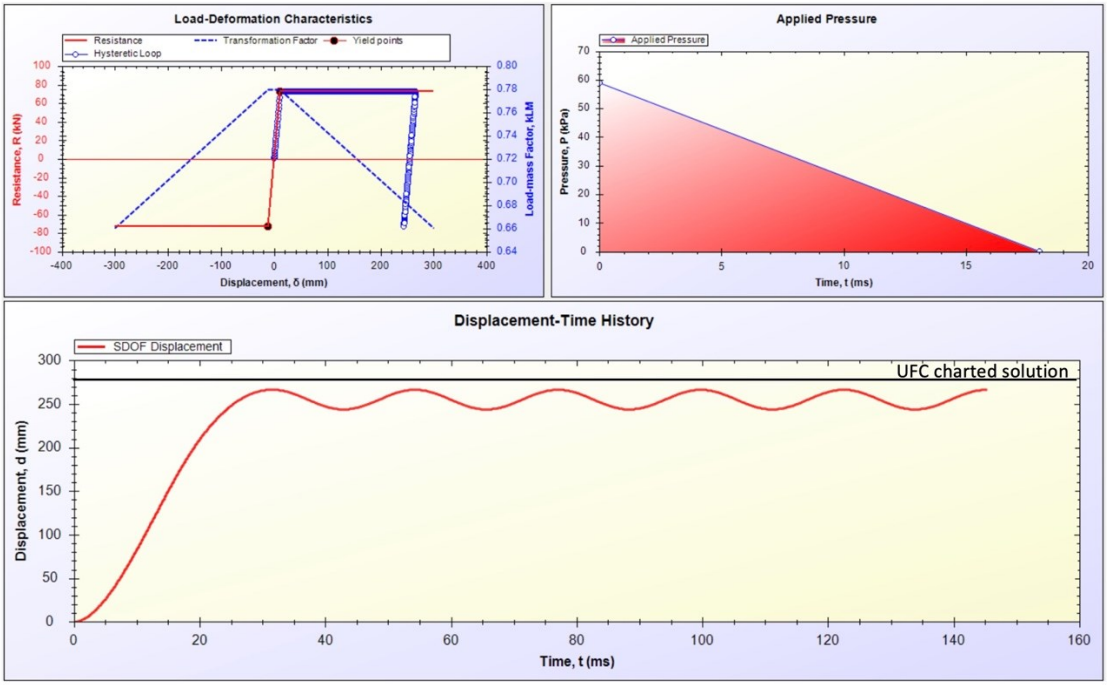

Figure 4 - 26 : Validation of UFC charted solution and RC-Blast software – Mullion 1H – simple supports

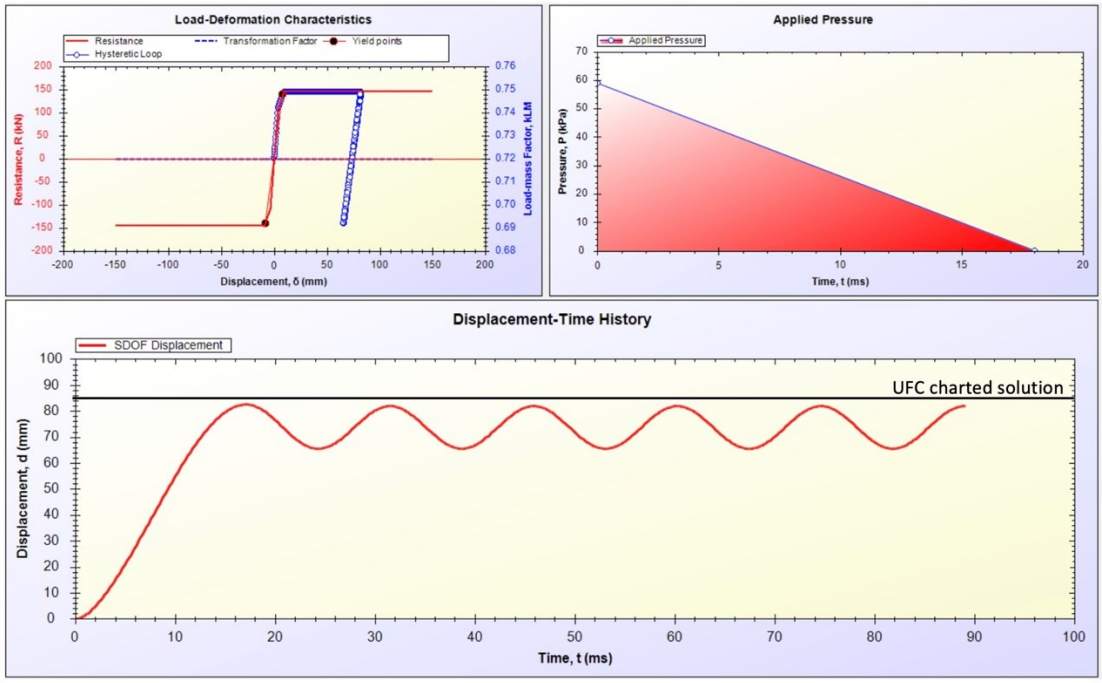

Figure 4 - 27 : Validation of UFC charted solution and RC-Blast software – Mullion 1H – fixed supports

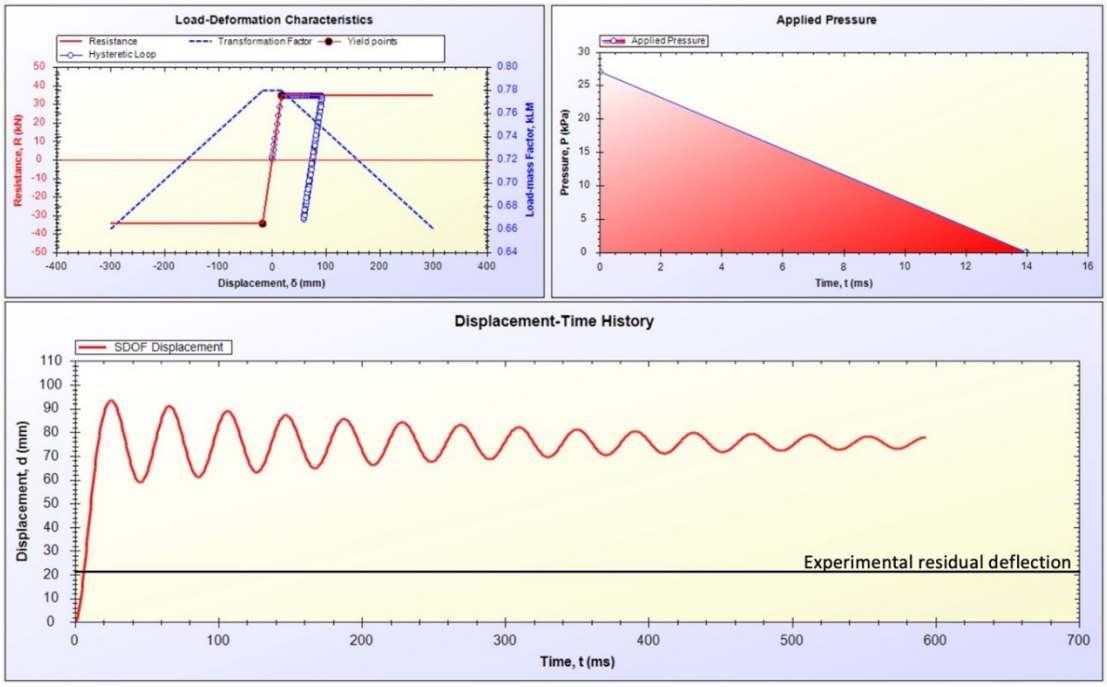

Figure 4 - 28 : Validation of RC-Blast analysis and experimental results – Mullion 1 – simple supports

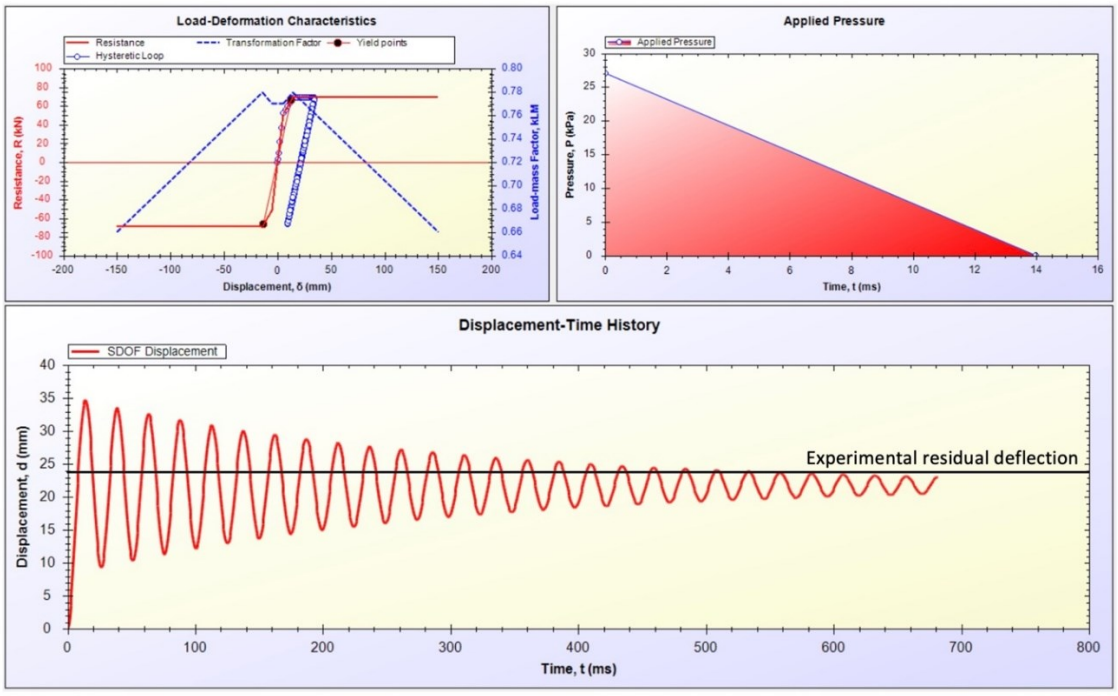

Figure 4 - 29 : Validation of RC-Blast analysis and experimental results – Mullion 1 – fixed supports

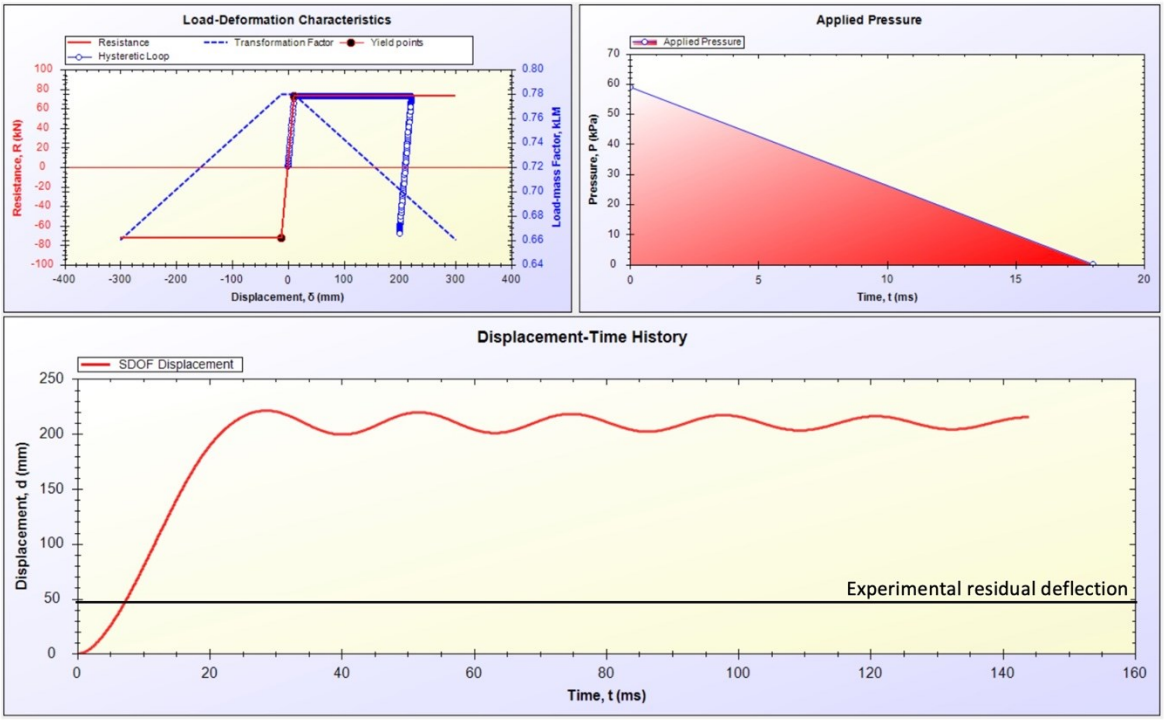

Figure 4 - 30 : Validation of RC-Blast analysis and experimental results – Mullion 1H – simple supports

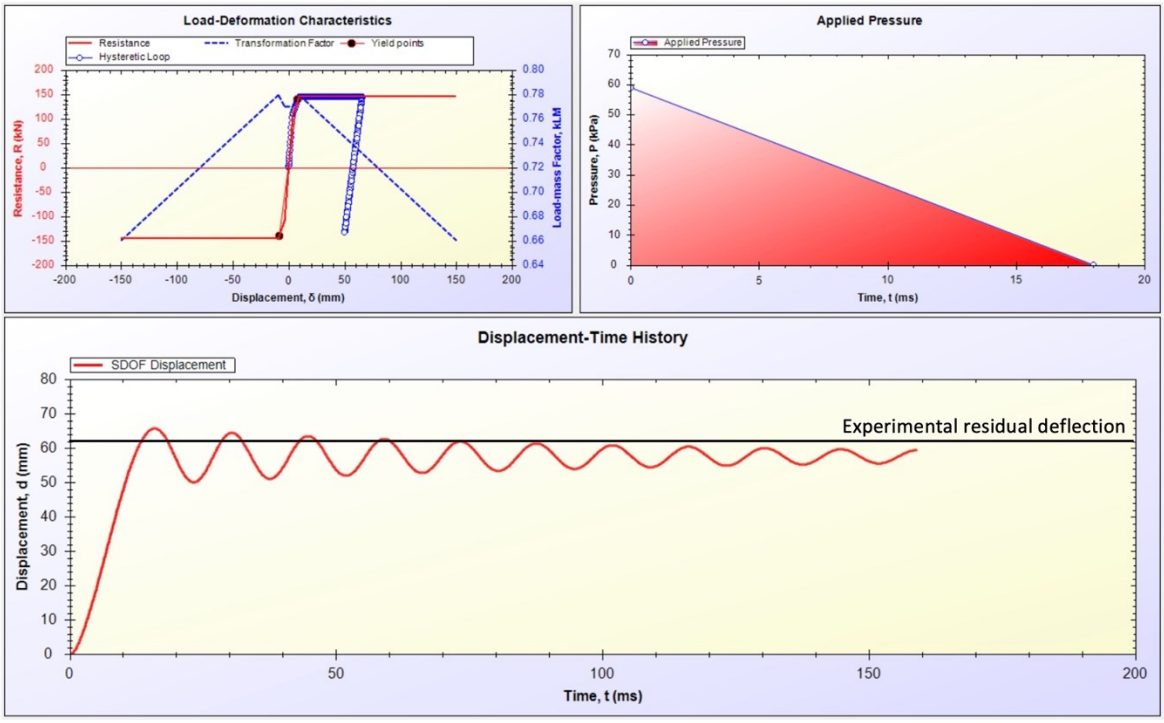

Figure 4 - 31 : Validation of RC-Blast analysis and experimental results – Mullion 1H – fixed supports

4.4.3 Validation procedures summary and discussion

The outcome of the validation procedures and the observations made are as follows.

- The UFC charted solution and the RC-Blast software results showed excellent agreement. Minor differences between the two analytical tools were observed. These differences were attributed to the differences in resistance functions for mullions with fixed end conditions, resulting in tri-linear resistance functions used in SDOF analysis and the UFC charted solution which is based on bilinear relationships.
- Figure 4-32 shows maximum mid-span displacements obtained from each analysis on the basis of the two analytical tools employed, indication very good agreement between the two, conforming the validity of the RC-Blast software and the analysis approach followed in establishing the resistance functions.

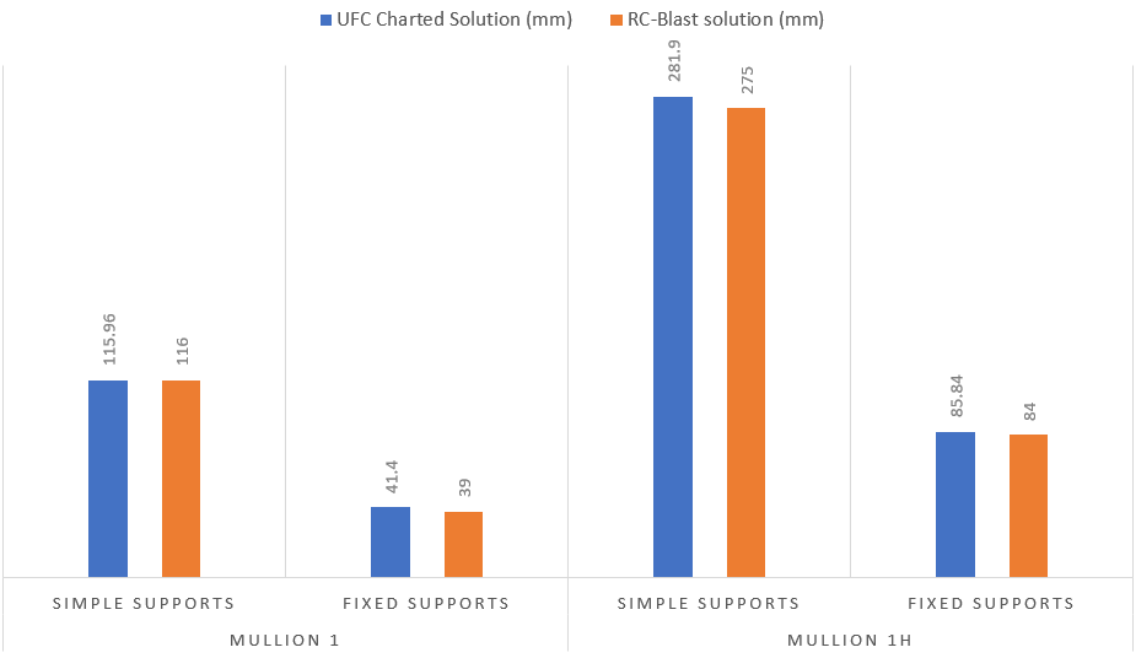

Figure 4 - 32 : Validation of UFC charted solution and RC-Blast software analysis

- The comparisons of the dynamic analysis results obtained from RC-Blast software and the test results indicate very good agreement, indicating the suitability of the analysis tool for further numerical work to generate P-I diagrams for the mullions considered, with and without the three types of hardening techniques considered.

- The comparisons of SDOF analysis results with experimental data was performed for both simply supported and fully fixed mullions. The actual support conditions created during the experimental program resulted in close-to full fixity support condition against rotations. Therefore, the test resulted agreed well with the analytical results when the supports were fully fixed.
- Any minor discrepancy observed in the results between the analytical and experimental displacements are attributed to the differences between the assumed full fixity condition in the analysis and the actual support conditions for the test specimens. Also, the assumed fully composite behavior in the analysis of hardened mullions may contribute to the minor discrepancies of results obtained. While the aluminum mullions and the steel plates performed in a composite manner, at high inelastic deformations this composite action may not have been maintained, as indicated by the bending of the plates between the self-tapping screws. The comparison of residual displacements is shown in Figure 4-33.

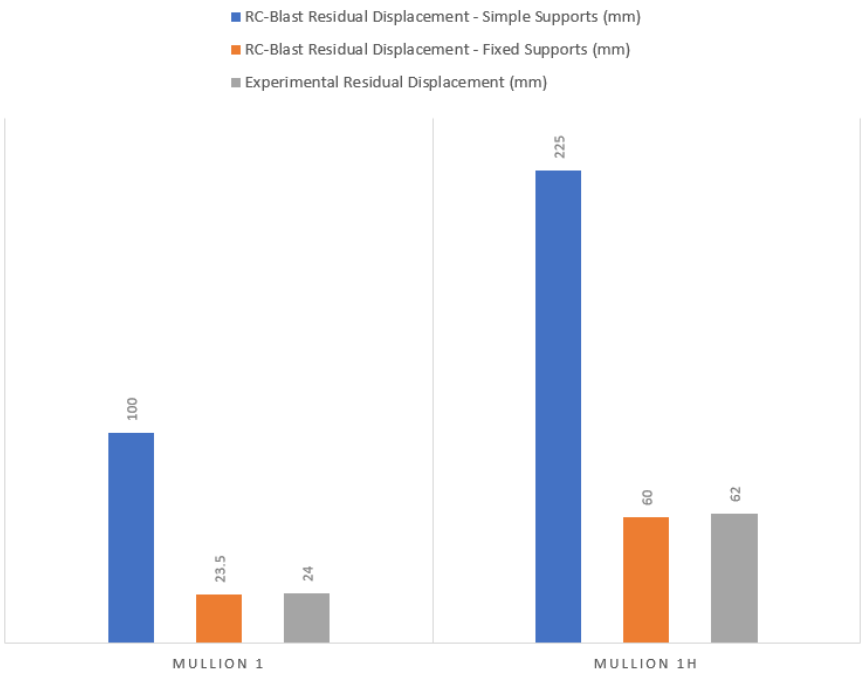

Figure 4 - 33 : Validation of RC-Blast software analysis and experimental results

4.5 PRESSURE-IMPULSE DIAGRAMS

Pressure impulse diagrams are commonly used design aids that show inelastic displacement capacity or damage level of a given element to different combinations of pressure and impulse. The vertical axis shows the applied pressure, and the horizontal axis shows applied impulse. Figure 4-34 illustrates different regions of P-I diagrams. In the impulsive region the damage increases with impulse under constant pressure. In this range of response, the damage is not sensitive to the level of pressure applied so long as the impulse remains constant. In the quasi-static region, the damage increases with pressure. In this range of response, for a given impulse the damage increases with pressure. In the dynamic region the damage varies both with pressure and impulse.

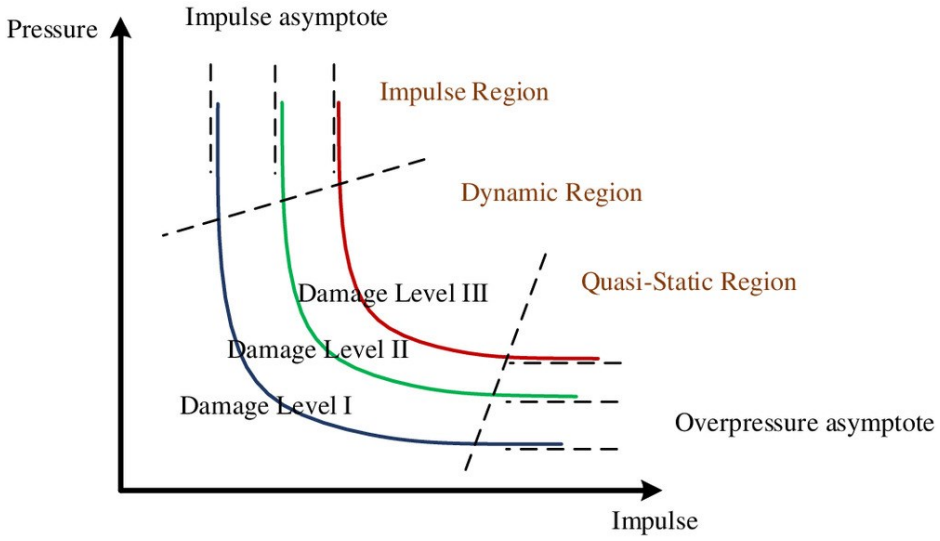

Figure 4 - 34 : Pressure-Impulse (P-I) diagrams (Parisi et al. 2016)

The RC-Blast software is equipped with a capability of plotting P-I diagrams. The user specifies the level of maximum displacement for which the combination of pressure and impulse is computed for the resistance function specified. The software follows an iterative approach and plots pressure and impulse that lead to the same maximum deflection. The P-I diagrams were generated for a range of displacements for the six mullions considered in the current research project for both simple and fixed support conditions, involving unhardened and hardened mullions with three different configurations of hardening steel plates. The P-I diagrams are plotted in Figures 4-35 through 4-46. They indicate the pressure-impulse combinations applied

during the experimental phase. They illustrate the range of blast threat that each mullion can resist, or the damage level sustained by different blast threats, recalling that pressure and impulse combinations correspond to different combinations of charge weight and standoff distance.

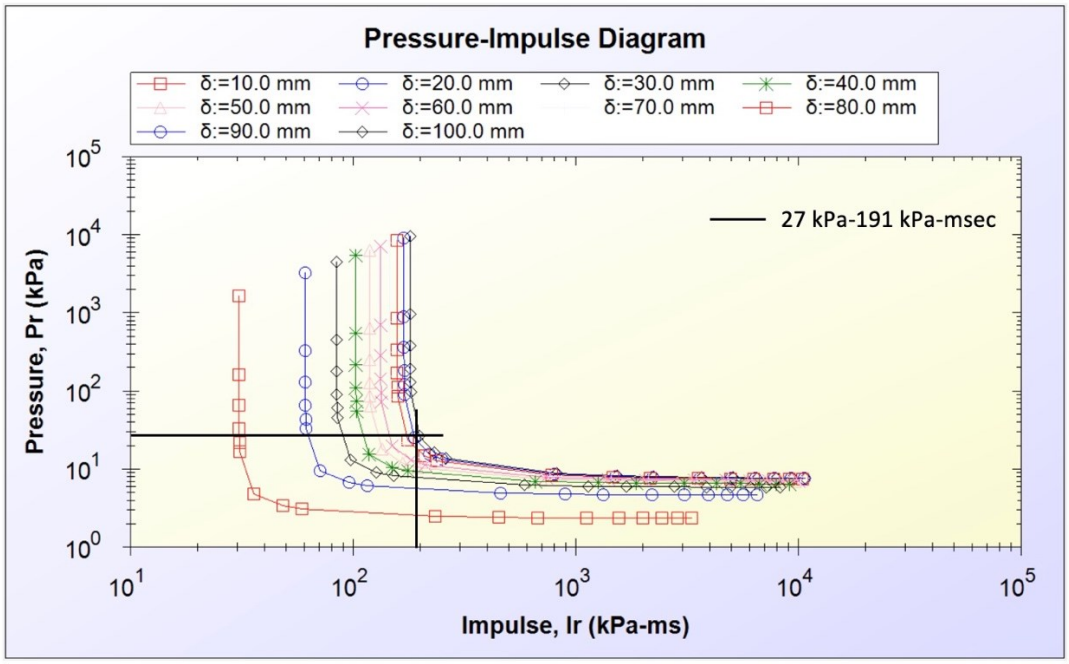

Figure 4 - 35 : P-I diagram for Mullion 1 – simple supports

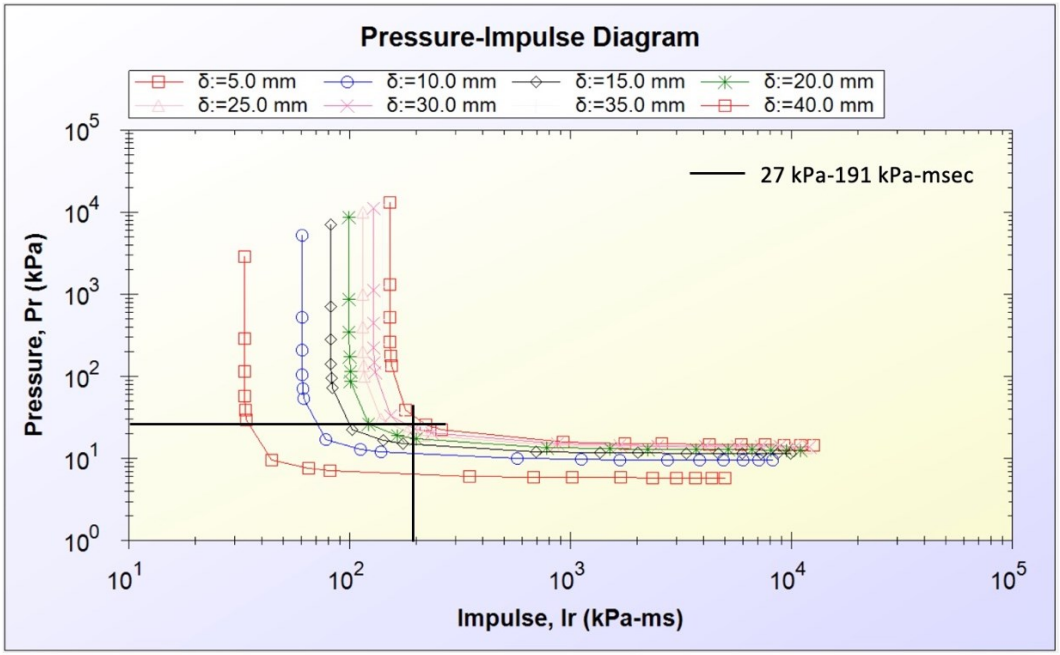

Figure 4 - 36 : P-I diagram for Mullion 1 – fixed supports

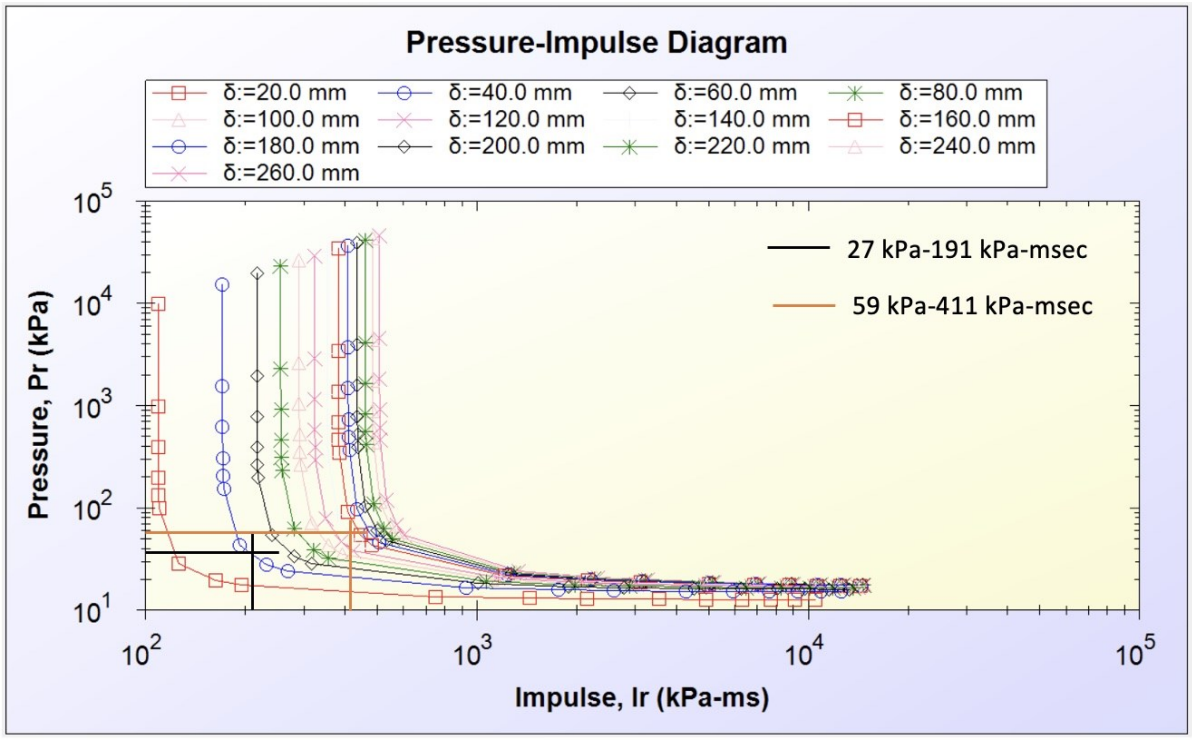

Figure 4 - 37 : P-I diagram for Mullion 1H – simple supports

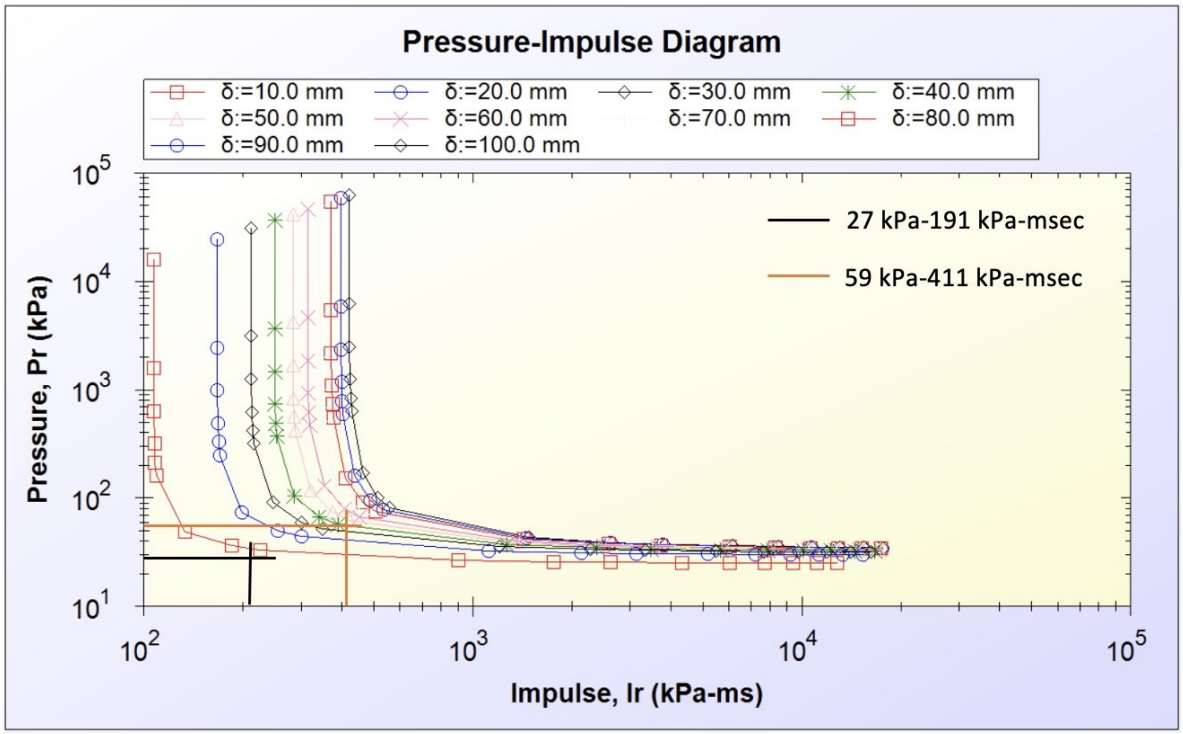

Figure 4 - 38 : P-I diagram for Mullion 1H – fixed supports

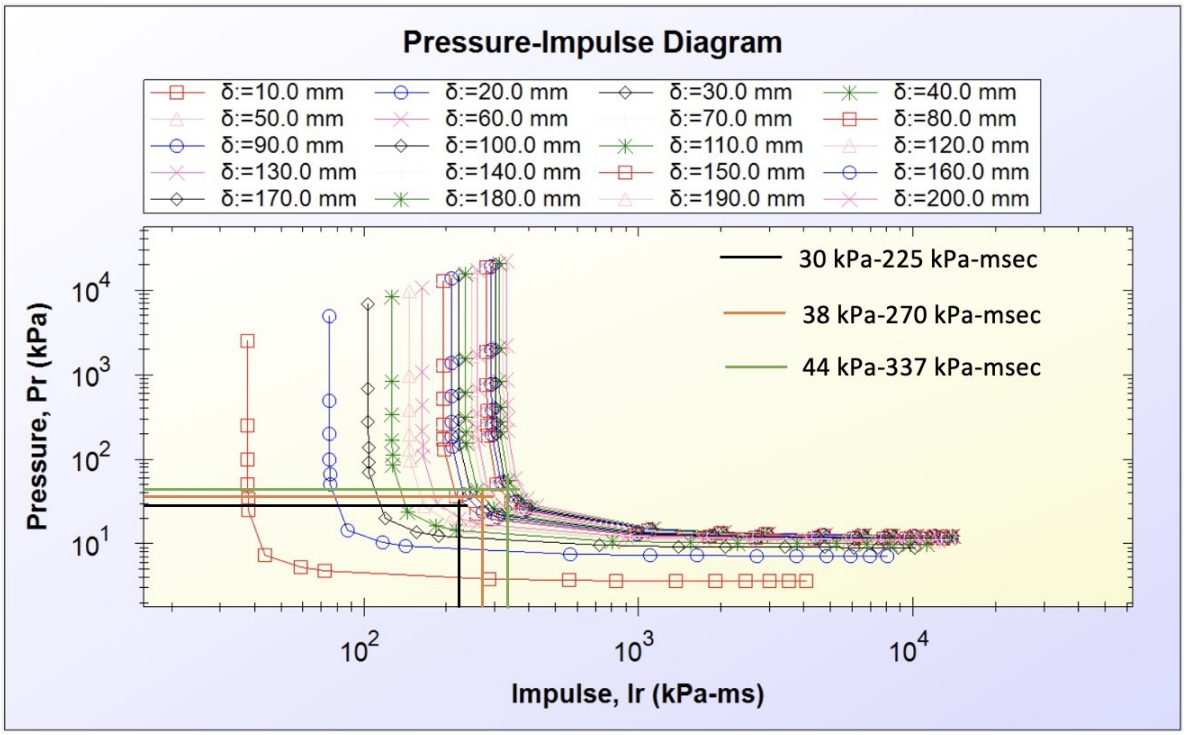

Figure 4 - 39 : P-I diagram for Mullion 2 – simple supports

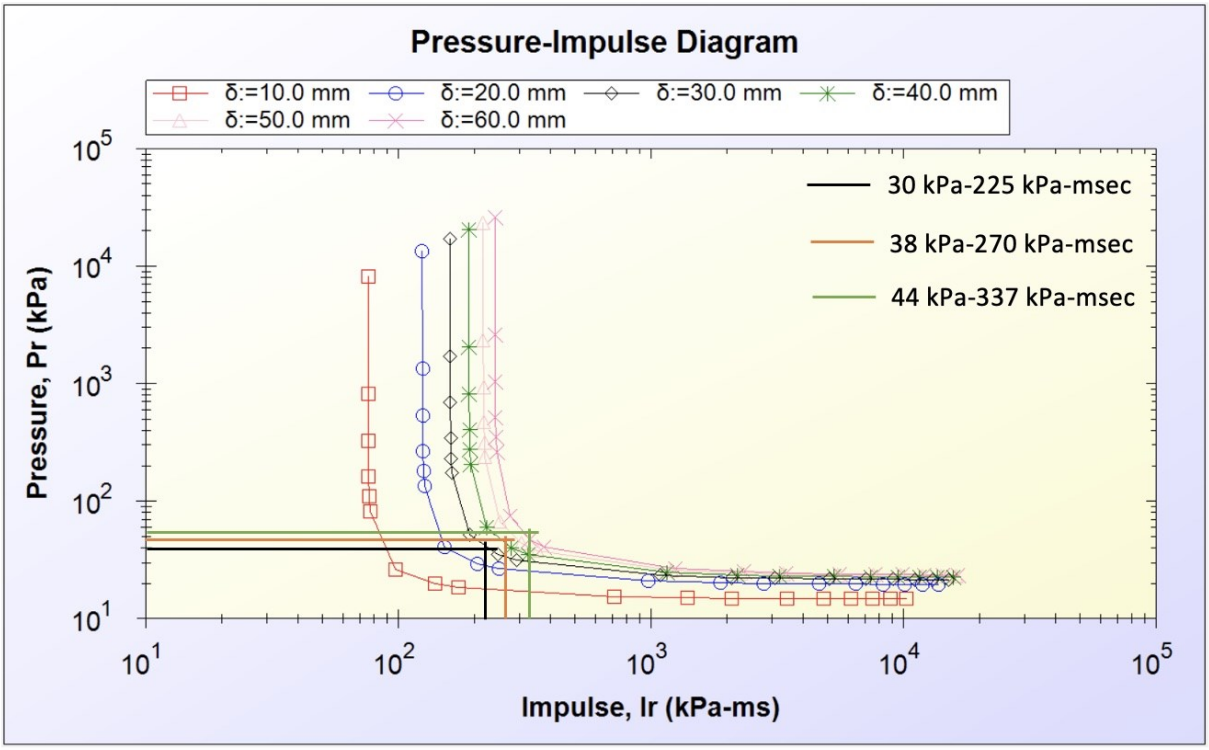

Figure 4 - 40 : P-I diagram for Mullion 2 – fixed supports

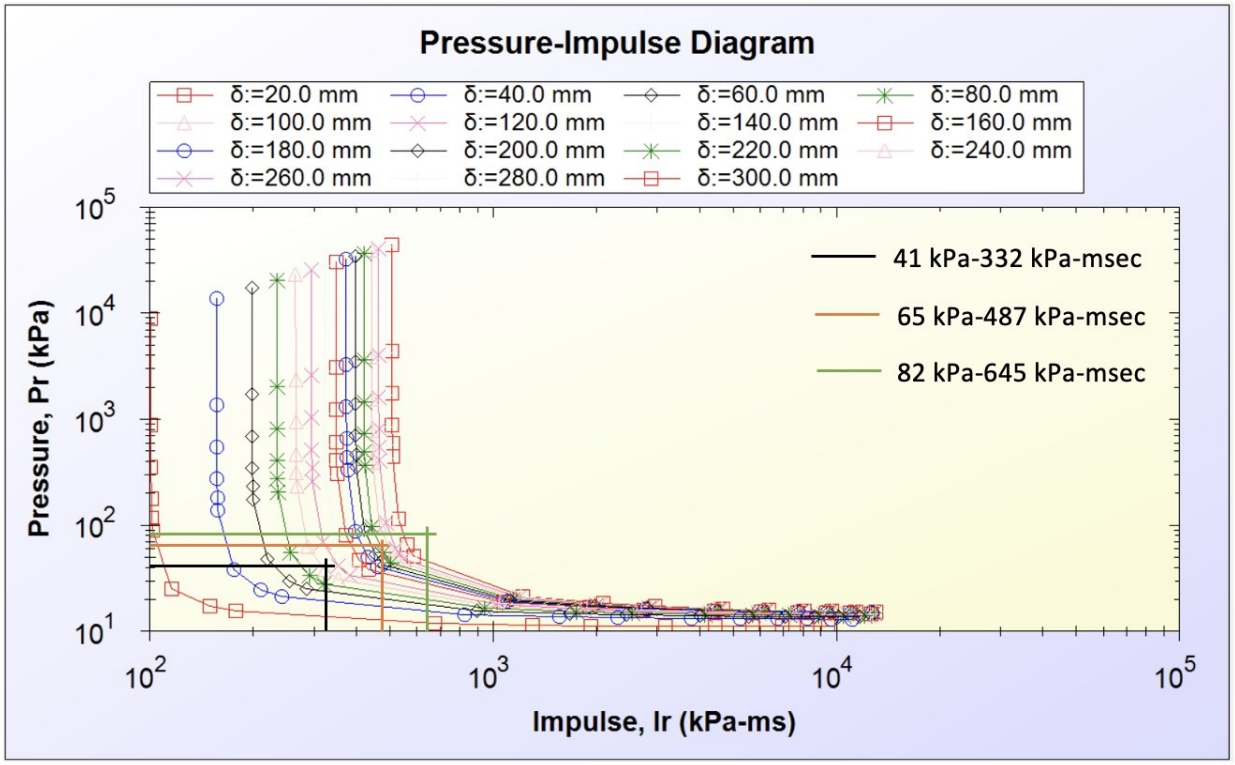

Figure 4 - 41 : P-I diagram for Mullion 2H – simple supports

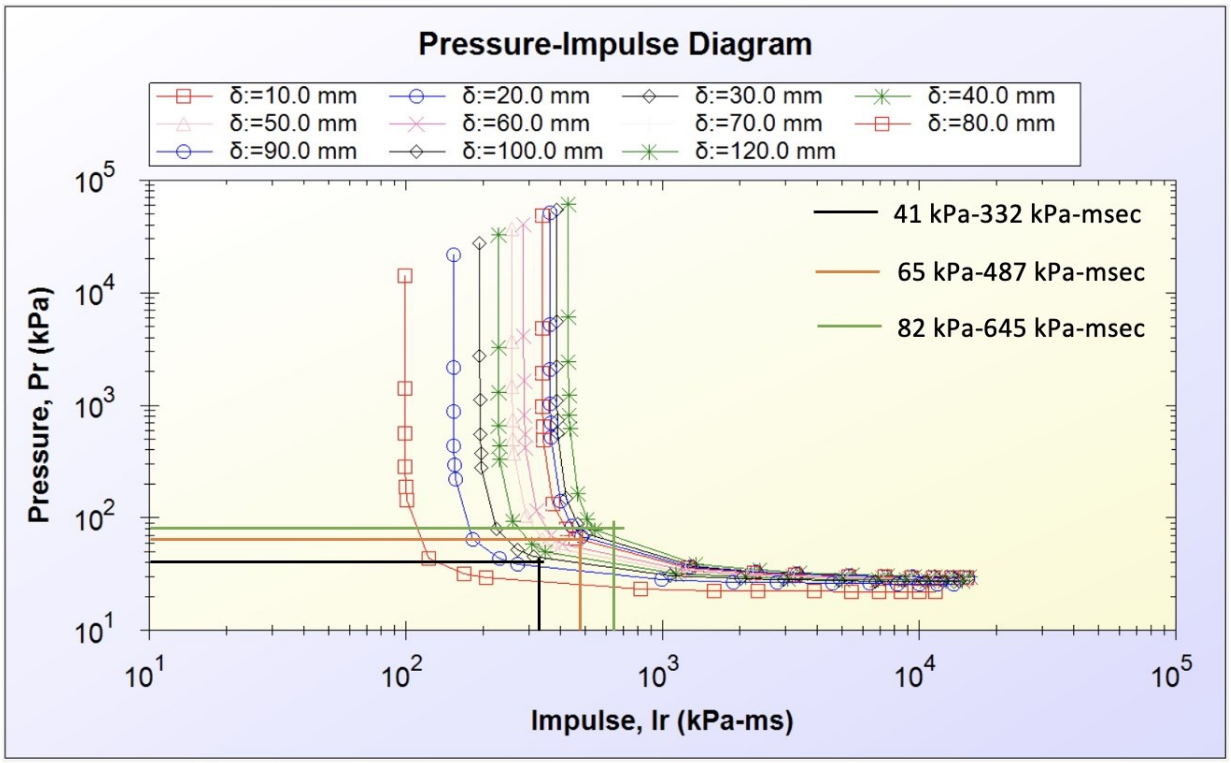

Figure 4 - 42 : P-I diagram for Mullion 2H – fixed supports

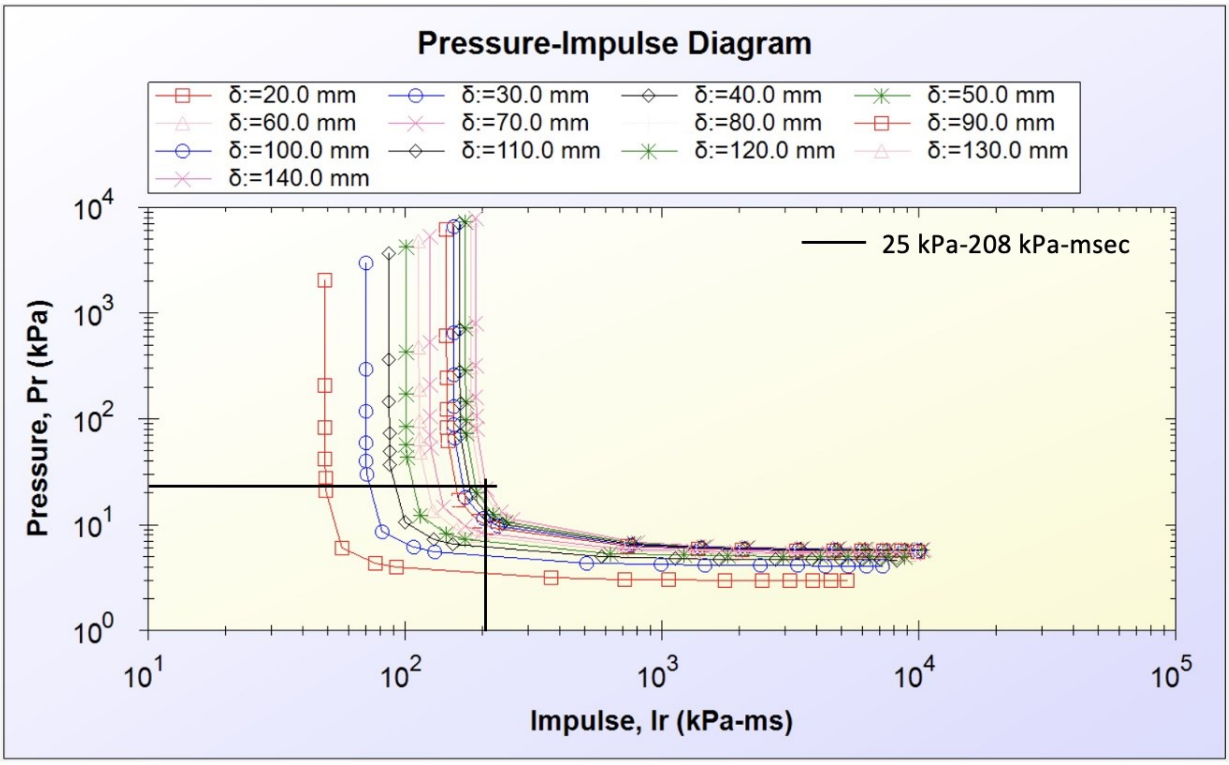

Figure 4 - 43 : P-I diagram for Mullion 3 – simple supports

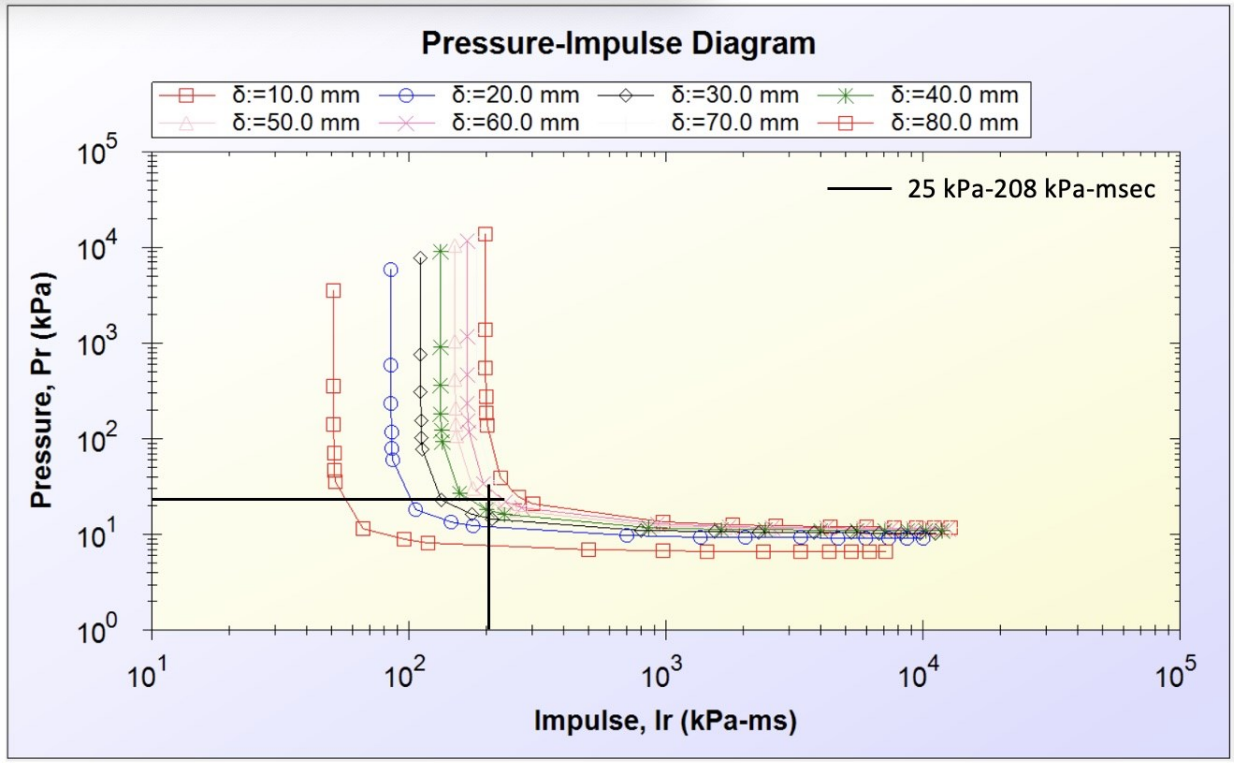

Figure 4 - 44 : P-I diagram for Mullion 3 – fixed supports

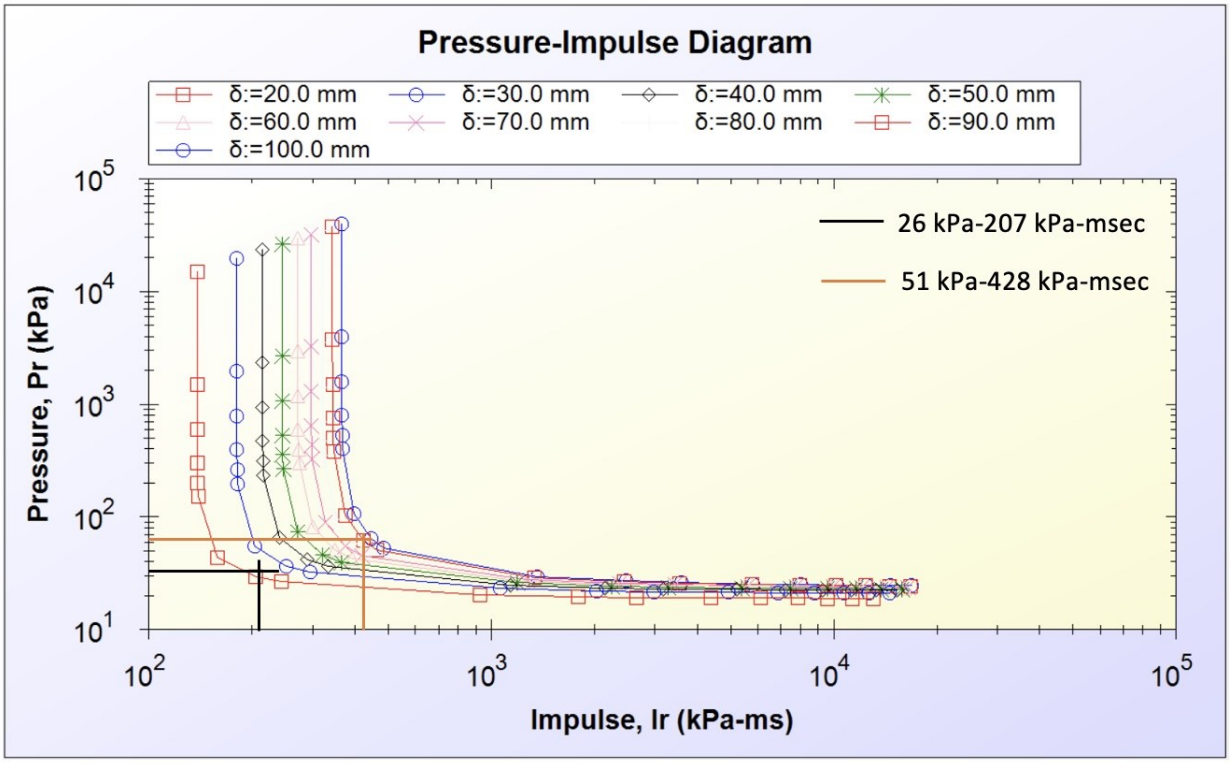

Figure 4 - 45 : P-I diagram for Mullion 3H – simple supports

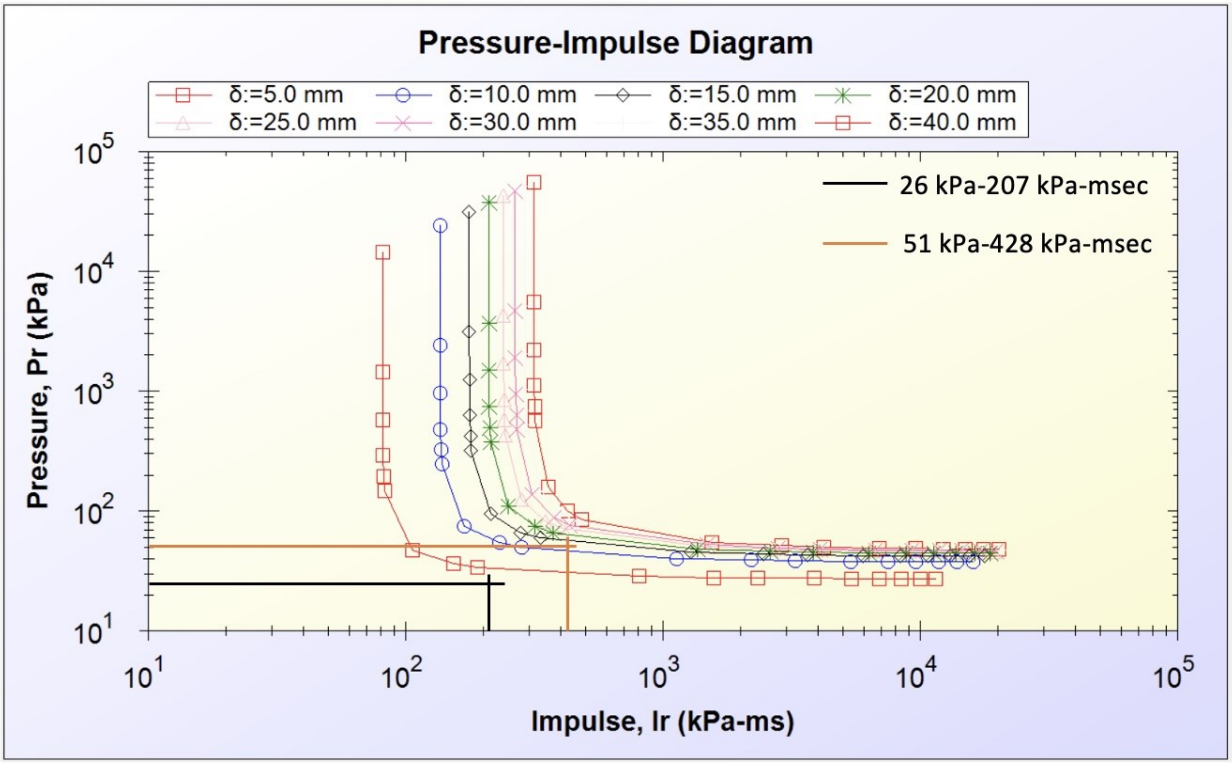

Figure 4 - 46 : P-I diagram for Mullion 3H – fixed supports

CHAPTER 5. BLAST HARDENING OF A PROTOTYPE BUILDING

5.1 INTRODUCTION

The mullion hardening techniques developed as part of the current research project is applied to a prototype building to assess the feasibility of using them for curtain wall retrofits in practice. The building is an imaginary reinforced concrete frame building covered with glass curtain walls. Curtain walls consist of double pane insulated glass units (IGU), glazed with protective film, mechanically connected to the vertical aluminum mullions. The geometry of the curtain wall is such that the blast loads are transmitted from the glazed glass panes to the vertical mullions that span between reinforced concrete slabs. The mullions are attached to the slabs with simple supports, without the end restraints against rotation. The curtain wall at the first-story level of the front elevation was judged to be the most critical. Figure 5-1 illustrates the tributary area of one of the critical vertical mullions and the geometric details of the curtain wall used in the building.

Blast risk assessment was conducted for the building. It was indicated that two blast scenarios had to be considered: i) 50 kg TNT at 20 m standoff distance and ii) 100 kg TNT at 20 m standoff distance. The first task was to assess the capacity of the existing critical mullion to establish mullion hardening requirements, if any. The second task was to consider the type of hardening required for the threat level given. These two tasks were fulfilled by conducting SDOF inelastic dynamic analysis using the RC-Blast software. The third task was to develop P-I diagrams for the mullions considered, in the event the blast risk for the building were to change in the future and the capacity of the mullions would be needed under different pressure-impulse scenarios.

5.2 ASSESSMENT OF THE EXISTING MULLION

Dynamic analysis of the critical first-story mullion was conducted using the RC-Blast software. The resistance function was established first as described in Appendix C with a yield displacement of 45 mm. The mullion was subjected to reflected pressure-impulse combination associated with the lower threat level (50 kg TNT at 20 m). The entire time history of the pressure variation was considered, including the negative phase. Figure 5-2 illustrates the displacement response time history, indicating significant yielding in the positive direction, reaching 260 mm (5.8 times the

yield deflection) and developing -180 mm permanent displacement. This corresponds to 10 degrees of support rotation, which was judged to be excessive. Therefore, the mullion was decided to be hardened by steel plates. P-I diagrams were also developed for the existing mullion, as depicted in Figure 5-3.

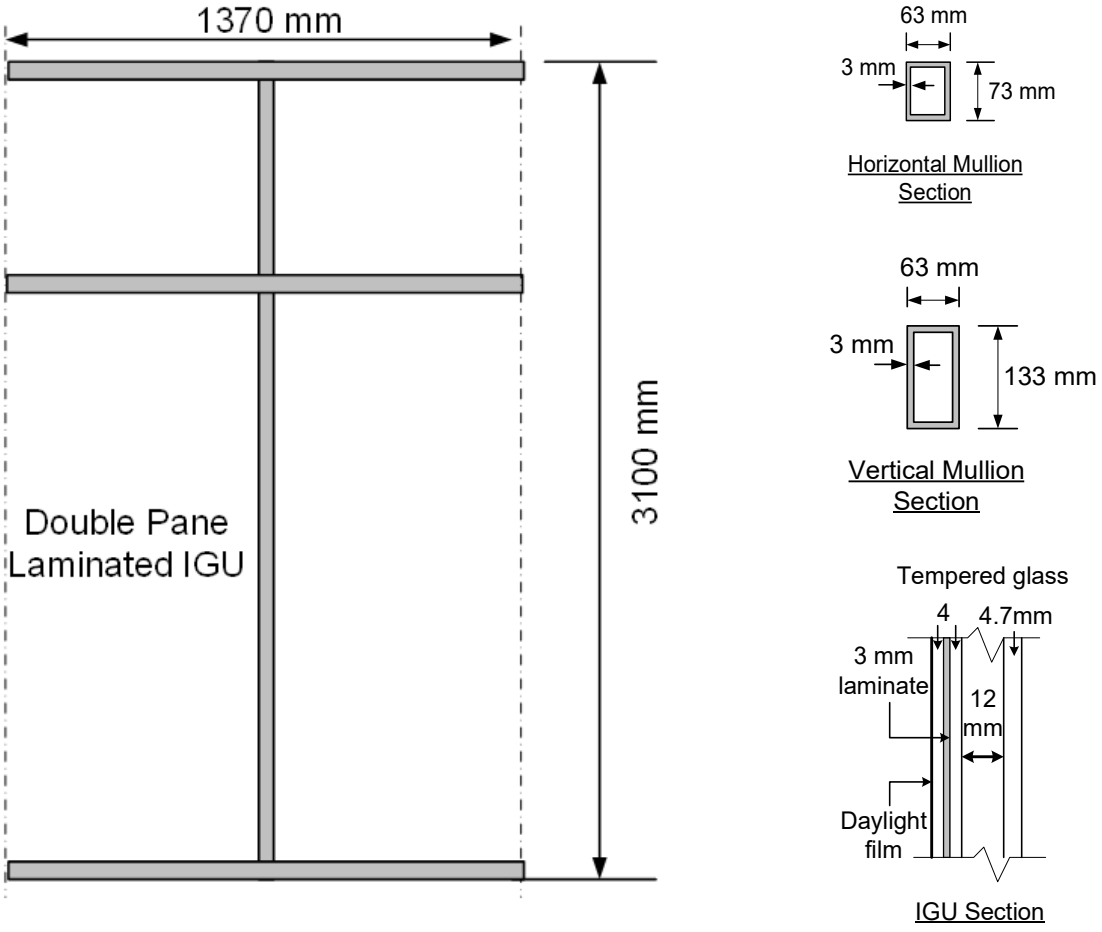

Figure 5 - 1 : Critical first-story curtain wall mullion details

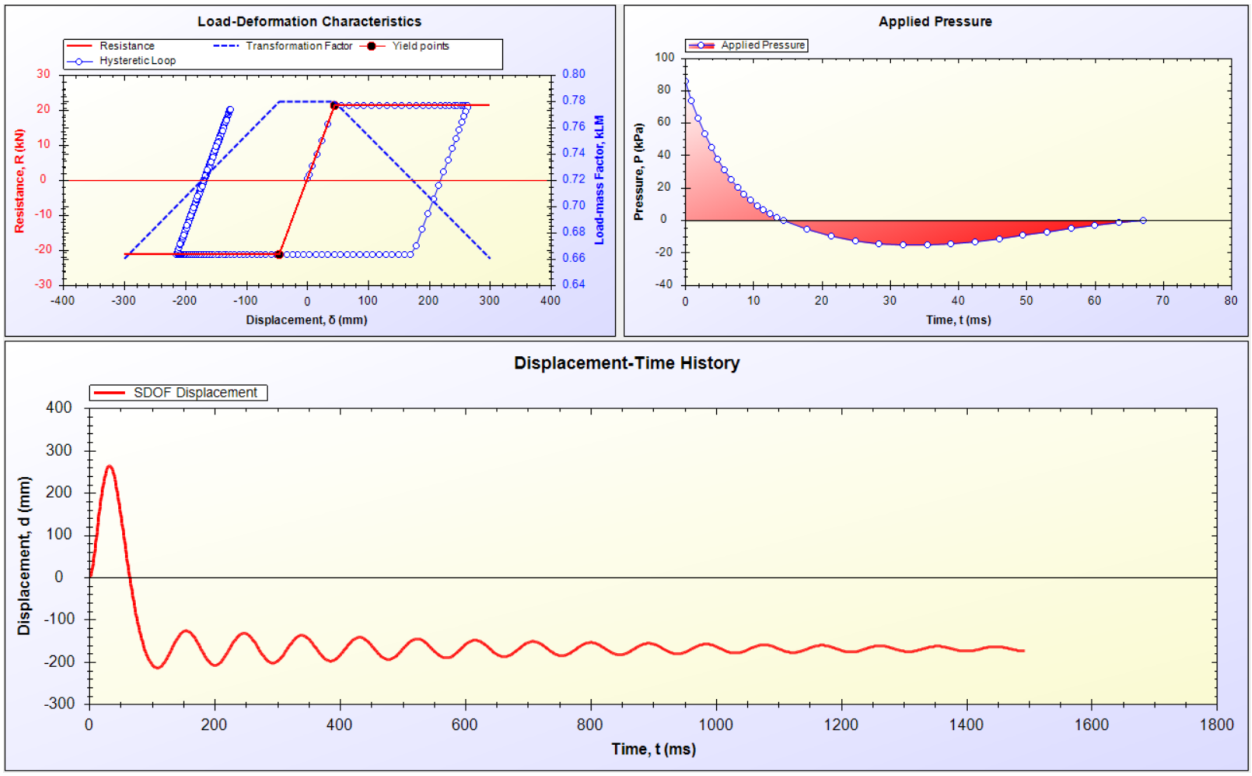

Figure 5 - 2 : Displacement time history for non-retrofitted first-story mullion

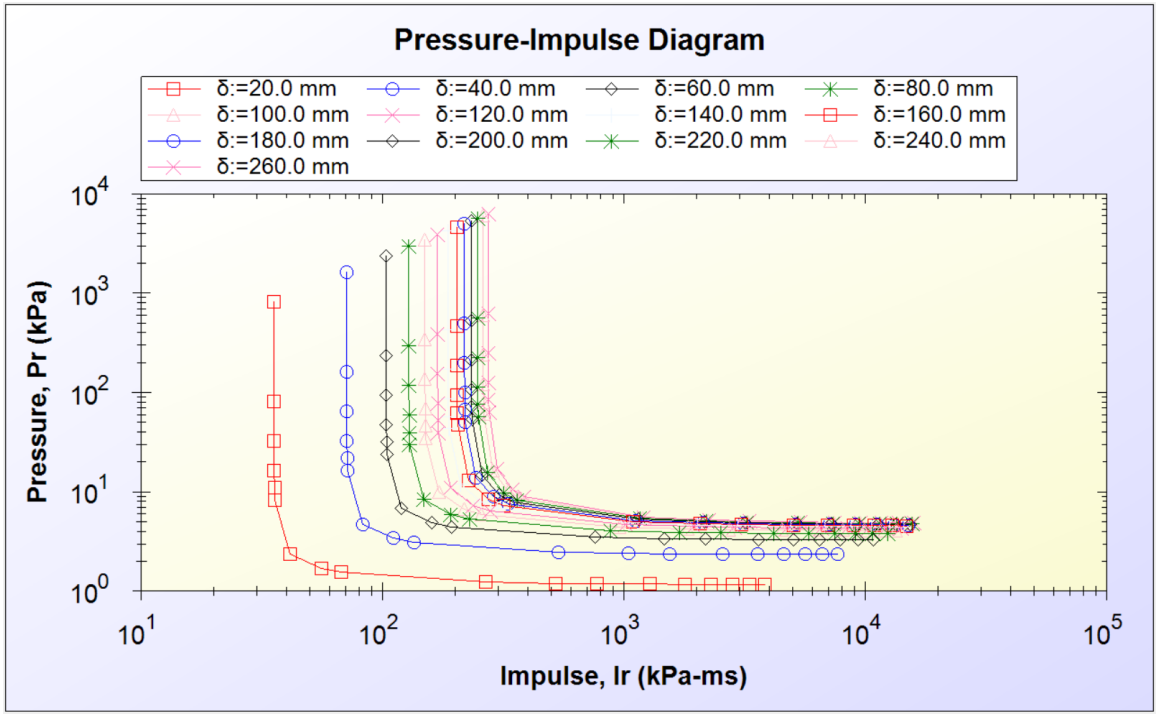

Figure 5 - 3 : P-I diagrams for the existing un-retrofitted mullion

5.3 RETROFITTING METHODOLOGIES AND RESULTS OF DYNAMIC ANALLYSIS

The first retrofit technique considered was to strengthen the mullion by attaching 3.0 mm thick L-shaped steel plates, covering the web, as well as the tension flange. This is illustrated in Figure 5-4. Nonlinear SDOF dynamic analysis was conducted to assess the resulting improvements resulting from the addition of the steel plates. The displacement time history under the same blast threat as the previous un-retrofitted mullion is shown in Figure 5-5. The retrofitting technique resulted in reduced response, from 275 mm maximum displacement to 170 mm. The residual displacement was also reduced from – 180 mm to -70 mm. This indicates a reduction in maximum ductility ratio from 6.0 to 4.0. PI diagrams have also been developed for the use of L-shaped steel plates as a hardening technique. They are shown in Figure 5-6.

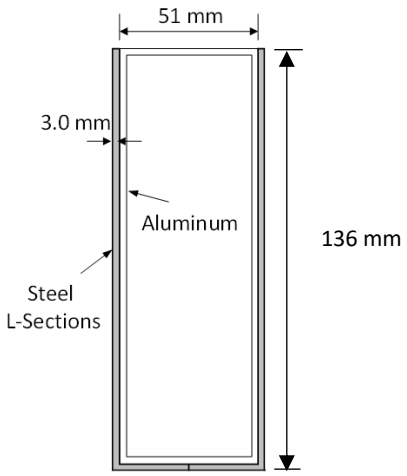

Figure 5 - 4 : L-shaped steel plates as hardening technique

Another hardening technique was tried for the existing mullion in an effort to increase the level of protection. The second type of retrofit consisted of a 3 mm thick steel HSS section placed on the tension flange, connected together by means of additional 3 mm steel plates attached by means of self-tapping screws. Figure 5-7 illustrates the cross-section of the hardened mullion. Dynamic analysis results are shown in Figure 5-8, showing significantly improved response with reduced inelastic displacements under the same blast threat. Because of the increased strength and stiffness of the use of combined HSS and side plates the maximum inelastic displacement was reduced to 85 mm with only -5 mm residual displacement. Figure 5-9 shows the P-I diagrams developed for this type of hardening technology.

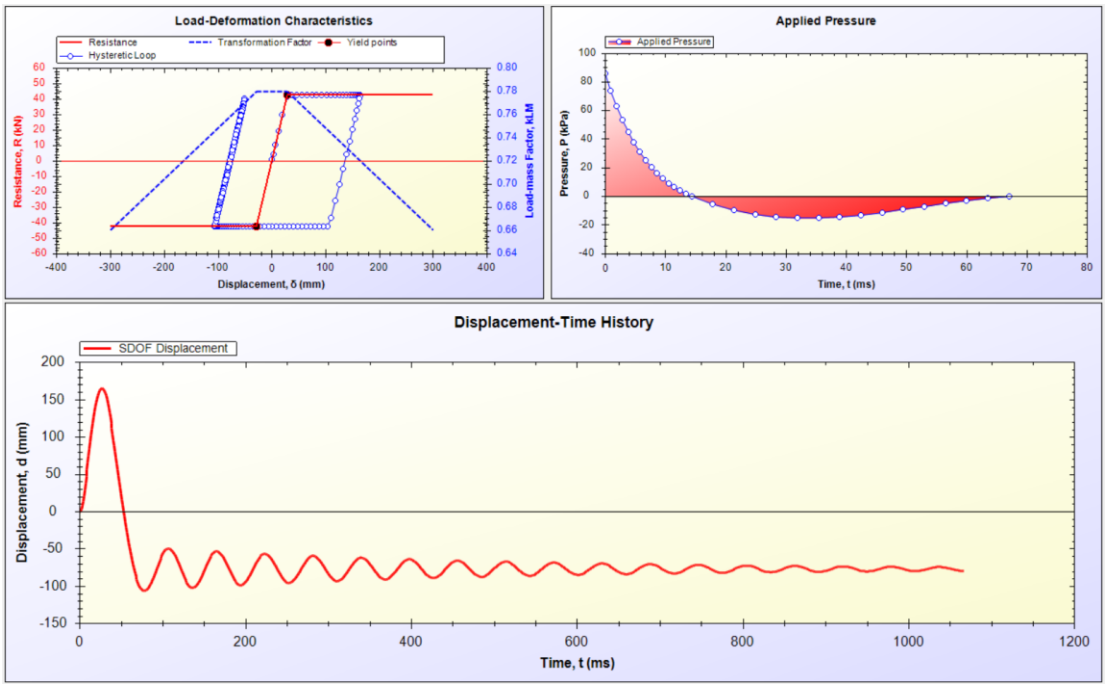

Figure 5 - 5 : Displacement time history for the mullion hardened with L-shaped steel plates

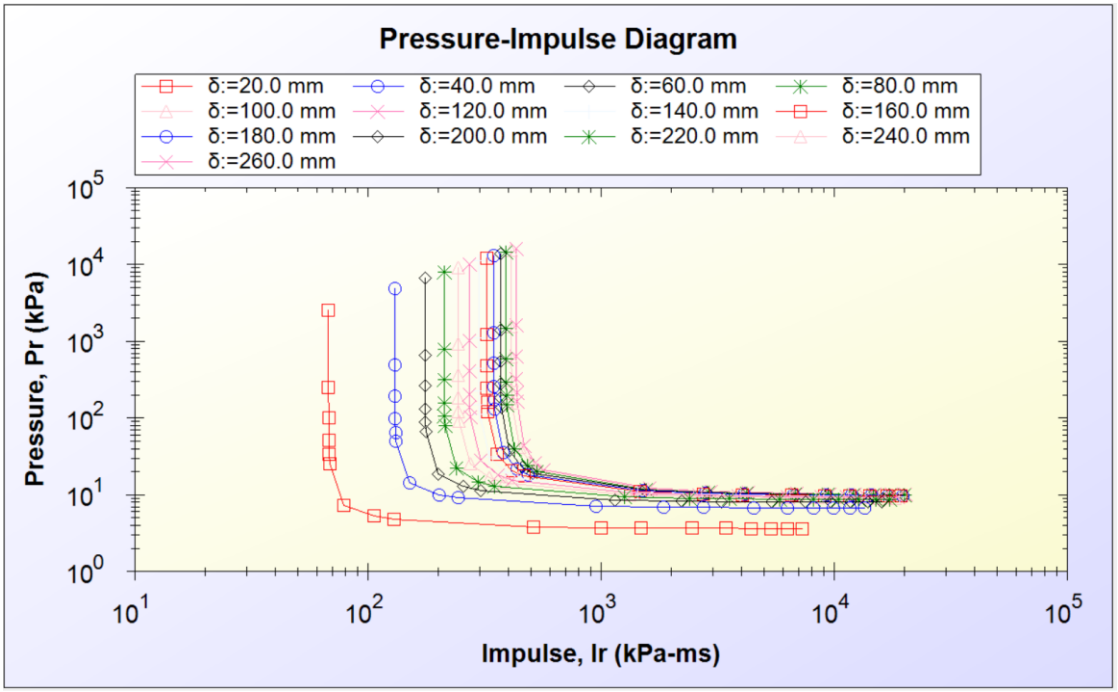

Figure 5 - 6 : P-I diagrams for hardened mullions with L-shaped steel plates

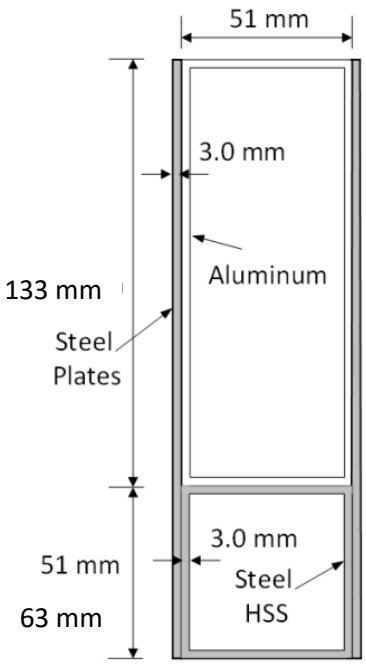

Figure 5 - 7 : Hardened mullion with 3.0 mm thick steel HSS and side plates

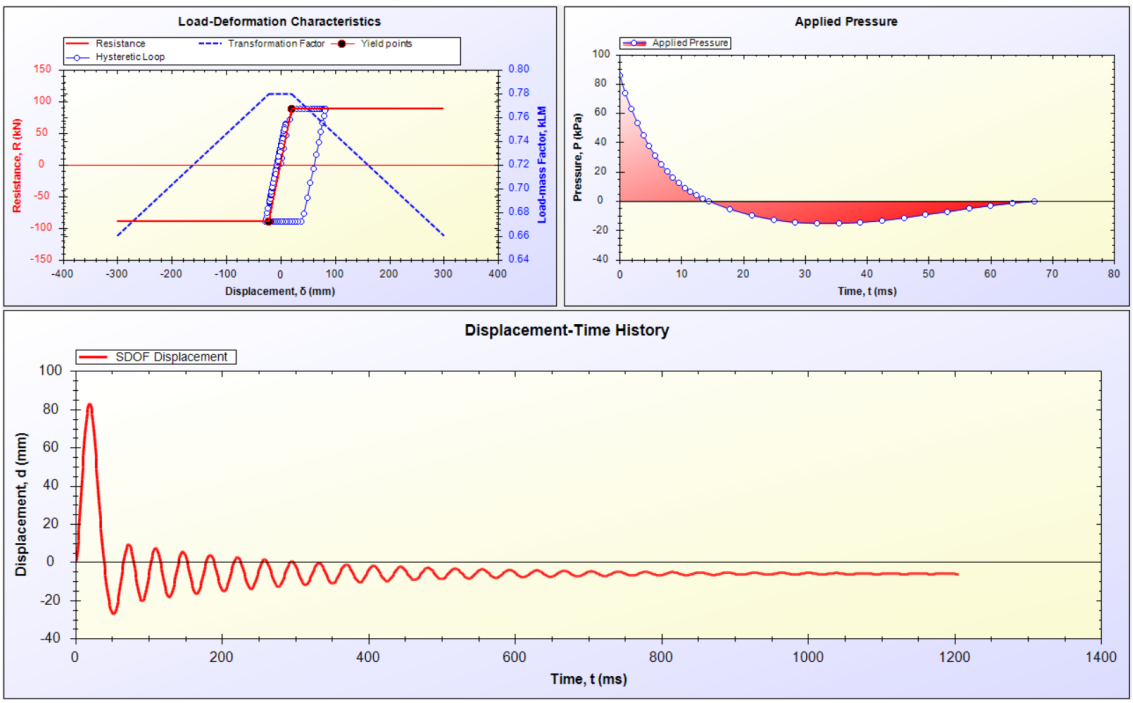

Figure 5 - 8 : Displacement time history for mullion hardened with 3.0 mm thick steel HSS and side plates

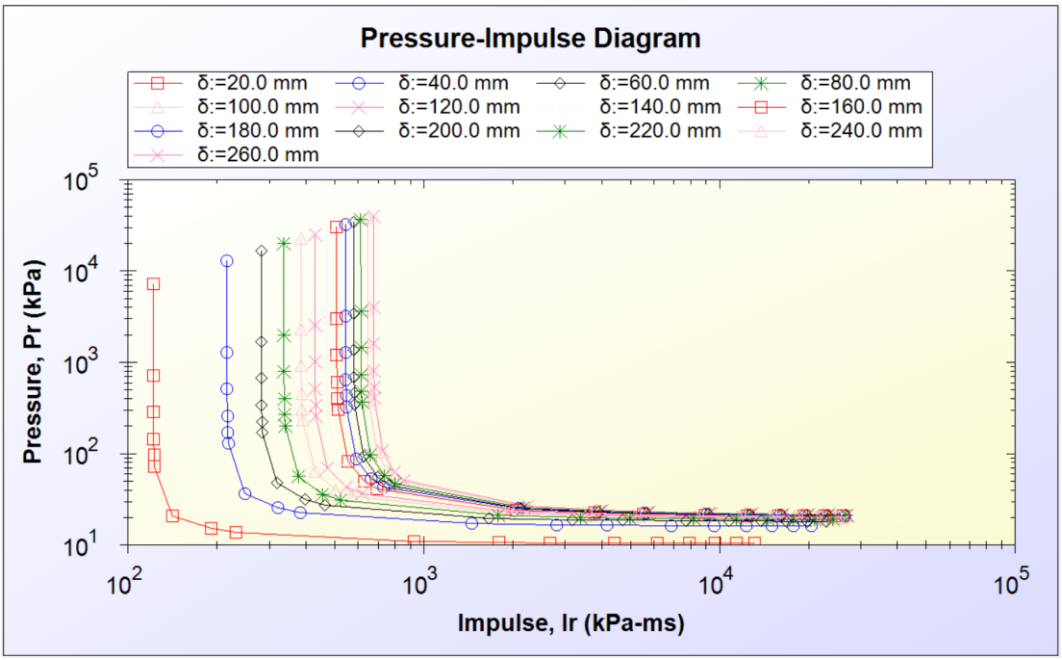

Figure 5 - 9 : P-I diagram for mullion hardened with 3.0 mm thick steel HSS and side plates

The same hardening technique was implemented to the aluminum mullion with increased steel thickness of 6.3 mm for both the HSS section and the plates as illustrated in Figure 5-10. Further increase in strength and stiffness resulted in a reduced maximum displacement of 40 mm and a permanent deflection of 4.0 mm. The results of dynamic analysis are shown in Figure 5-11 with the P-I diagram depicted in Figure 5-12.

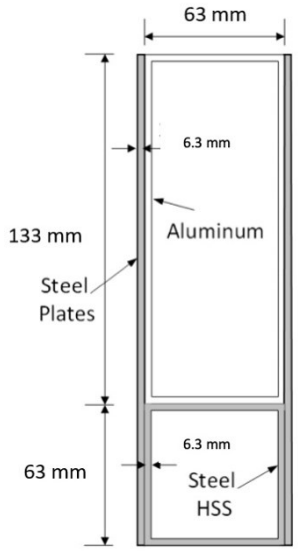

Figure 5 - 10 : Mullion hardened with 6.3 mm thick steel HSS and side plates

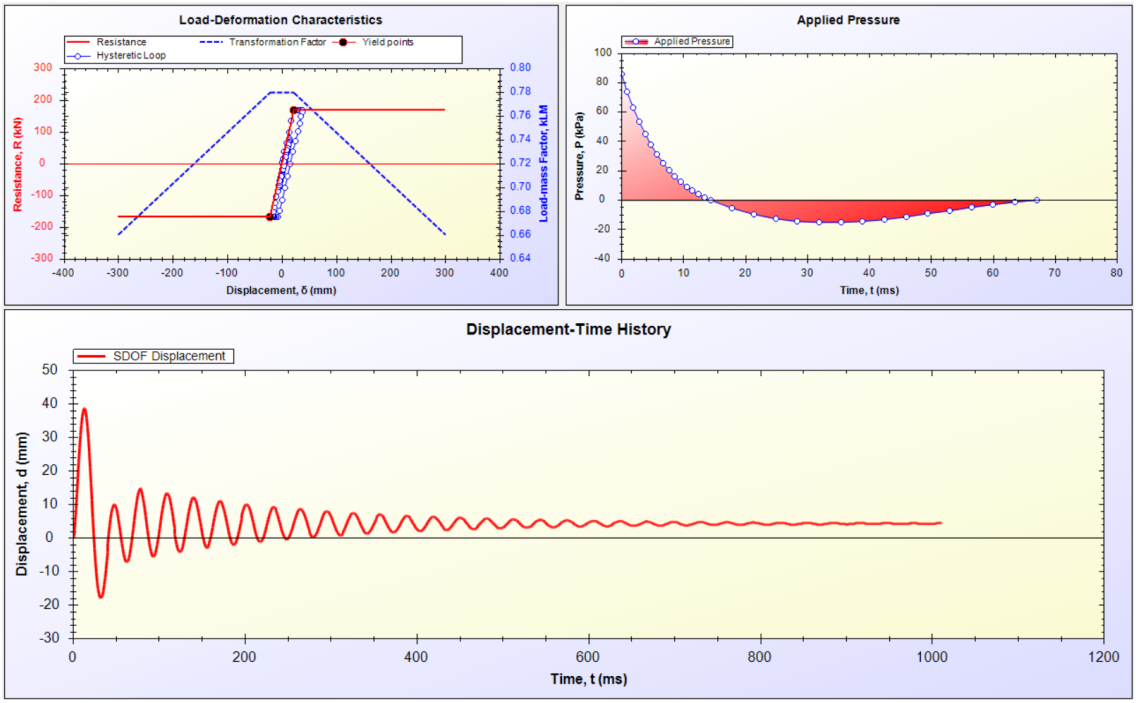

Figure 5 - 11 : Displacement time history for mullion hardened with 6.3 mm thick steel HSS and side plates

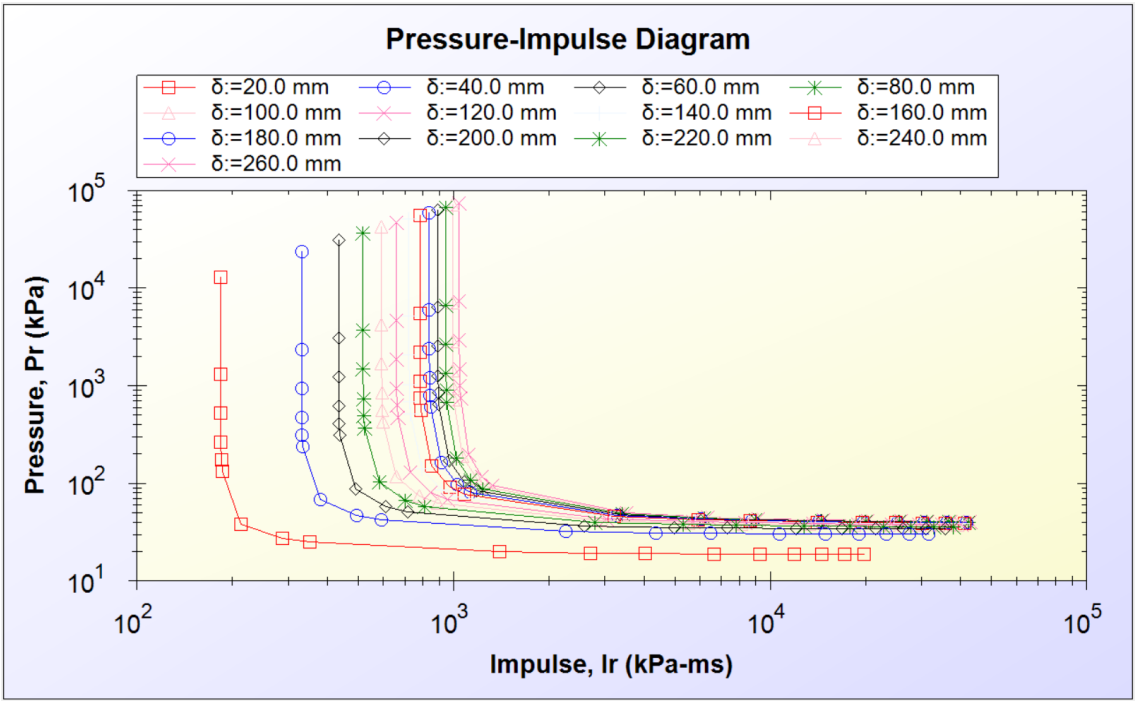

Figure 5 - 12 : P-I diagram for mullion hardened with 6.3 mm thick steel HSS and side plates

Because of the superior performance of the mullion hardened with 6.3 mm thick steel HSS and side plate assembly, it was further investigated under an increased blast threat. This time reflected pressure associated with 100 kg TNT was placed at 20 m distance. The displacement time history is illustrated in Figure 5-13 indicating a maximum inelastic displacement of 87 mm and a residual plastic displacement of 50 mm. This performance is deemed to be acceptable, considering the increased blast load.

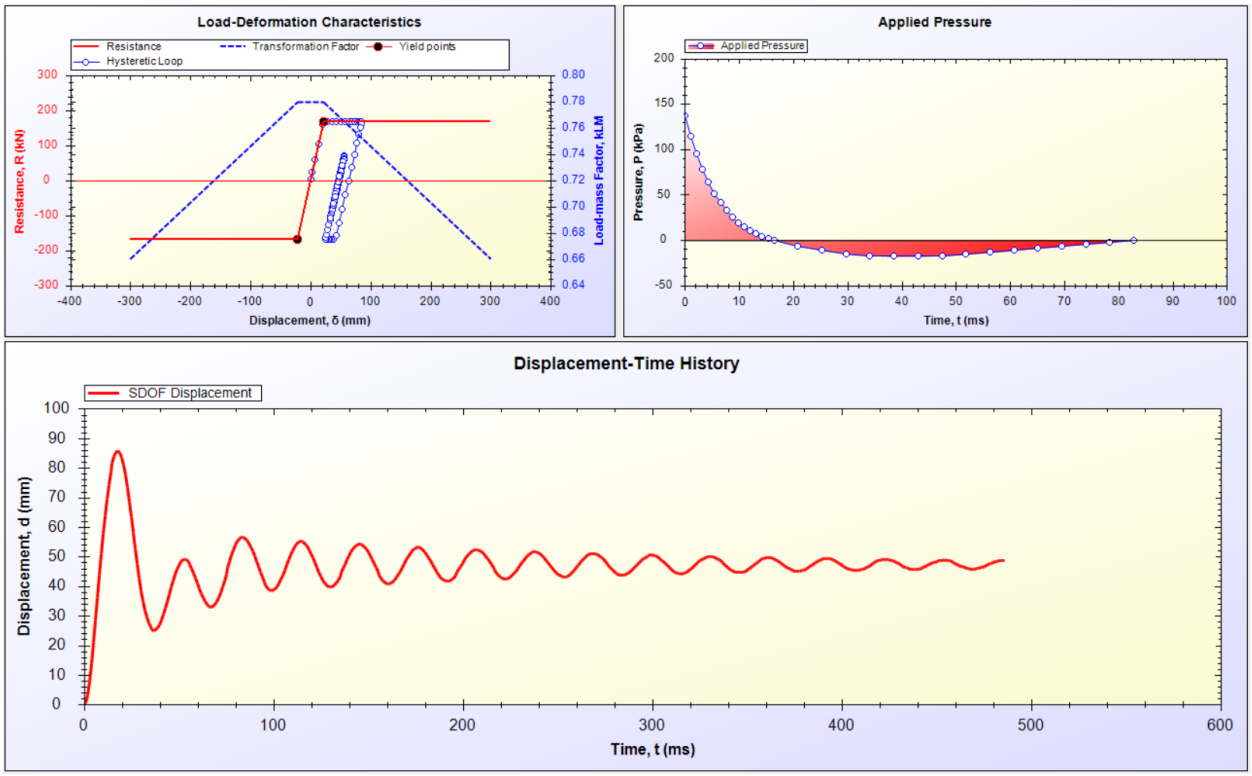

Figure 5 - 13 : Displacement time history for mullion hardened with 6.3 mm thick steel HSS and side plates under an increased blast threat of 100 kg TNT at 20 m standoff distance

5.4 DISCUSSION OF RESULTS

The critical vertical mullion component of a curtain wall in the prototype building was investigated for performance under two levels of blast threats: 50 kg TNT at 20 m and 100 kg TNT at 20 m. Under the lower threat level, the mullion experienced excessive inelastic deformation, potentially exceeding its deformation capacity. It was clear that he mullions needed hardening if it were to provide protection to the building. Two of the three hardening techniques developed in the experimental phase of research were considered. These include the two systems that had

steel components strengthening the tension flange as well as the web. All the hardening options implemented improved performance. Figure 5-14 provides a summary of computed maximum displacement for each case. The results indicate reductions in maximum displacements proportional to the increase in sectional rigidity. It appears that both the L-shaped steel plates and the HSS side plate assembly are suitable for retrofitting the curtain wall, so long as the required rigidity in the mullion section is provided for the thread level considered.

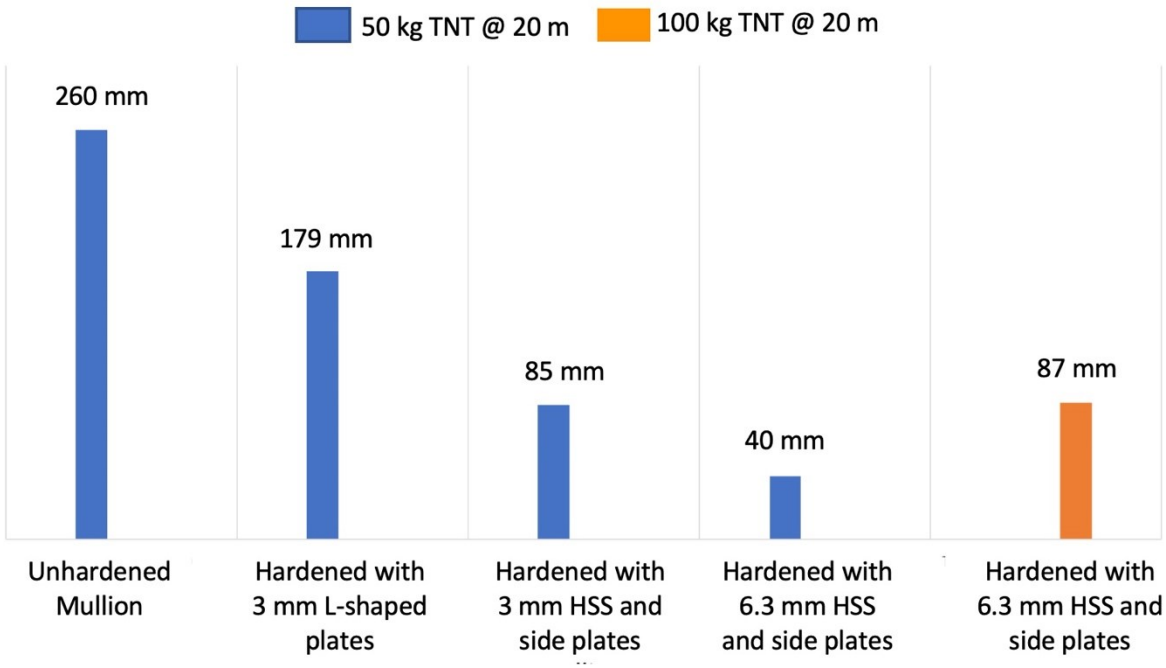

Figure 5 - 14 : Summary of computed maximum displacements for the prototype building mullions

CHAPTER 6. CONCLUSIONS

6.1 SUMMARY AND CONCLUSIONS

A combined experimental and analytical investigation was carried out to develop hardening techniques for curtain wall mullions subjected to blast loads. A total of six full size aluminum mullions with three different steel hardening techniques were tested using the University of Ottawa Shock Tube under progressively increasing intensity of blast loads. The hardening techniques consisted of the use of steel plates secured on the mullion web, with or without the bend extensions to cover the tension flange (forming L-shapes plates), as well as a combination of side plates and a HSS section on the tension flange. The results were compared with those obtained by the computer software RC-Blast, developed at the University of Ottawa, which is capable of conducting non-linear dynamic analysis of the mullions. The software was first validated against the analysis charts developed by the US Department of Defence (UFC 2008). A prototype building was selected to assess the feasibility of the curtain wall hardening techniques in practice. Two different threat levels were considered for the building and SDOF analyses were conducted to demonstrate the applicability of the retrofit systems.

The following conclusions can be drawn for the research project presented:

- The steel hardening techniques investigated for strengthening and stiffening existing aluminum curtain wall mullions provide significant improvements in blast response of otherwise deficient curtainwall mullions. Of the three types of hardening strategies considered, all three resulted in reduced deformations and increased strength.
- Steel plates secured on aluminum mullions are able to develop fully composite behavior until after significant inelastic deformations are developed, followed by the buckling of the plates between the self-tapping screws used for securing the plates. The initial experimental trial of using 200 mm screw spacing resulted in premature bending of the plates between the screws. Reducing the spacing to 100 mm consistently produced good results. This observation was validated by the analysis of retrofitted mullions as discussed below.
- The SDOF inelastic dynamic analysis of retrofitted mullions based on fully composite behavior resulted in good correlations with experimental data, confirming the

experimental observations relative to the full composite behavior with a screw spacing of 100 mm.

- The choice of a mullion hardening technique using steel plates depends on the required strength and stiffness as dictated by the threat level. It was observed through tests and dynamic analyses that the required enhancement in stiffness can be attained either with side plates only, in which case a thicker plate may have to be used, or with the use of L-shaped bent plates with higher rigidity. Even higher rigidity may be introduced by a combination of steel HSS sections placed on the tension flange of the mullion in combination with side plates. Other practical or aesthetic requirements my dictate the type of hardening technique that is to be implemented for a given application.
- Maximum dynamic response of aluminum curtain wall mullions, with or without steel hardening assemblies, can be predicted accurately by using nonlinear SDOF dynamic analysis. The same type of analysis may be conducted by using UFC charts for elasto-plastic systems. The results of both analysis methods provide good correlations.
- The P-I diagrams generated for the curtain wall mullion selected with and without the three hardening techniques can be used to design steel plate retrofit strategies for different threat levels that may need to be considered under different threat scenarios.
- Existing glass curtain walls in practice can be protected against civilian bomb attacks or accidental explosions by implementing any one of the steel retrofit techniques developed, as demonstrated by the dynamic response of hardened mullions for the prototype building selected.

CHAPTER 7. REFERENCES

- Bedon, C. and Amadiao, C. (2017). “Passive Control Systems for the Blast Enhancement of Glazing Curtain Walls Under Explosive Loads.”
- Brewer, T. R., Morrill, K. B., and Crawford, J.E. (2015). “A New Kind of Blast-Resistant Curtain Wall Façade.”
- Deng, Rong-Bing and Jin, Xiang-Long (2010). “Numerical Simulation for Blast Analysis of Insulating Glass in a Curtain Wall, International Journal for Computational Methods in Engineering Science and Mechanics.”
- Kennedy, B. T., Weggel, D. C. & Keanini, R. G. (2013). “Experimental Program and Simplified Nonlinear Design Expression for Glass Curtain Walls with Low-Level Blast Resistance.”
- Marchand, K., Davis, C., Sammarco, E., Bui, J., and Casper, J. (2016). “Coupled Glass and Structure Response of Conventional Curtain Walls Subjected to Blast Loads: Validation Tests and Analysis.”
- Nawar, M., Salim, H., Lusk, B., and Kiger, S. (2014). “Numerical Simulation and Verification of Curtain Wall Systems under Shock Pressure.”
- Northview Inc (2021). https://northviewsales.com.
- Ralston, A D., Weggel D C., Whelan, M. J. & Hongbing, F. (2015). “Experimental and Numerical Investigations of Glass Curtain Walls Subjected to Low- Level Blast Loads.”
- Parisi, F., Balestrieri, C., and Asprone, D. (2016). “Out-of-plane Capacity of Load-bearing Masonry Walls.” 16th International Brick and Block Masonry Conference.” Padova, Italy.
- Saatcioglu M., Alameer A., and Elnabelsy G. (2017a). “Blast Tests of Curtain Walls – Phase I: Windows Protected by Guardian Coil,” Report submitted to Global Affairs, Canada, HMDM Research Centre, University of Ottawa, Ottawa, December 2017.
- Saatcioglu M., Alameer A., and Elnabelsy G. (2017b). “Blast Tests of Curtain Walls – Phase II: Windows Protected by Guardian Coil,” Report submitted to Global Affairs, Canada, HMDM Research Centre, University of Ottawa, Ottawa, December 2017.
- Saatcioglu, M. (2020). “Building Envelop Hardening Measures.” Report submitted to Global Affairs Canada.

- Unified Facilities Criteria (2008). “Structures to Resist the Effects of Accidental Explosions.”
- Weggel, D. C., Zapata, B. J., and Keifer, M. J. (2007). “Properties and Dynamic Behavior of Glass Curtain Walls with Split Screw Spline Mullions.”

APPENDIX A DEVELOPMENT OF RESISTANCE FUNCTIONS

A.1 RESISTANCE FUNCTIONS FOR MULLION 1

A.1.1 Resistance function for simple supports

The cross section details of specimen Mullion 1 are given as follows,

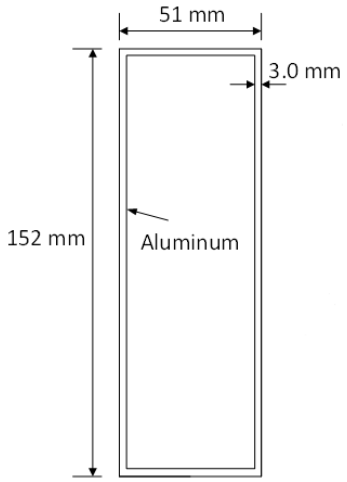

Figure A - 1 : Mullion 1 c/s details

The numerical values of the properties required for establishing resistance function are given as follows:

Yield Strength of Aluminum (f_y) = 210 MPa

Modulus of Elasticity (E_A) = 70000 N/mm^2

Length of tributary area (L) = 2083 mm

Width of tributary area (W) = 2083 mm

Total mass of load application device (m) = 107 kg

Moment of inertia for mullion-1 (I) = $\frac{(51*152^3) - (45*146^3)}{12}$ = 3254674 mm^4

Stiffness for simply supported beam assembly,

$$k_s = \frac{(384)\mathrm{EI}}{5L^3} = \frac{384 * 70000*3254674}{5 * 2083^3} = 1935.97 \text{ N/mm}$$

Moment Capacity of section,

$$M^- = M^+ = \frac{(f_y)\, I}{y}$$

Here, M^- and M^+ are negative and positive moment capacities. Here, *'y'* is the maximum distance to the tension fibers from the neutral axis which is half of the section depth (152/2 = 76 mm). Thus, substituting the above calculated values in the moment equation,

$$M = \frac{210*3254674}{76} = 8993178.2 \text{ N.mm} = 8.99 \text{ kN.m}$$

Elastic Resistance of mullion,

$$R_m = \frac{8M}{L} = \frac{8*8.99}{2.083} = 34.53 \text{ kN}$$

Yield displacement,

$$u_y = \frac{R_m}{k_s} = \frac{(34.53)(1000)}{(1935.97)} = 17.84 \text{ mm}$$

Now, considering the yield displacement calculated as above, the maximum inelastic displacement is calculated by the use of UFC charts and RC-Blast software for the applied combination of pressure-impulse loading.

A.1.2 Resistance function for fixed supports

The resistance function for the fixed end conditions is calculated as follows for the mullion section properties considered for the above calculation of simple support conditions.

Stiffness for simply supported beam assembly,

$$k_s = \frac{(384)\text{EI}}{5L^3} = \frac{384 * 70000*3254674}{5 * 2083^3} = 1935.97 \text{ N/mm}$$

Stiffness for fixed supported beam assembly,

$$k_f = \frac{(384)\text{EI}}{L^3} = \frac{384 * 70000*3254674}{2083^3} = 9679.857 \text{ N/mm}$$

The resistance function for fixed support condition exhibits a trilinear relationship. The resistance offered by the beam is divided into two parts. In the first one, due to the loading, the yielding occurs at the supports. Now, the beam behaves as a simply supported beam, as hinges are created at the supports. Now, the moment capacity of the original beam is reduced to half due to the formation of hinges at supports. In the second part, the beam resists the loading until a hinge is formed in the centre of the beam.

Considering the fixity at the supports, initial yield resistance is calculated as follows,

$$R_{y1} = \frac{12M}{L} = \frac{12 * 8.99}{2.083} = 51.81\ kN$$

Corresponding displacement at the supports is calculated as follows,

$$u_{y1} = \frac{R_{y1}}{k_f} = \frac{51.81 * 1000}{9679.85} = 5.36\ mm$$

Now, hinges are formed at the supports, and the moment carrying capacity is reduced to half, which will be 4.49 kN.m. The beam will now behave as simply supported beam with the yield resistance calculated as follows,

$$R_{y2} = \frac{8M}{L} = \frac{8 * 4.49}{2.083} = 17.27\ kN$$

Now, the total resistance is the summation of R_{y1} and R_{y2}. Thus, R_m = 69.08 kN. The displacement at the formation of the hinge at support is given as follows,

$$u_{y2} = u_{y1} + \frac{R_{y2}}{k_s} = 5.36 + \frac{17.27 * 1000}{1935.97} = 14.27\ mm$$

Now, the trilinear resistance function needs to be converted into bilinear resistance function. For doing this, the area under the trilinear and bilinear function is to be equated, which gives an equivalent yield displacement value for the corresponding yield resistance R_m. Following are the calculated values for the same.

$$u_y = 12.94\ mm \qquad k_{eff} = \frac{R_m}{u_y} = \frac{69.08}{12.94} = 5340.61\ N/mm$$

Now, considering the yield displacement calculated as above, the maximum inelastic displacement is calculated by the use of UFC charts and RC-Blast software for the applied combination of pressure-impulse loading.

A.2 RESISTANCE FUNCTIONS FOR MULLION 1H

A.2.1 Resistance function for simple supports

The cross section details of specimen Mullion 1H are given as follows,

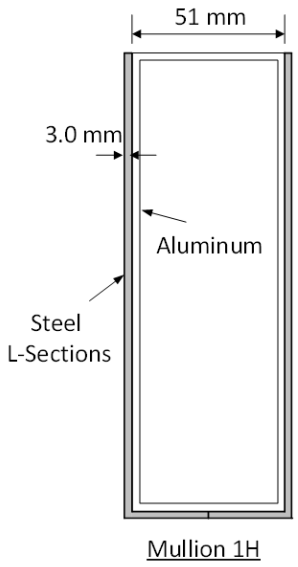

Figure A - 2 : Mullion 1H c/s details

The numerical values of the properties required for establishing resistance function are given as follows:

Modulus of Elasticity of aluminum (E_A) = 70000 N/mm^2

Modulus of Elasticity of steel (E_S) = 200000 N/mm^2

Density of steel = 7850 kg/m^3

Yield Strength of steel (f_y) = 350 MPa

Length of tributary area (L) = 2083 mm

Width of tributary area (W) = 2083 mm

Total mass of load application device (m) = 107 kg

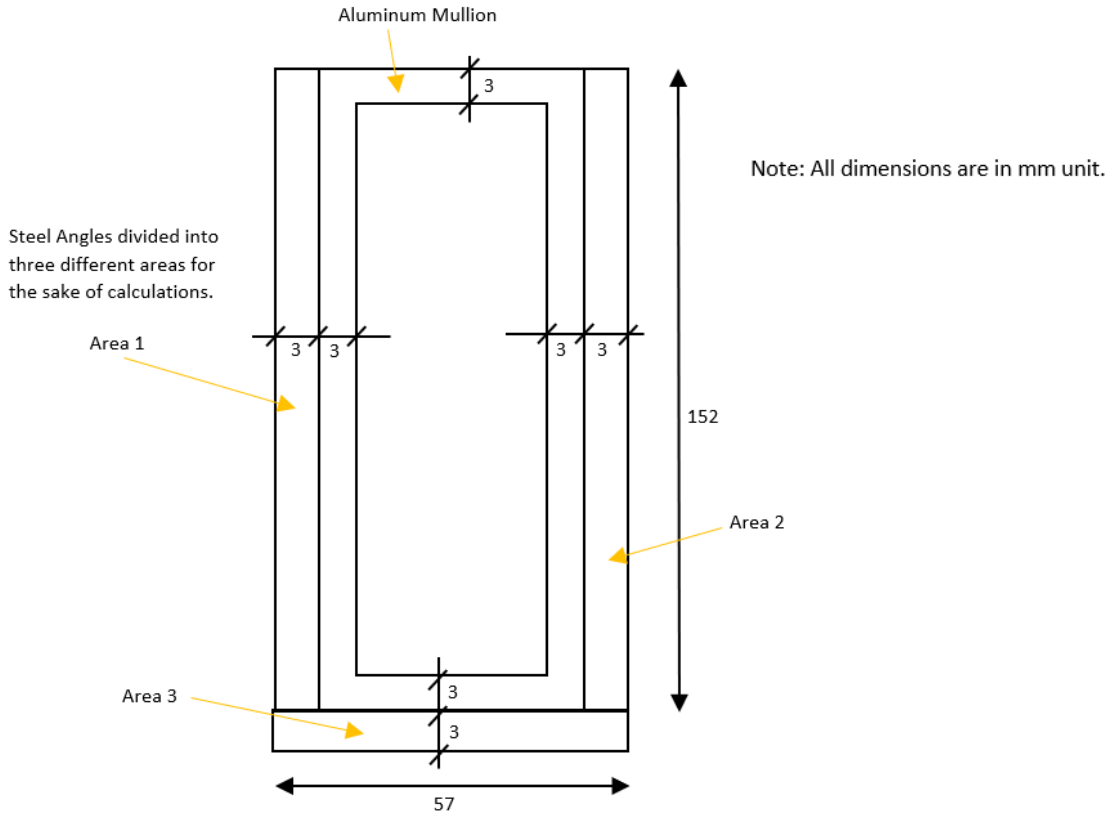

Figure A - 3 : Area division for Mullion 1H

Calculation of transformed M.I for the composite section:

Transformation factor to convert aluminum section into equivalent steel section: $n = E_A/E_s = 0.35$

Area of aluminum mullion = (152 x 51 – 146 x 45) = 1182 mm^2

Transformed area of aluminum to steel section = 0.35 x 1182 = 413.72 mm^2

M.I of aluminum mullion = $\frac{(51*152^3)-(45*146^3)}{12}$ = 3254674 mm^4

Transformed M.I of aluminum to steel section = 0.35 x 3254674 = 1139135.9 mm^4

Area of steel area 1 and area 2 = 152 x 3 = 456 mm^2

M.I for area 1 and area 2 = $\frac{3*152^3}{12}$ = 877952 mm^4

M.I for area 3 = $\frac{57*3^3}{12}$ = 128.25 mm^4

Area of steel area 3 = 57 x 3 = 171 mm^2

Distance of the neutral axis from the extreme bottom (tension) fibers,

$$y = \frac{2 * 456 * 79 + 413 * 79 + 171 * 1.5}{413.72 + 912 + 171} = 70.146\ mm$$

Moment of inertia for the transformed section,

I_{TR} = [1139135.9 + 413.72 x (79 – 70.146)^2] + 2 x [877952 + 456 x (79 – 70.146)^2] + [128.25 + 171 x (70.146 – 1.5)^2 = 3804894.47 mm^4

Stiffness for simply supported beam assembly,

$$k_s = \frac{(384)\mathrm{EI}}{5L^3} = \frac{384 * 200000 * 3804894.47}{5 * 2083^3} = 6466.4519\ \text{N/mm}$$

Moment Capacity of section,

$$M^- = M^+ = \frac{(f_y)\ I}{y}$$

Here, M^- and M^+ are negative and positive moment capacities. Here, *'y'* is the maximum distance to the tension fibers from the neutral axis. Thus, substituting the above calculated values in the moment equation,

$$M = \frac{350 * 3804849.47}{70.146} = 18984650.79\ \text{N.mm} = 18.99\ \text{kN.m}$$

Elastic Resistance of mullion,

$$R_m = \frac{8M}{L} = \frac{8 * 18.99}{2.083} = 72.914\ \text{kN}$$

Yield displacement,

$$u_y = \frac{R_m}{k_s} = \frac{(72.914)(1000)}{(6466.452)} = 11.276\ \text{mm}$$

Now, considering the yield displacement calculated as above, the maximum inelastic displacement is calculated by the use of UFC charts and RC-Blast software for the applied combination of pressure-impulse loading.

A.2.2 Resistance function for fixed supports

The resistance function for the fixed end conditions is calculated as follows for the mullion section properties considered for the above calculation of simple support conditions.

Stiffness for simply supported beam assembly,

$$k_s = \frac{(384)\mathrm{EI}}{5L^3} = \frac{384 * 200000 * 3804894.47}{5 * 2083^3} = 6466.45 \text{ N/mm}$$

Stiffness for fixed supported beam assembly,

$$k_f = \frac{(384)\mathrm{EI}}{L^3} = \frac{384 * 200000 * 3804894.47}{2083^3} = 32332.26 \text{ N/mm}$$

Considering the fixity at the supports, initial yield resistance is calculated as follows,

$$R_{y1} = \frac{12M}{L} = \frac{12 * 18.99}{2.083} = 109.37\ kN$$

Corresponding displacement at the supports is calculated as follows,

$$u_{y1} = \frac{R_{y1}}{k_f} = \frac{109.37 * 1000}{32332.26} = 3.39\ mm$$

Now, hinges are formed at the supports, and the moment carrying capacity is reduced to half, which will be 9.49 kN.m. The beam will now behave as simply supported beam with the yield resistance calculated as follows,

$$R_{y2} = \frac{8M}{L} = \frac{8 * 9.49}{2.083} = 36.45\ kN$$

Now, the total resistance is the summation of R_{y1} and R_{y2}. Thus, R_m = 145.83 kN. The displacement at the formation of the hinge at support is given as follows,

$$u_{y2} = u_{y1} + \frac{R_{y2}}{k_s} = 3.39 + \frac{36.45 * 1000}{6466.45} = 9.02\ mm$$

Now, the trilinear resistance function needs to be converted into bilinear resistance function. For doing this, the area under the trilinear and bilinear function is to be equated, which gives an equivalent yield displacement value for the corresponding yield resistance R_m. Following are the calculated values for the same.

$$u_y = 8.18\,mm \qquad k_{eff} = \frac{R_m}{u_y} = \frac{145.83 * 1000}{8.18} = 17838.49\,N/mm$$

Now, considering the yield displacement calculated as above, the maximum inelastic displacement is calculated by the use of UFC charts and RC-Blast software for the applied combination of pressure-impulse loading.

A.3 RESISTANCE FUNCTIONS FOR MULLION 2

A.3.1 Resistance function for simple supports

The cross section details of specimen Mullion 2 are given as follows,

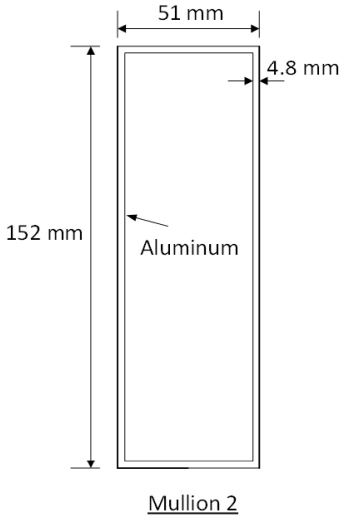

Figure A - 4 : Mullion 2 c/s details

The numerical values of the properties required for establishing resistance function are given as follows:

Yield Strength of Aluminum (f_y) = 210 MPa

Modulus of Elasticity (E_A) = 70000 N/mm^2

Length of tributary area (L) = 2083 mm

Width of tributary area (W) = 2083 mm

Total mass of load application device (m) = 107 kg

Moment of inertia for mullion-2 (I) = $\frac{(51*152^3) - (41.4*142.4^3)}{12}$ = 4963126.1 mm^4

Stiffness for simply supported beam assembly,

$$k_s = \frac{(384)\mathrm{EI}}{5L^3} = \frac{384 * 70000 * 4963126.1}{5 * 2083^3} = 2952.20 \text{ N/mm}$$

Moment Capacity of section,

$$M^- = M^+ = \frac{(f_y)\, I}{y}$$

Here, M^- and M^+ are negative and positive moment capacities. Here, *'y'* is the maximum distance to the tension fibers from the neutral axis which is half of the section depth (152/2 = 76 mm). Thus, substituting the above calculated values in the moment equation,

$$M = \frac{210 * 4963126.1}{76} = 13713901.07 \text{ N.mm} = 13.72 \text{ kN.m}$$

Elastic Resistance of mullion,

$$R_m = \frac{8M}{L} = \frac{8 * 13.72}{2.083} = 52.67 \text{ kN}$$

Yield displacement,

$$u_y = \frac{R_m}{k_s} = \frac{(52.67)(1000)}{(2952.20)} = 17.84 \text{ mm}$$

Now, considering the yield displacement calculated as above, the maximum inelastic displacement is calculated by the use of UFC charts and RC-Blast software for the applied combination of pressure-impulse loading.

A.3.2 Resistance function for fixed supports

The resistance function for the fixed end conditions is calculated as follows for the mullion section properties considered for the above calculation of simple support conditions.

Stiffness for simply supported beam assembly,

$$k_s = \frac{(384)\mathrm{EI}}{5L^3} = \frac{384 * 70000 * 4963126.1}{5 * 2083^3} = 2952.20 \text{ N/mm}$$

Stiffness for fixed supported beam assembly,

$$k_f = \frac{(384)\mathrm{EI}}{L^3} = \frac{384 * 70000 * 4963126.1}{2083^3} = 14761.03 \text{ N/mm}$$

The resistance function for fixed support condition exhibits a trilinear relationship. The resistance offered by the beam is divided into two parts. In the first one, due to the loading, the yielding occurs at the supports. Now, the beam behaves as a simply supported beam, as hinges are created at the supports. Now, the moment capacity of the original beam is reduced to half due to the formation of hinges at supports. In the second part, the beam resists the loading until a hinge is formed in the centre of the beam.

Considering the fixity at the supports, initial yield resistance is calculated as follows,

$$R_{y1} = \frac{12M}{L} = \frac{12 * 13.72}{2.083} = 79\ kN$$

Corresponding displacement at the supports is calculated as follows,

$$u_{y1} = \frac{R_{y1}}{k_f} = \frac{79 * 1000}{14761.03} = 5.35\ mm$$

Now, hinges are formed at the supports, and the moment carrying capacity is reduced to half, which will be 6.857 kN.m. The beam will now behave as simply supported beam with the yield resistance calculated as follows,

$$R_{y2} = \frac{8M}{L} = \frac{8 * 6.857}{2.083} = 26.335\ kN$$

Now, the total resistance is the summation of R_{y1} and R_{y2}. Thus, R_m = 105.34 kN. The displacement at the formation of the hinge at support is given as follows,

$$u_{y2} = u_{y1} + \frac{R_{y2}}{k_s} = 5.35 + \frac{26.335 * 1000}{2952.20} = 14.273\ mm$$

Now, the trilinear resistance function needs to be converted into bilinear resistance function. For doing this, the area under the trilinear and bilinear function is to be equated, which gives an equivalent yield displacement value for the corresponding yield resistance R_m. Following are the calculated values for the same.

$$u_y = 12.94\ mm \qquad k_{eff} = \frac{R_m}{u_y} = \frac{105.34*1000}{12.94} = 8144.02\ N/mm$$

Now, considering the yield displacement calculated as above, the maximum inelastic displacement is calculated by the use of UFC charts and RC-Blast software for the applied combination of pressure-impulse loading.

A.4 RESISTANCE FUNCTIONS FOR MULLION 2H

A.4.1 Resistance function for simple supports

The cross-section details of specimen Mullion 2H are given as follows,

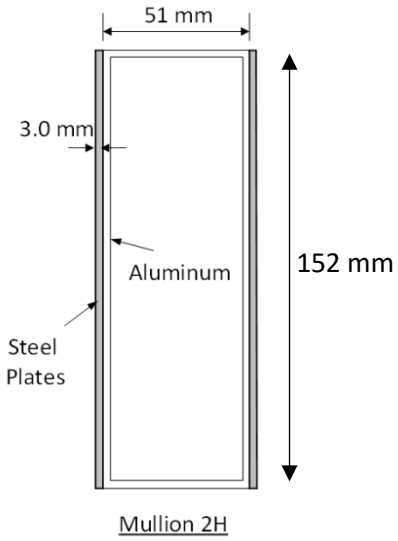

Figure A - 5 : Mullion 2H c/s details

The numerical values of the properties required for establishing resistance function are given as follows:

Modulus of Elasticity of aluminum (E_A) = 70000 N/mm^2

Modulus of Elasticity of steel (E_S) = 200000 N/mm^2

Density of steel = 7850 kg/m^3

Yield Strength of steel (f_y) = 350 MPa

Length of tributary area (L) = 2083 mm

Width of tributary area (W) = 2083 mm

Total mass of load application device (m) = 121.92 kg

Calculation of transformed M.I for the composite section:

Transformation factor to convert aluminum section into equivalent steel section: $n = E_A/E_s = 0.35$

Area of aluminum mullion = (152 x 51 – 142.4 x 41.4) = 1856.64 mm^2

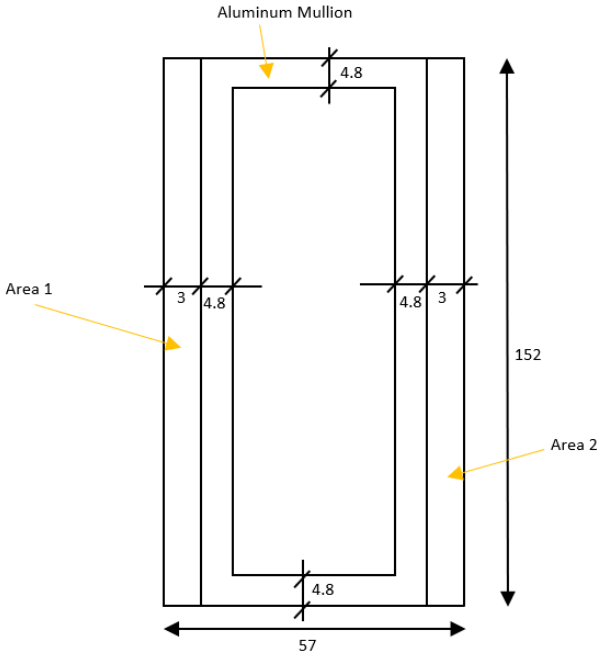

Note: All dimensions are in mm unit.

Figure A - 6 : Area division for Mullion 2H

Transformed area of aluminum to steel section = 0.35 x 1856.64 = 649.824 mm^2

M.I of aluminum mullion = $\frac{(51*152^3)-(41.4*142.4^3)}{12}$ = 4963126.067 mm^4

Transformed M.I of aluminum to steel section = 0.35 x 4963126.067 = 1737094.124 mm^4

Area of steel area 1 and area 2 = 152 x 3 = 456 mm^2

M.I for area 1 and area 2 = $\frac{3*152^3}{12}$ = 877952 mm^4

Distance of the neutral axis from the extreme bottom (tension) fibers,

$$y = 76\ mm$$

Moment of inertia for the transformed section,

I_{TR} = 1737094.124 + 2 x 877952 = 3492998.124 mm^4

Stiffness for simply supported beam assembly,

$$k_s = \frac{(384)\mathrm{EI}}{5L^3} = \frac{384 * 200000 * 3492998.124}{5 * 2083^3} = 5936.38 \text{ N/mm}$$

Moment Capacity of section,

$$M^- = M^+ = \frac{(f_y)\, I}{y}$$

Here, M^- and M^+ are negative and positive moment capacities. Here, *'y'* is the maximum distance to the tension fibers from the neutral axis. Thus, substituting the above calculated values in the moment equation,

$$M = \frac{350 * 3492998.124}{76} = 16086176 \text{ N.mm} = 16.086 \text{ kN.m}$$

Elastic Resistance of mullion,

$$R_m = \frac{8M}{L} = \frac{8 * 16.086}{2.083} = 61.78 \text{ kN}$$

Yield displacement,

$$u_y = \frac{R_m}{k_s} = \frac{(61.78)(1000)}{(5936.38)} = 10.407 \text{ mm}$$

Now, considering the yield displacement calculated as above, the maximum inelastic displacement is calculated by the use of UFC charts and RC-Blast software for the applied combination of pressure-impulse loading.

A.4.2 Resistance function for fixed supports

The resistance function for the fixed end conditions is calculated as follows for the mullion section properties considered for the above calculation of simple support conditions.

Stiffness for simply supported beam assembly,

$$k_s = \frac{(384)\mathrm{EI}}{5L^3} = \frac{384 * 200000 * 3492998.1}{5 * 2083^3} = 5936.38 \text{ N/mm}$$

Stiffness for fixed supported beam assembly,

$$k_f = \frac{(384)\mathrm{EI}}{L^3} = \frac{384 * 200000 * 3492998.1}{2083^3} = 29681.9 \text{ N/mm}$$

Considering the fixity at the supports, initial yield resistance is calculated as follows,

$$R_{y1} = \frac{12M}{L} = \frac{12 * 16.08}{2.083} = 92.67\ kN$$

Corresponding displacement at the supports is calculated as follows,

$$u_{y1} = \frac{R_{y1}}{k_f} = \frac{92.67 * 1000}{29681.9} = 3.122\ mm$$

Now, hinges are formed at the supports, and the moment carrying capacity is reduced to half, which will be 8.043 kN.m. The beam will now behave as simply supported beam with the yield resistance calculated as follows,

$$R_{y2} = \frac{8M}{L} = \frac{8 * 8.043}{2.083} = 30.89\ kN$$

Now, the total resistance is the summation of R_{y1} and R_{y2}. Thus, R_m = 123.562 kN. The displacement at the formation of the hinge at support is given as follows,

$$u_{y2} = u_{y1} + \frac{R_{y2}}{k_s} = 3.122 + \frac{30.89 * 1000}{5936.38} = 8.326\ mm$$

Now, the trilinear resistance function needs to be converted into bilinear resistance function. For doing this, the area under the trilinear and bilinear function is to be equated, which gives an equivalent yield displacement value for the corresponding yield resistance R_m. Following are the calculated values for the same.

$$u_y = 7.55\ mm \qquad k_{eff} = \frac{R_m}{u_y} = \frac{123.562 * 1000}{7.55} = 16376.223\ N/mm$$

Now, considering the yield displacement calculated as above, the maximum inelastic displacement is calculated by the use of UFC charts and RC-Blast software for the applied combination of pressure-impulse loading.

A.5 RESISTANCE FUNCTIONS FOR MULLION 3

A.5.1 Resistance function for simple supports

The cross-section details of specimen Mullion 3 are given as follows,

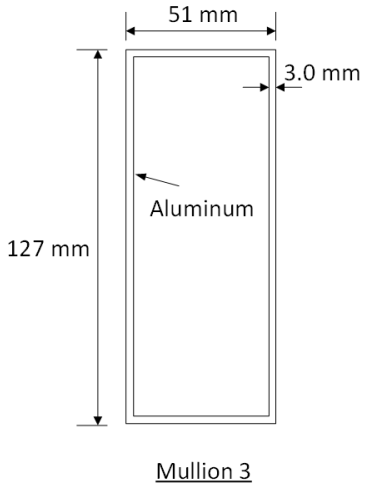

Figure A - 7 : Mullion 3 c/s details

The numerical values of the properties required for establishing resistance function are given as follows:

Yield Strength of Aluminum (f_y) = 210 MPa

Modulus of Elasticity (E_A) = 70000 N/mm^2

Length of tributary area (L) = 2083 mm

Width of tributary area (W) = 2083 mm

Total mass of load application device (m) = 107 kg

Moment of inertia for mullion-3 (I) = $\frac{(51*127^3) - (45*121^3)}{12}$ = 2062274 mm^4

Stiffness for simply supported beam assembly,

$$k_s = \frac{(384)\mathrm{EI}}{5L^3} = \frac{384 * 70000*2062274}{5 * 2083^3} = 1226.7 \text{ N/mm}$$

Moment Capacity of section,

$$M^- = M^+ = \frac{(f_y)\, I}{y}$$

Here, M^- and M^+ are negative and positive moment capacities. Here, *'y'* is the maximum distance to the tension fibers from the neutral axis which is half of the section depth (127/2 = 63.5 mm). Thus, substituting the above calculated values in the moment equation,

$$M = \frac{210*2062274}{63.5} = 6820118.7 \text{ N.mm} = 6.82 \text{ kN.m}$$

Elastic Resistance of mullion,

$$R_m = \frac{8M}{L} = \frac{8*6.82}{2.083} = 26.2 \text{ kN}$$

Yield displacement,

$$u_y = \frac{R_m}{k_s} = \frac{(26.2)(1000)}{(1226.7)} = 21.353 \text{ mm}$$

Now, considering the yield displacement calculated as above, the maximum inelastic displacement is calculated by the use of UFC charts and RC-Blast software for the applied combination of pressure-impulse loading.

A.5.2 Resistance function for fixed supports

The resistance function for the fixed end conditions is calculated as follows for the mullion section properties considered for the above calculation of simple support conditions.

Stiffness for simply supported beam assembly,

$$k_s = \frac{(384)\text{EI}}{5L^3} = \frac{384 * 70000*2062274}{5 * 2083^3} = 1226.7 \text{ N/mm}$$

Stiffness for fixed supported beam assembly,

$$k_f = \frac{(384)\text{EI}}{L^3} = \frac{384 * 70000*2062274}{2083^3} = 6133.49 \text{ N/mm}$$

The resistance function for fixed support condition exhibits a trilinear relationship. The resistance offered by the beam is divided into two parts. In the first one, due to the loading, the yielding occurs at the supports. Now, the beam behaves as a simply supported beam, as hinges are created at the supports. Now, the moment capacity of the original beam is reduced to half due to the formation of hinges at supports. In the second part, the beam resists the loading until a hinge is formed in the centre of the beam.

Considering the fixity at the supports, initial yield resistance is calculated as follows,

$$R_{y1} = \frac{12M}{L} = \frac{12 * 6.82}{2.083} = 39.29\ kN$$

Corresponding displacement at the supports is calculated as follows,

$$u_{y1} = \frac{R_{y1}}{k_f} = \frac{39.29 * 1000}{6133.49} = 6.405\ mm$$

Now, hinges are formed at the supports, and the moment carrying capacity is reduced to half, which will be 3.41 kN.m. The beam will now behave as simply supported beam with the yield resistance calculated as follows,

$$R_{y2} = \frac{8M}{L} = \frac{8 * 3.41}{2.083} = 13.097\ kN$$

Now, the total resistance is the summation of R_{y1} and R_{y2}. Thus, R_m = 52.387 kN. The displacement at the formation of the hinge at support is given as follows,

$$u_{y2} = u_{y1} + \frac{R_{y2}}{k_s} = 6.405 + \frac{13.097 * 1000}{1226.7} = 17.083\ mm$$

Now, the trilinear resistance function needs to be converted into bilinear resistance function. For doing this, the area under the trilinear and bilinear function is to be equated, which gives an equivalent yield displacement value for the corresponding yield resistance R_m. Following are the calculated values for the same.

$$u_y = 15.48\ mm \qquad k_{eff} = \frac{R_m}{u_y} = \frac{52.387 * 1000}{15.48} = 3383.996\ N/mm$$

Now, considering the yield displacement calculated as above, the maximum inelastic displacement is calculated by the use of UFC charts and RC-Blast software for the applied combination of pressure-impulse loading.

A.6 RESISTANCE FUNCTIONS FOR MULLION 3H

A.6.1 Resistance function for simple supports

The cross-section details of specimen Mullion 3H are given as follows,

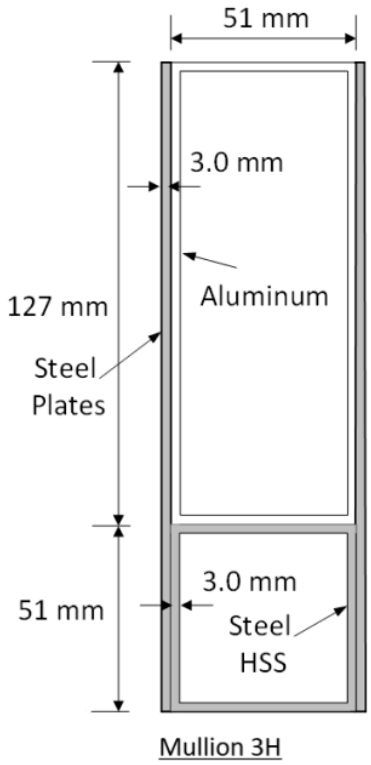

Figure A - 8 : Mullion 3H c/s details

The numerical values of the properties required for establishing resistance function are given as follows:

Modulus of Elasticity of aluminum (E_A) = 70000 N/mm^2

Modulus of Elasticity of steel (E_S) = 200000 N/mm^2

Density of steel = 7850 kg/m^3

Yield Strength of steel (f_y) = 350 MPa

Length of tributary area (L) = 2083 mm

Width of tributary area (W) = 2083 mm

Total mass of load application device (m) = 133.89 kg

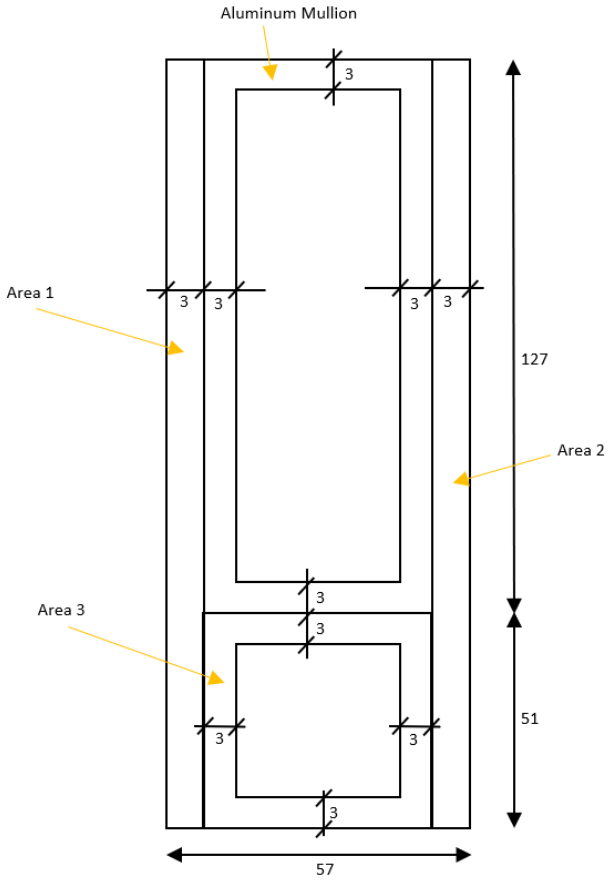

Note: All dimensions are in mm unit.

Figure A - 9 : Area division for Mullion 3H

Calculation of transformed M.I for the composite section:

Transformation factor to convert aluminum section into equivalent steel section: $n = E_A/E_s = 0.35$

Area of aluminum mullion = (127 x 51 – 121 x 45) = 1032 mm^2

Transformed area of aluminum to steel section = 0.35 x 1032 = 361.2 mm^2

M.I of aluminum mullion = $\frac{(51*127^3)-(45*121^3)}{12}$ = 2062274 mm^4

Transformed M.I of aluminum to steel section = 0.35 x 2062274 = 721795.9 mm^4

Area of steel area 1 and area 2 = 178 x 3 = 534 mm^2

M.I for area 1 and area 2 = $\frac{3*178^3}{12}$ = 1409938 mm^4

M.I for area 3 = $\frac{(51*51^3)-(45*45^3)}{12}$ = 222048 mm^4

Area of steel area 3 = (51 x 51) – (45 x 45) = 576 mm^2

Distance of the neutral axis from the extreme bottom (tension) fibers,

$$y = \frac{361.2 * 114.5 + 2 * 534 * 89 + 576 * 25.5}{361.2 + 2 * 534 + 576} = 75.353\ mm$$

Moment of inertia for the transformed section,

I_{TR} = [721795.9 + 361.2 x (114.5 – 75.353)^2] + 2 x [1409938 + 534 x (89 – 75.353)^2] + [222048 + 576 x (75.353 – 25.5)^2 = 5947704.64 mm^4

Stiffness for simply supported beam assembly,

$$k_s = \frac{(384)\mathrm{EI}}{5L^3} = \frac{384 * 200000 * 5947704.64}{5 * 2083^3} = 10108.18\ \mathrm{N/mm}$$

Moment Capacity of section,

$$M^- = M^+ = \frac{(f_y)\ I}{y}$$

Here, M^- and M^+ are negative and positive moment capacities. Here, *'y'* is the maximum distance to the tension fibers from the neutral axis. Thus, substituting the above calculated values in the moment equation,

$$M = \frac{350 * 5947704.64}{75.353} = 27625929\ \mathrm{N.mm} = 27.626\ \mathrm{kN.m}$$

Elastic Resistance of mullion,

$$R_m = \frac{8M}{L} = \frac{8 * 27.626}{2.083} = 106.1\ \mathrm{kN}$$

Yield displacement,

$$u_y = \frac{R_m}{k_s} = \frac{(106.1)(1000)}{(10108.18)} = 10.5\ \mathrm{mm}$$

Now, considering the yield displacement calculated as above, the maximum inelastic displacement is calculated by the use of UFC charts and RC-Blast software for the applied combination of pressure-impulse loading.

A.6.2 Resistance function for fixed supports

The resistance function for the fixed end conditions is calculated as follows for the mullion section properties considered for the above calculation of simple support conditions.

Stiffness for simply supported beam assembly,

$$k_s = \frac{(384)\mathrm{EI}}{5L^3} = \frac{384 * 200000 * 5947704.64}{5 * 2083^3} = 10108.18 \text{ N/mm}$$

Stiffness for fixed supported beam assembly,

$$k_f = \frac{(384)\mathrm{EI}}{L^3} = \frac{384 * 200000 * 5947704.64}{2083^3} = 50540.88 \text{ N/mm}$$

Considering the fixity at the supports, initial yield resistance is calculated as follows,

$$R_{y1} = \frac{12M}{L} = \frac{12 * 27.626}{2.083} = 159.15\ kN$$

Corresponding displacement at the supports is calculated as follows,

$$u_{y1} = \frac{R_{y1}}{k_f} = \frac{159.15 * 1000}{50540.88} = 3.15\ mm$$

Now, hinges are formed at the supports, and the moment carrying capacity is reduced to half, which will be 13.813 kN.m. The beam will now behave as simply supported beam with the yield resistance calculated as follows,

$$R_{y2} = \frac{8M}{L} = \frac{8 * 13.813}{2.083} = 53.05\ kN$$

Now, the total resistance is the summation of R_{y1} and R_{y2}. Thus, R_m = 212.20 kN. The displacement at the formation of the hinge at support is given as follows,

$$u_{y2} = u_{y1} + \frac{R_{y2}}{k_s} = 3.15 + \frac{53.05 * 1000}{10108.18} = 8.398\ mm$$

Now, the trilinear resistance function needs to be converted into bilinear resistance function. For doing this, the area under the trilinear and bilinear function is to be equated, which gives an equivalent yield displacement value for the corresponding yield resistance R_m. Following are the calculated values for the same.

$$u_y = 7.61\ mm \qquad k_{eff} = \frac{R_m}{u_y} = \frac{212.20 * 1000}{7.61} = 27884.624\ N/mm$$

Now, considering the yield displacement calculated as above, the maximum inelastic displacement is calculated by the use of UFC charts and RC-Blast software for the applied combination of pressure-impulse loading.

APPENDIX B VALIDATION OF UFC CHARTED SOLUTION AND RC-BLAST SOFTWARE

B.1 VALIDATION PROCEDURES FOR MULLION 1

B.1.1 Validation procedure for simple supports

The parameters recorded from the experiment for testing of Mullion 1 are P_r = 27 kPa, I_r = 191 kPa-ms and t_d = 14 ms. Thus, time period of mullions is calculated as follows,

$$T_s = 2\pi\sqrt{\frac{K_{LM}m}{k}}$$

Where, K_{LM} is the load mass factor and K_{LM} = 0.78 for elastic range and K_{LM} = 0.66 for plastic range. Considering the elastic response, implies the load mass factor to be 0.78,

$$T_s = 2\pi\sqrt{\frac{0.78 * 107}{1.9 * 10^6}} = 0.0413 \text{ s} = 41.3 \text{ ms}$$

Now, the blast force on tributary area (F_1) = 27 * 2.083 * 2.083 = 117.15 kN. Using UFC chart,

$$\frac{t_d}{T_s} = \frac{14}{41.3} = 0.339, for\ \mu = 1.0\ \ gives\ \ \frac{R_m}{F_1} = 1.2$$

Thus, $(R_m)_{demand}$ = 1.2 * 117.15 = 140.58 kN > $(R_m)_{capacity}$ = 34.53 kN. Thus, mullions are behaving in plastic range. Thus, assume K_{LM} = 0.72 as an average load mass factor for the entire elasto-plastic range, the time period of the mullion is modified as follows,

$$T_s = 2\pi\sqrt{\frac{0.72 * 107}{1.9 * 10^6}} = 0.03965 \text{ s} = 39.65 \text{ ms}$$

Now, for R_m/F_1 = 34.53/117.15 = 0.295, using UFC Chart, the ductility demand is calculated as follows,

$$\frac{t_d}{T_s} = \frac{14}{39.65} = 0.353 \; and \; \frac{R_m}{F_1} = 0.295 \; gives \; \mu = 6.5$$

Thus, the deflection at mid height responsible for rupture is u_m = 6.5 * 17.84 = 115.96 mm. The obtained inelastic displacement is now compared with nonlinear single degree of freedom (SDOF) analysis done with the help of RC-Blast software.

B.1.2 Validation procedure for fixed supports

The parameters recorded from the experiment for testing of Mullion 1 are P_r = 27 kPa, I_r = 191 kPa-ms and t_d = 14 ms. Thus, time period of mullions is calculated as follows,

$$T_s = 2\pi\sqrt{\frac{K_{LM}m}{k}}$$

Where, K_{LM} is the load mass factor and K_{LM} = 0.78 for elastic range and K_{LM} = 0.66 for plastic range. Considering the elastic response, implies the load mass factor to be 0.78,

$$T_s = 2\pi\sqrt{\frac{0.78*107}{5.34*10^6}} = 0.02387 \text{ s} = 23.87 \text{ ms}$$

Now, the blast force on tributary area (F_1) = 27 * 2.083 * 2.083 = 117.15 kN. Using UFC chart,

$$\frac{t_d}{T_s} = \frac{14}{24.9} = 0.5864, for \; \mu = 1.0 \; gives \; \frac{R_m}{F_1} = 1.3$$

Thus, $(R_m)_{demand}$ = 1.3 * 117.15 = 152.3 kN > $(R_m)_{capacity}$ = 69.08 kN. Thus, mullions are behaving in plastic range. Thus, assume K_{LM} = 0.72 as an average load mass factor for the entire elasto-plastic range, the time period of the mullion is modified as follows,

$$T_s = 2\pi\sqrt{\frac{0.72*107}{5.34*10^6}} = 0.02384 \text{ s} = 23.84 \text{ ms}$$

Now, for R_m/F_1 = 69.08/117.15 = 0.59, using UFC Chart, the ductility demand is calculated as follows,

$$\frac{t_d}{T_s} = \frac{14}{39.65} = 0.587 \; and \; \frac{R_m}{F_1} = 0.59 \; gives \; \mu = 3.2$$

Thus, the deflection at mid height responsible for rupture is u_m = 3.2 * 12.94 = 41.4 mm. The obtained inelastic displacement is now compared with nonlinear single degree of freedom (SDOF) analysis done with the help of RC-Blast software.

B.2 VALIDATION PROCEDURES FOR MULLION 1H

B.2.1 Validation procedure for simple supports

The parameters recorded from the experiment for testing of Mullion 1H are P_r = 59 kPa, I_r = 411 kPa-ms and t_d = 18 ms. Thus, time period of mullions is calculated as follows,

$$T_s = 2\pi\sqrt{\frac{K_{LM}m}{k}}$$

Where, K_{LM} is the load mass factor and K_{LM} = 0.78 for elastic range and K_{LM} = 0.66 for plastic range. Here, the mass of steel sections which is 17.71 kgs is to be added to the entire load application device. Thus, the total mass of the system is 124.71 kgs. Considering the plastic response implies the load mass factor to be 0.78,

$$T_s = 2\pi\sqrt{\frac{0.78*124.71}{6.467*10^6}} = 0.02437 \text{ s} = 24.37 \text{ ms}$$

Now, the blast force on tributary area (F_1) = 59 * 2.083 * 2.083 = 255.995 kN. Using UFC chart,

$$\frac{t_d}{T_s} = \frac{18}{24.37} = 0.74, for\ \mu = 1.0\ \ gives\ \ \frac{R_m}{F_1} = 1.4$$

Thus, $(R_m)_{demand}$ = 1.4 * 255.995 = 358.4 kN > $(R_m)_{capacity}$ = 72.914 kN. Thus, mullions are behaving in plastic range. Thus, assume K_{LM} = 0.72 as an average load mass factor for the entire elasto-plastic range, the time period of the mullion is modified as follows,

$$T_s = 2\pi\sqrt{\frac{0.72*124.71}{6.467*10^6}} = 0.02342 \text{ s} = 23.42 \text{ ms}$$

Now, for R_m/F_1 = 72.914/255.995 = 0.29, using UFC Chart, the ductility demand is calculated as follows,

$$\frac{t_d}{T_s} = \frac{18}{23.42} = 0.77\ and\ \ \frac{R_m}{F_1} = 0.29\ \ gives\ \ \mu = 25$$

Thus, the deflection at mid height responsible for rupture is u_m = 25 * 11.276 = 281.9 mm. The obtained inelastic displacement is now compared with nonlinear single degree of freedom (SDOF) analysis done with the help of RC-Blast software.

B.2.2 Validation procedure for fixed supports

The parameters recorded from the experiment for testing of Mullion 1H are P_r = 59 kPa, I_r = 411 kPa-ms and t_d = 18 ms. Thus, time period of mullions is calculated as follows,

$$T_s = 2\pi\sqrt{\frac{K_{LM}m}{k}}$$

Where, K_{LM} is the load mass factor and K_{LM} = 0.78 for elastic range and K_{LM} = 0.66 for plastic range. Here, the mass of steel sections which is 17.71 kgs is to be added to the entire load application device. Thus, the total mass of the system is 124.71 kgs. Considering the plastic response implies the load mass factor to be 0.78,

$$T_s = 2\pi\sqrt{\frac{0.78*124.71}{17.839*10^6}} = 0.01468 \text{ s} = 14.68 \text{ ms}$$

Now, the blast force on tributary area (F_1) = 59 * 2.083 * 2.083 = 255.995 kN. Using UFC chart,

$$\frac{t_d}{T_s} = \frac{18}{14.68} = 1.23, for\ \mu = 1.0\ \ gives\ \ \frac{R_m}{F_1} = 1.6$$

Thus, $(R_m)_{demand}$ = 1.6 * 255.995 = 409.6 kN > $(R_m)_{capacity}$ = 145.83 kN. Thus, mullions are behaving in plastic range. Thus, assume K_{LM} = 0.72 as an average load mass factor for the entire elasto-plastic range, the time period of the mullion is modified as follows,

$$T_s = 2\pi\sqrt{\frac{0.72*124.71}{17.839*10^6}} = 0.0141 \text{ s} = 14.1 \text{ ms}$$

Now, for R_m/F_1 = 145.83/255.995 = 0.57, using UFC Chart, the ductility demand is calculated as follows,

$$\frac{t_d}{T_s} = \frac{18}{14.1} = 1.28\ and\ \ \frac{R_m}{F_1} = 0.57\ \ gives\ \ \mu = 10.5$$

Thus, the deflection at mid height responsible for rupture is u_m = 10.5 * 8.18 = 85.84 mm. The obtained inelastic displacement is now compared with nonlinear single degree of freedom (SDOF) analysis done with the help of RC-Blast software.

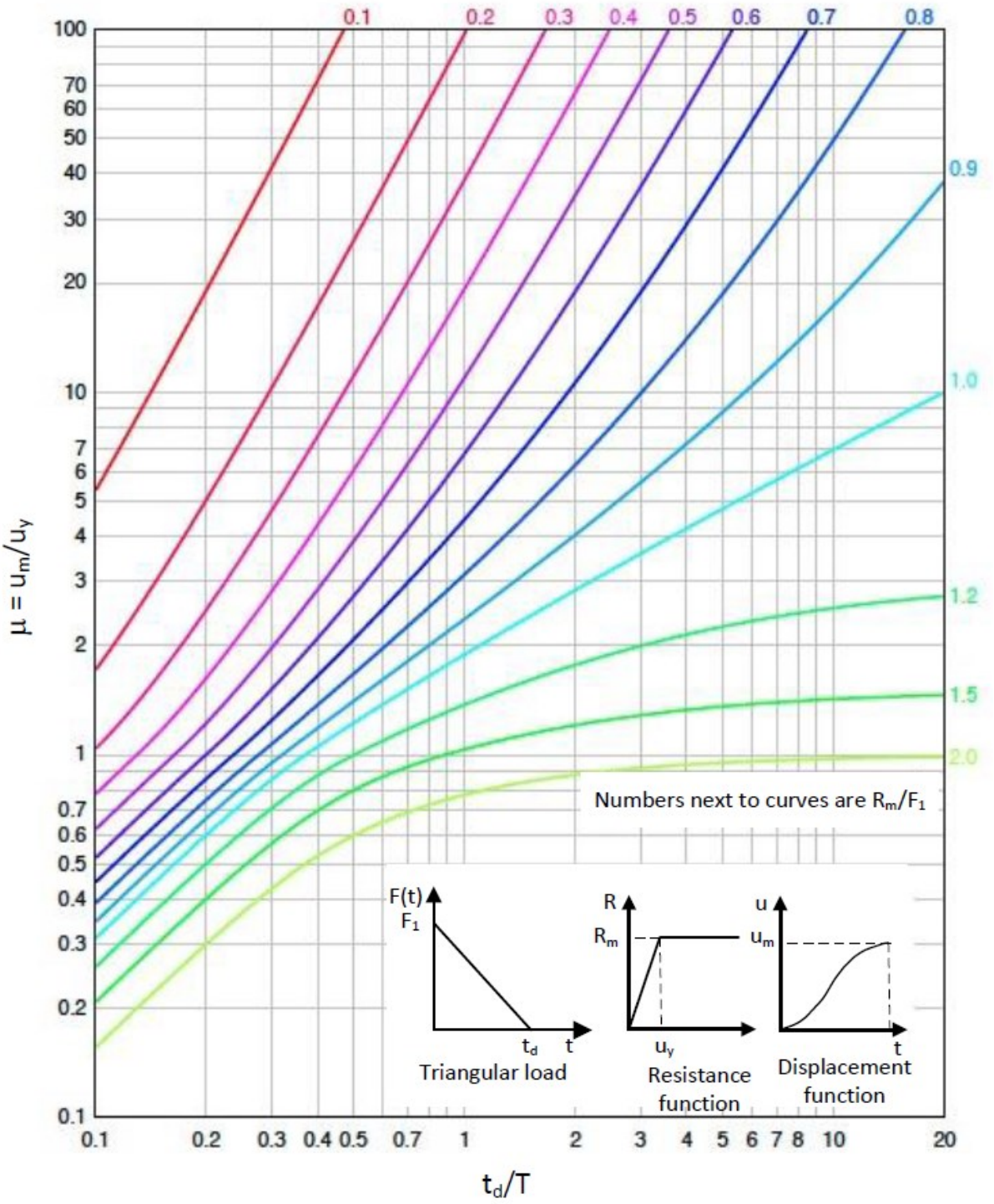

Figure B - 1 : UFC chart for calculating ductility ratio

APPENDIX C PROTOTYPE BUILDING RETROFIT PARAMETRIC CALCULATIONS

C.1 MASS CALCULATION CURTAIN WALL

Mass density of glass = 2400 kg/m^3

Area of glass panes = 1.307 x 2.911 = 3.805 m^2

Mass of glass panes = 3.805 x (4 + 4 + 4.7) x 10^{-3} x 2400 = 115.977 kg

Mass density of laminate = 1000 kg/m^3

Mass of laminate = 3.805 x 0.003 x 1000 = 11.415 kg

Mass density of daylight films = 1000 kg/m^3

Mass of 2 - daylight films = 2 x 3.805 x 0.000176 x 1000 = 1.34 kg

Mass density of aluminum = 2700 kg/m^3

Mass of 1 - vertical mullion = (133 x 63 – 127 x 57) x 10^{-6} x 3.1 x 2700 = 9.542 kg

Mass of 3 - horizontal mullions = (73 x 63 – 67 x 57) x 10^{-6} x 1.37 x 2700 = 2.886 kg

Total mass of curtain wall = 115.977 + 11.415 + 1.34 + 9.542 + 2.886 = 141.16 kg

C.2 RESISTANCE FUNCTION OF ALUMINUM FRAME

The cross-section details of Case A Mullion are given as follows,

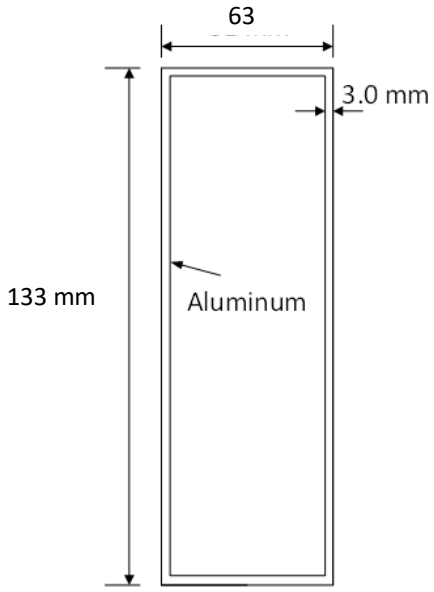

Figure C - 1 : Critical curtain wall mullion c/s details

The numerical values of the properties required for establishing resistance function are given as follows:

Yield Strength of Aluminum (f_y) = 210 MPa

Modulus of Elasticity (E_A) = 70000 N/mm^2

Length of tributary area (L) = 3100 mm

Width of tributary area (W) = 1370 mm

Total mass of curtain wall assembly (m) = 141.16 kg

Moment of inertia for mullion-1 (I) = $\frac{(63*133^3) - (57*127^3)}{12}$ = 2621525 mm^4

Stiffness for simply supported beam assembly,

$$k_s = \frac{(384)\mathrm{EI}}{5L^3} = \frac{384 * 70000*2621525}{5 * 3100^3} = 473.07 \text{ N/mm}$$

Moment Capacity of section,

$$M^- = M^+ = \frac{(f_y)\, I}{y}$$

Here, M^- and M^+ are negative and positive moment capacities. Here, *'y'* is the maximum distance to the tension fibers from the neutral axis which is half of the section depth (133/2 = 66.5 mm). Thus, substituting the above calculated values in the moment equation,

$$M = \frac{210*2621525}{66.5} = 8278500 \text{ N.mm} = 8.279 \text{ kN.m}$$

Elastic Resistance of mullion,

$$R_m = \frac{8M}{L} = \frac{8*8.279}{3.1} = 21.364 \text{ kN}$$

Yield displacement,

$$u_y = \frac{R_m}{k_s} = \frac{(21.364)(1000)}{(473.07)} = 45.16 \text{ mm}$$

Now, considering the yield displacement calculated as above, the maximum inelastic displacement is calculated by the use of RC-Blast software for the applied combination of pressure-impulse loading equivalent to 50 kg of TNT at 20 m of standoff distance and the pressure impulse charts are developed.

C.3 RESISTANCE FUNCTION FOR MULLION WITH L-SHAPED STEEL PLATES HARDENING TECHNIQUE

The numerical values of the properties required for establishing resistance function are given as follows:

Modulus of Elasticity of aluminum (E_A) = 70000 N/mm^2

Modulus of Elasticity of steel (E_S) = 200000 N/mm^2

Density of steel = 7850 kg/m^3

Yield Strength of steel (f_y) = 350 MPa

Length of tributary area (L) = 3100 mm

Width of tributary area (W) = 1370 mm

Total mass of curtain wall assembly (m) = 165.179 kg

Calculation of transformed M.I for the composite section:

Transformation factor to convert aluminum section into equivalent steel section: n = E_A/E_s = 0.35

Area of aluminum mullion = (133 x 63 – 127 x 57) = 1140 mm^2

Transformed area of aluminum to steel section = 0.35 x 1140 = 399 mm^2

M.I of aluminum mullion = 2621525 mm^4

Transformed M.I of aluminum to steel section = 0.35 x 2621525 = 917533.75 mm^4

Area of steel area 1 and area 2 = 133 x 3 = 399 mm^2

M.I for area 1 and area 2 = $\frac{3 * 133^3}{12}$ = 588159.25 mm^4

M.I for area 3 = $\frac{63 * 3^3}{12}$ = 141.75 mm^4

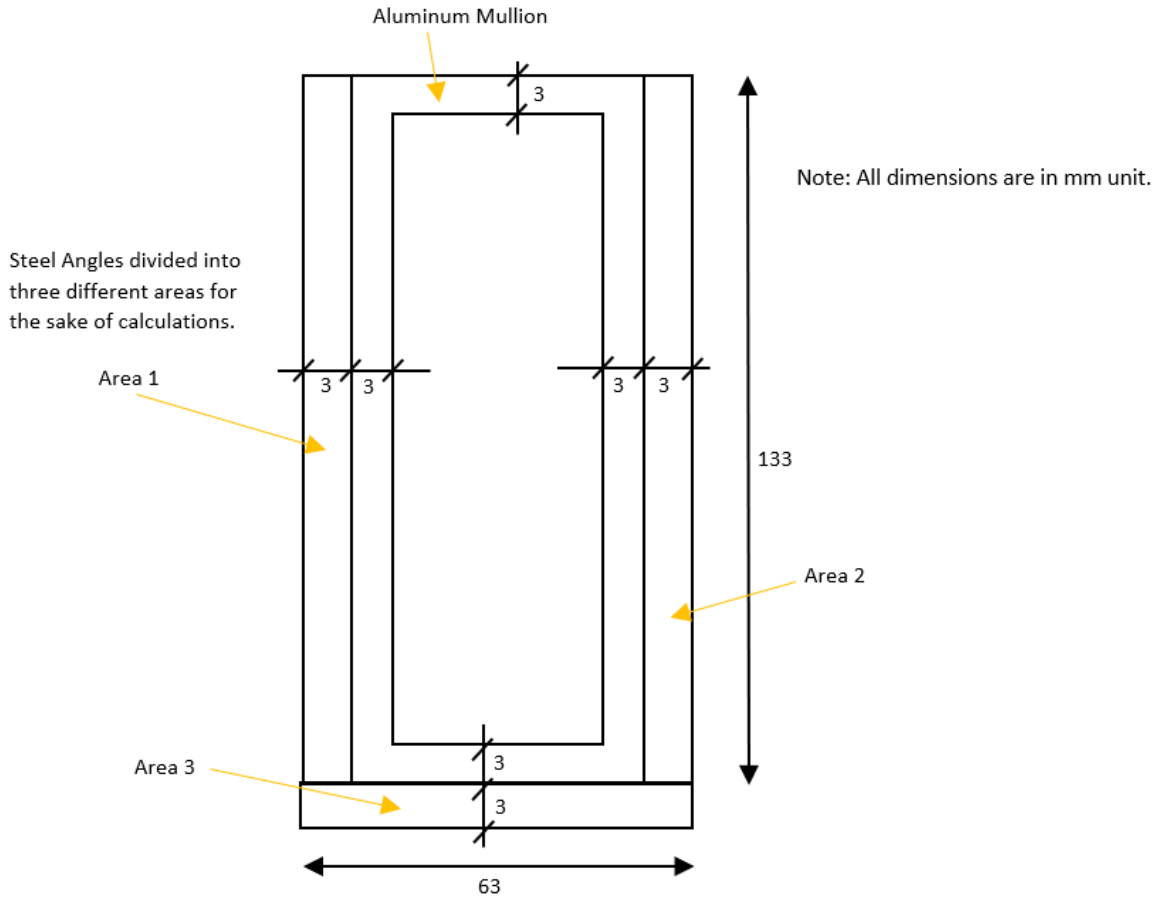

Figure C - 2 : Area division for mullion with L-Shaped steel plates

Area of steel area 3 = 63 x 3 = 189 mm^2

Distance of the neutral axis from the extreme bottom (tension) fibers,

$$y = \frac{2 * 399 * 69.5 + 399 * 69.5 + 189 * 1.5}{399 + 798 + 189} = 60.23\ mm$$

Moment of inertia for the transformed section,

I_{TR} = [917533.75 + 399 x (69.5 - 60.23)^2] + 2 x [588159.25 + 399 x (69.5 – 60.23)^2] + [141.75 + 189 x (60.23 – 1.5)^2 = 2848756.919 mm^4

Stiffness for simply supported beam assembly,

$$k_s = \frac{(384)\mathrm{EI}}{5L^3} = \frac{384 * 200000 * 2848756.919}{5 * 3100^3} = 1468.796\ \mathrm{N/mm}$$

Moment Capacity of section,

$$M^- = M^+ = \frac{(f_y)\, I}{y}$$

Here, M^- and M^+ are negative and positive moment capacities. Here, *'y'* is the maximum distance to the tension fibers from the neutral axis. Thus, substituting the above calculated values in the moment equation,

$$M = \frac{350*2848756.919}{60.23} = 16554291 \text{ N.mm} = 16.555 \text{ kN.m}$$

Elastic Resistance of mullion,

$$R_m = \frac{8M}{L} = \frac{8*16.555}{3.1} = 42.72 \text{ kN}$$

Yield displacement,

$$u_y = \frac{R_m}{k_s} = \frac{(42.72)(1000)}{(1468.796)} = 29.08 \text{ mm}$$

Now, considering the yield displacement calculated as above, the maximum inelastic displacement is calculated by the use of RC-Blast software for the applied combination of pressure-impulse loading equivalent to 50 kg of TNT at 20 m of standoff distance and the pressure impulse charts are developed.

C.4 RESISTANCE FUNCTION FOR MULLION WITH 3.0 MM THICK STEEL HSS AND SIDE PLATES HARDENING TECHNIQUE

The numerical values of the properties required for establishing resistance function are given as follows:

Modulus of Elasticity of aluminum (E_A) = 70000 N/mm^2

Modulus of Elasticity of steel (E_S) = 200000 N/mm^2

Density of steel = 7850 kg/m^3

Yield Strength of steel (f_y) = 350 MPa

Length of tributary area (L) = 3100 mm

Width of tributary area (W) = 1370 mm

Total mass of load application device (m) = 187.3 kg

Calculation of transformed M.I for the composite section:

Transformation factor to convert aluminum section into equivalent steel section: $n = E_A/E_s = 0.35$

Area of aluminum mullion = (133 x 63 – 127 x 57) = 1140 mm^2

Transformed area of aluminum to steel section = 0.35 x 1140 = 399 mm^2

M.I of aluminum mullion = 2621525 mm^4

Transformed M.I of aluminum to steel section = 0.35 x 2621525 = 917533.75 mm^4

Area of steel area 1 and area 2 = 196 x 3 = 588 mm^2

M.I for area 1 and area 2 = $\frac{3 * 196^3}{12}$ = 1882384 mm^4

M.I for area 3 = $\frac{(63*63^3)-(57*57^3)}{12}$ = 433080 mm^4

Area of steel area 3 = (63 x 63) – (57 x 57) = 720 mm^2

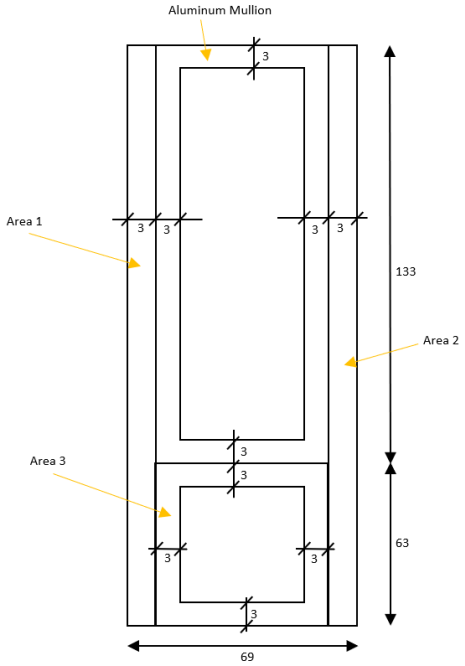

Note: All dimensions are in mm unit.

Figure C - 3 : Area division for mullion with 3 mm thick steel HSS and side plates

Distance of the neutral axis from the extreme bottom (tension) fibers,

$$y = \frac{399 * 129.5 + 2 * 588 * 98 + 720 * 31.5}{399 + 2 * 588 + 720} = 82.614\ mm$$

Moment of inertia for the transformed section,

I_{TR} = [917533.75 + 399 x (129.5 – 82.614)^2] + 2 x [1882384 + 588 x (98 – 82.614)^2] + [433080 + 720 x (82.614 – 31.5)^2 = 8151997.068 mm^4

Stiffness for simply supported beam assembly,

$$k_s = \frac{(384)\mathrm{EI}}{5L^3} = \frac{384 * 200000 * 8151997.068}{5 * 3100^3} = 4203.11\ \mathrm{N/mm}$$

Moment Capacity of section,

$$M^- = M^+ = \frac{(f_y)\ I}{y}$$

Here, M^- and M^+ are negative and positive moment capacities. Here, *'y'* is the maximum distance to the tension fibers from the neutral axis. Thus, substituting the above calculated values in the moment equation,

$$M = \frac{350 * 8151997.068}{82.614} = 34536507\ \mathrm{N.mm} = 34.54\ \mathrm{kN.m}$$

Elastic Resistance of mullion,

$$R_m = \frac{8M}{L} = \frac{8 * 34.54}{3.1} = 89.126\ \mathrm{kN}$$

Yield displacement,

$$u_y = \frac{R_m}{k_s} = \frac{(89.126)(1000)}{(4203.11)} = 21.205\ \mathrm{mm}$$

Now, considering the yield displacement calculated as above, the maximum inelastic displacement is calculated by the use of RC-Blast software for the applied combination of pressure-impulse loading equivalent to 50 kg of TNT at 20 m of standoff distance and the pressure impulse charts are developed.

C.5 RESISTANCE FUNCTION FOR MULLION WITH 6.3 MM THICK STEEL HSS AND SIDE PLATES HARDENING TECHNIQUE

The numerical values of the properties required for establishing resistance function are given as follows:

Modulus of Elasticity of aluminum (E_A) = 70000 N/mm^2

Modulus of Elasticity of steel (E_S) = 200000 N/mm^2

Density of steel = 7850 kg/m^3

Yield Strength of steel (f_y) = 350 MPa

Length of tributary area (L) = 3100 mm

Width of tributary area (W) = 1370 mm

Total mass of load application device (m) = 236 kg

Calculation of transformed M.I for the composite section:

Transformation factor to convert aluminum section into equivalent steel section: n = E_A/E_s = 0.35

Area of aluminum mullion = (133 x 63 – 127 x 57) = 1140 mm^2

Transformed area of aluminum to steel section = 0.35 x 1140 = 399 mm^2

M.I of aluminum mullion = 2621525 mm^4

Transformed M.I of aluminum to steel section = 0.35 x 2621525 = 917533.75 mm^4

Area of steel area 1 and area 2 = 196 x 6.3 = 1234.8 mm^2

M.I for area 1 and area 2 = $\frac{6.3 * 196^3}{12}$ = 3953006.4 mm^4

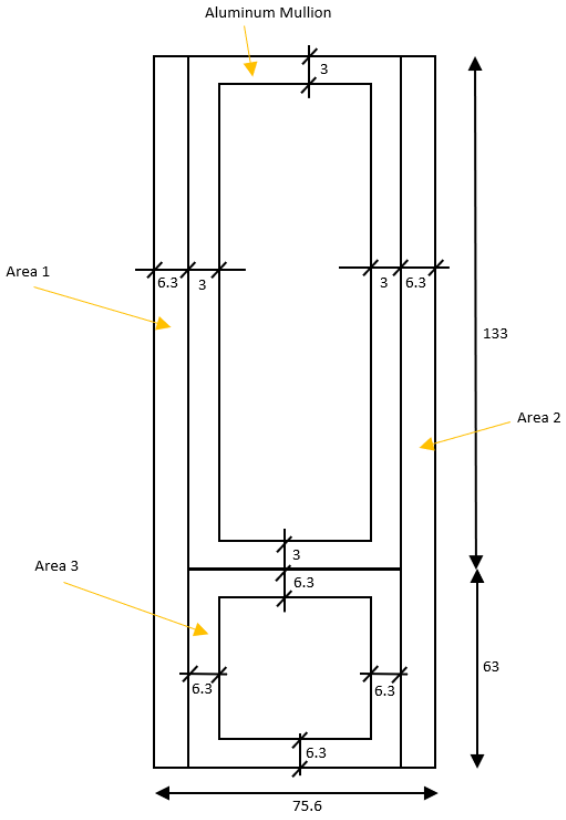

Note: All dimensions are in mm unit.

Figure C - 4 : Area division for mullion with 6.3 mm thick steel HSS and side plates

M.I for area 3 = $\frac{(63*63^3)-(50.4*50.4^3)}{12}$ = 775045.681 mm^4

Area of steel area 3 = (63 x 63) – (50.4 x 50.4) = 1428.84 mm^2

Distance of the neutral axis from the extreme bottom (tension) fibers,

$$y = \frac{399 * 129.5 + 2 * 1234.8 * 98 + 1428.84 * 31.5}{399 + 2 * 1234.8 + 1428.84} = 78.82\ mm$$

Moment of inertia for the transformed section,

I_{TR} = [917533.75 + 399 x (129.5 – 78.82)^2] + 2 x [3953006.4 + 1234.8 x (98 – 78.82)^2] + [775045.681 + 1428.84 x (78.82 – 31.5)^2 = 14731339.79 mm^4

Stiffness for simply supported beam assembly,

$$k_s = \frac{(384)\mathrm{EI}}{5L^3} = \frac{384 * 200000 * 14731339.79}{5 * 3100^3} = 7595.36\ \mathrm{N/mm}$$

Moment Capacity of section,

$$M^- = M^+ = \frac{(f_y)\, I}{y}$$

Here, M^- and M^+ are negative and positive moment capacities. Here, *'y'* is the maximum distance to the tension fibers from the neutral axis. Thus, substituting the above calculated values in the moment equation,

$$M = \frac{350*14731339.79}{78.82} = 65414475 \text{ N.mm} = 65.42 \text{ kN.m}$$

Elastic Resistance of mullion,

$$R_m = \frac{8M}{L} = \frac{8*65.42}{3.1} = 168.82 \text{ kN}$$

Yield displacement,

$$u_y = \frac{R_m}{k_s} = \frac{(168.82)(1000)}{(7595.3603)} = 22.23 \text{ mm}$$

Now, considering the yield displacement calculated as above, the maximum inelastic displacement is calculated by the use of RC-Blast software for the applied combination of pressure-impulse loading equivalent to 50 kg of TNT at 20 m of standoff distance and the pressure impulse charts are developed.

APPENDIX D EXPERIMENTAL DAMAGE PROGRESSION OF CURTAIN WALL MULLIONS

D.1 EXPERIMENTAL DAMAGE PROGRESSION FOR MULLION 1

D.1.1 Mullion 1 – Before test

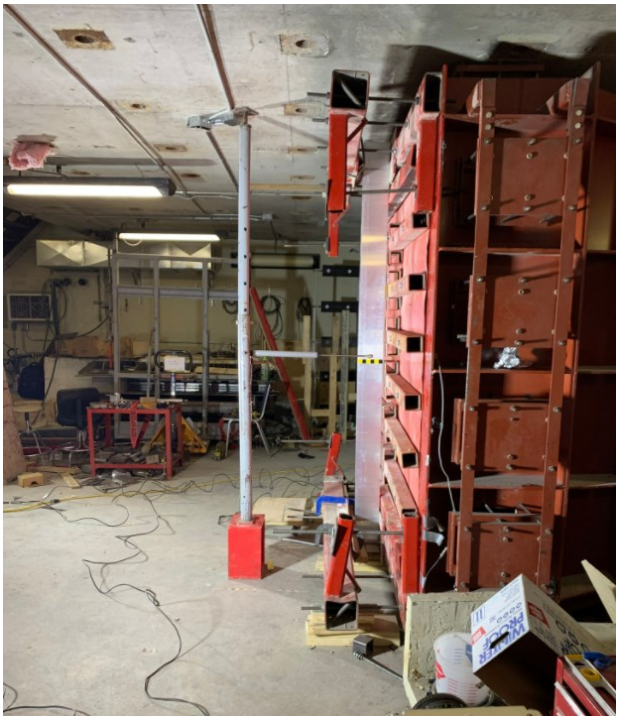

D.1.2 Mullion 1 – After test

D.1.2.1 Damage progression at Blast Shot – 1 (27 kPa – 191 kPa-msec)

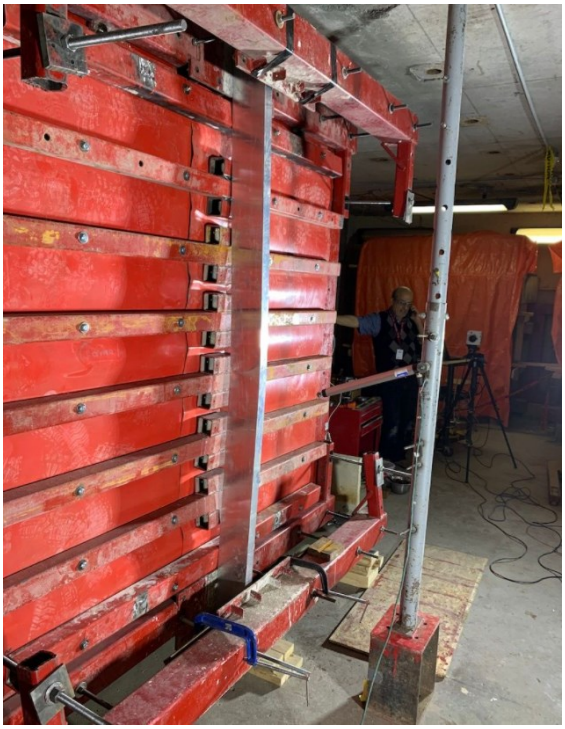

D.2 EXPERIMENTAL DAMAGE PROGRESSION FOR MULLION 1H

D.2.1 Mullion 1H – Before test

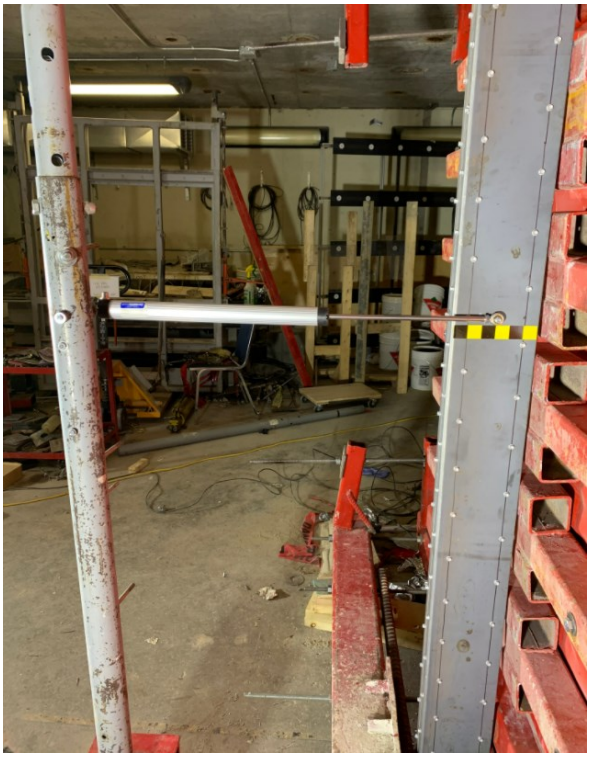

D.2.2 Mullion 1H – After test

D.2.2.1 Damage progression at Blast Shot – 1 (27 kPa – 210 kPa-msec)

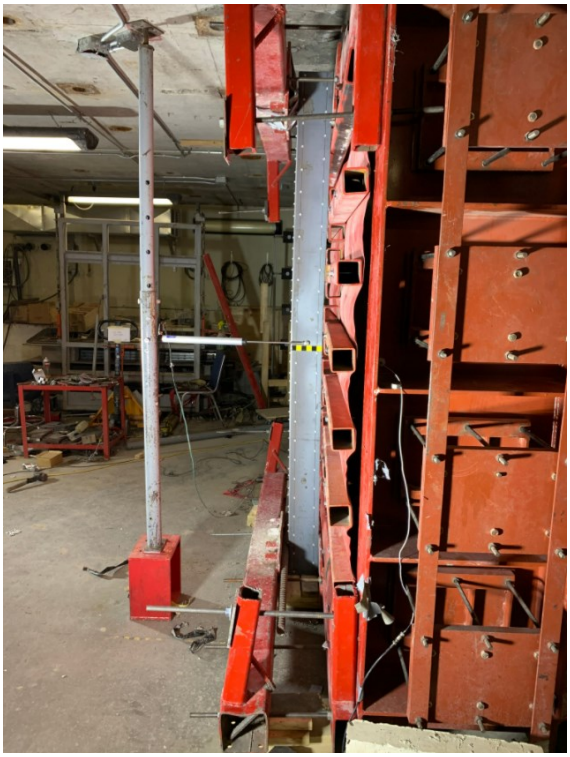

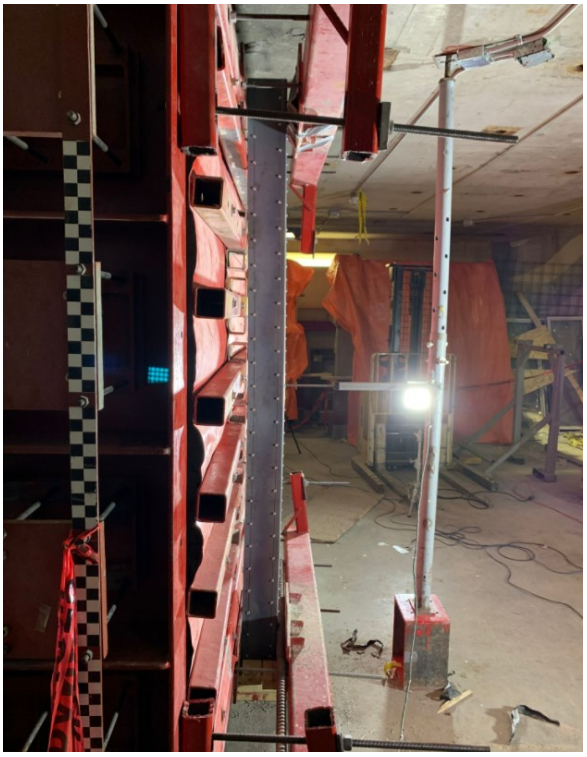

D.2.2.2 Damage progression at Blast Shot – 2 (59 kPa – 411 kPa-msec)

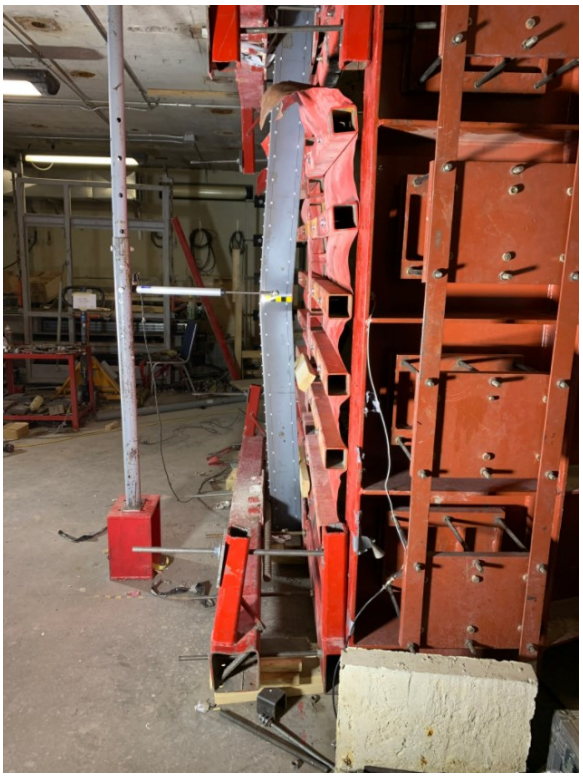

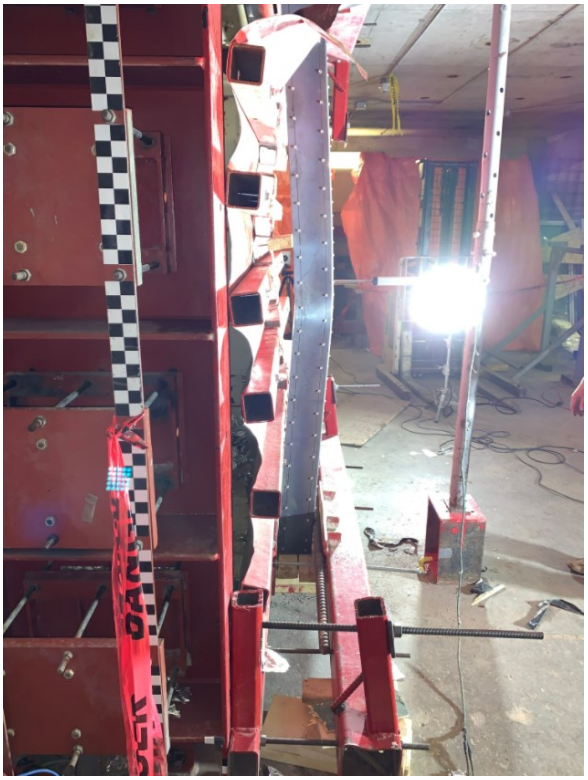

D.3 EXPERIMENTAL DAMAGE PROGRESSION FOR MULLION 2

D.3.1 Mullion 2 – Before test

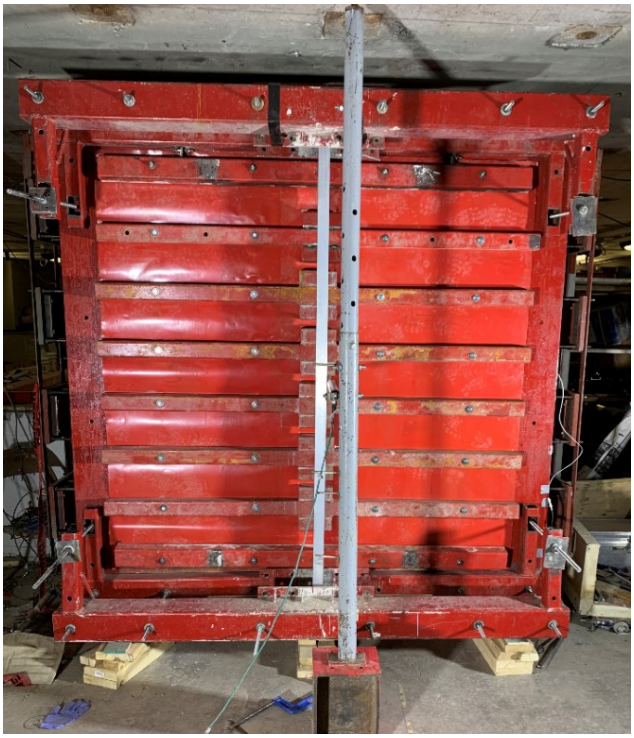

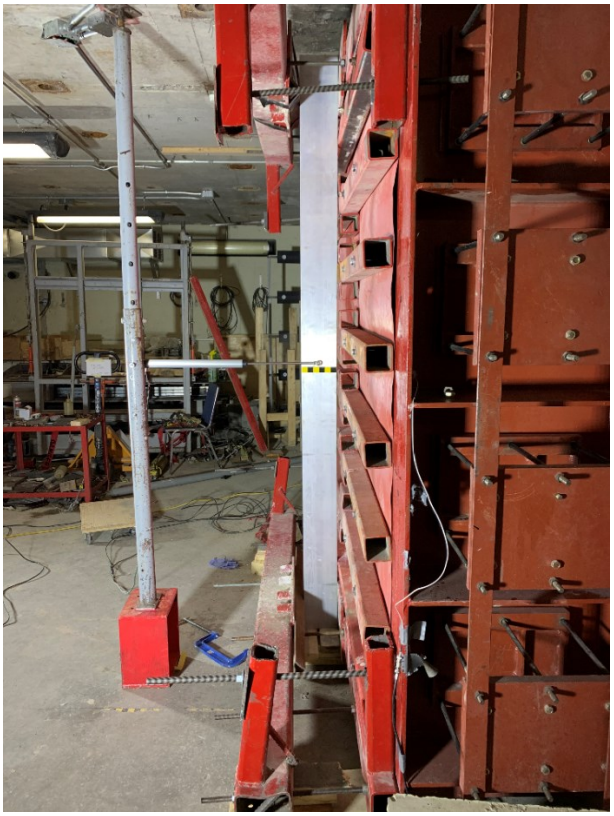

D.3.2 Mullion 2 – After test

D.3.2.1 Damage progression at Blast Shot – 1 (30 kPa – 225 kPa-msec)

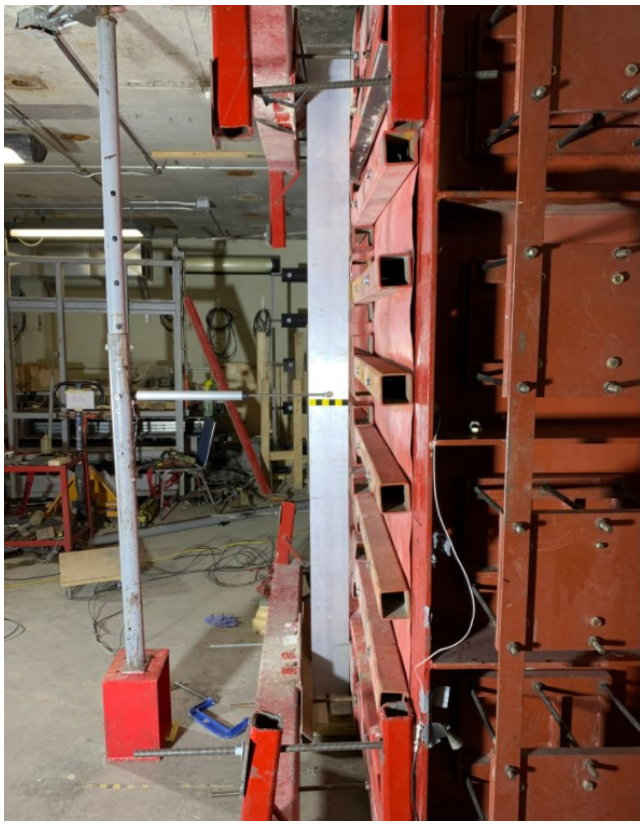

D.3.2.2 Damage progression at Blast Shot – 2 (38 kPa – 270 kPa-msec)

D.3.2.3 Damage progression at Blast Shot – 3 (44 kPa – 337 kPa-msec)

D.4 EXPERIMENTAL DAMAGE PROGRESSION FOR MULLION 2H

D.4.1 Mullion 2H – Before test

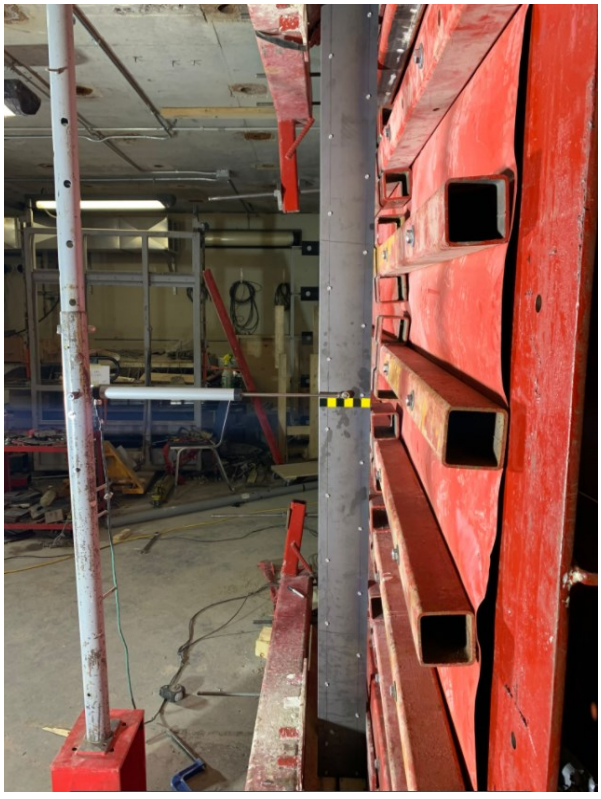

D.4.2 Mullion 2H – After test

D.4.2.1 Damage progression at Blast Shot – 1 (41 kPa – 332 kPa-msec)

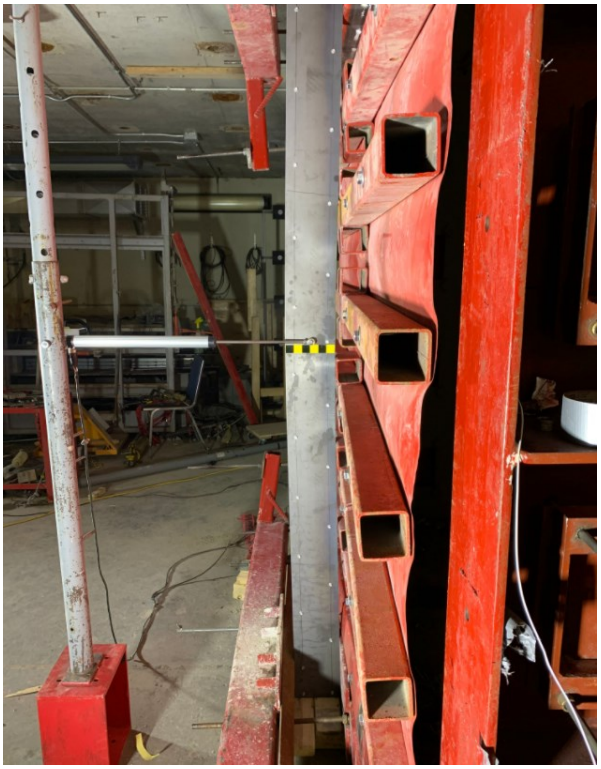

D.4.2.2 Damage progression at Blast Shot – 2 (65 kPa – 487 kPa-msec)

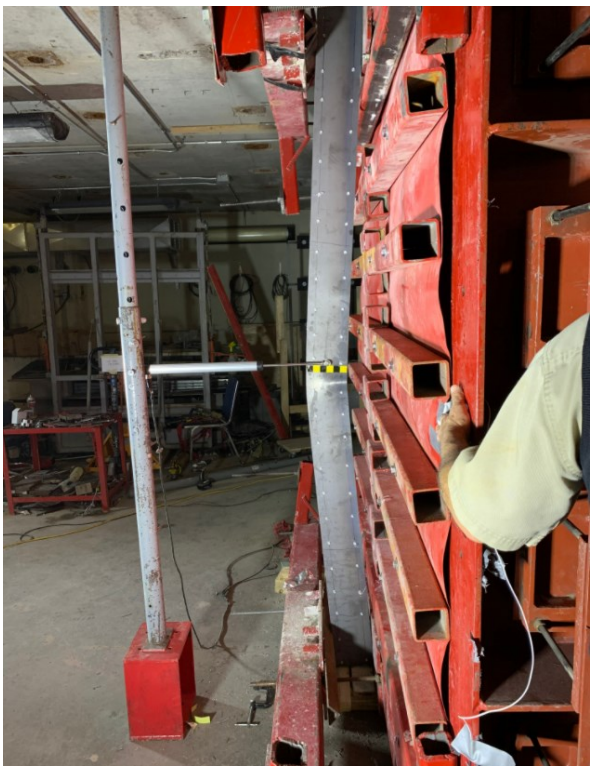

D.4.2.3 Damage progression at Blast Shot – 3 (82 kPa – 654 kPa-msec)

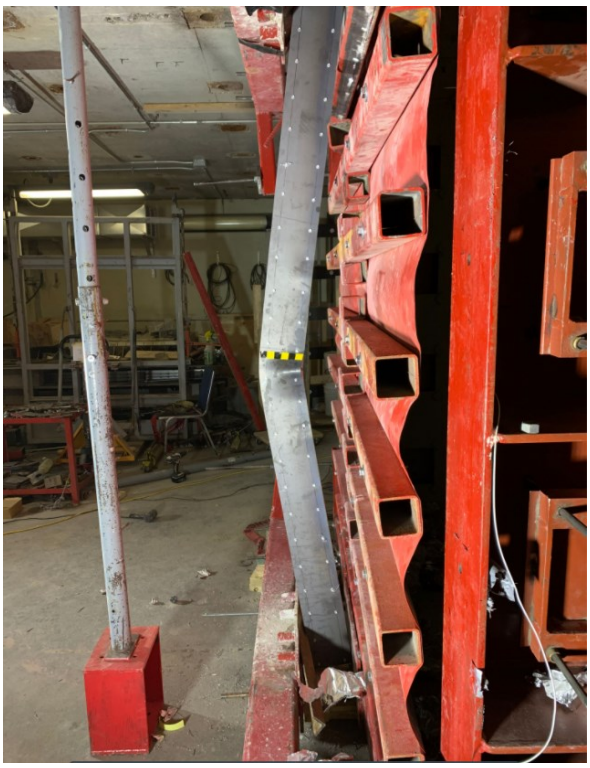

D.5 EXPERIMENTAL DAMAGE PROGRESSION FOR MULLION 3

D.5.1 Mullion 3 – Before test

D.5.2 Mullion 3 – After test

D.5.2.1 Damage progression at Blast Shot – 1 (25 kPa – 208 kPa-msec)

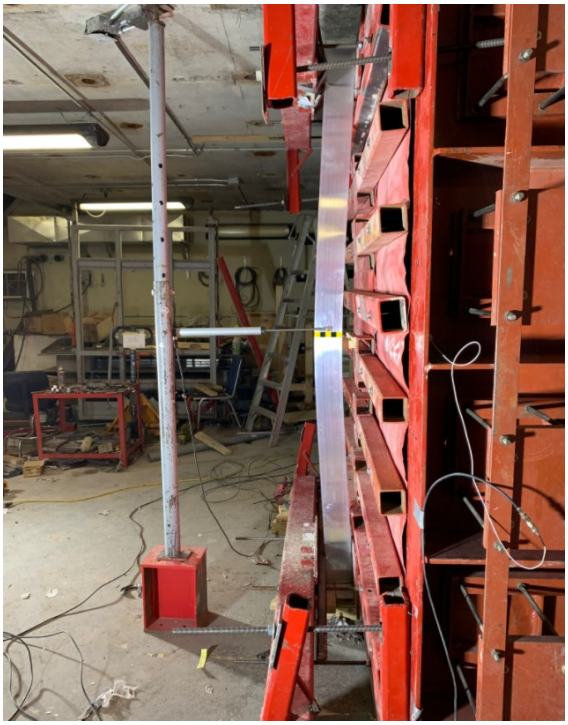

D.6 EXPERIMENTAL DAMAGE PROGRESSION FOR MULLION 3H

D.6.1 Mullion 3H – Before test

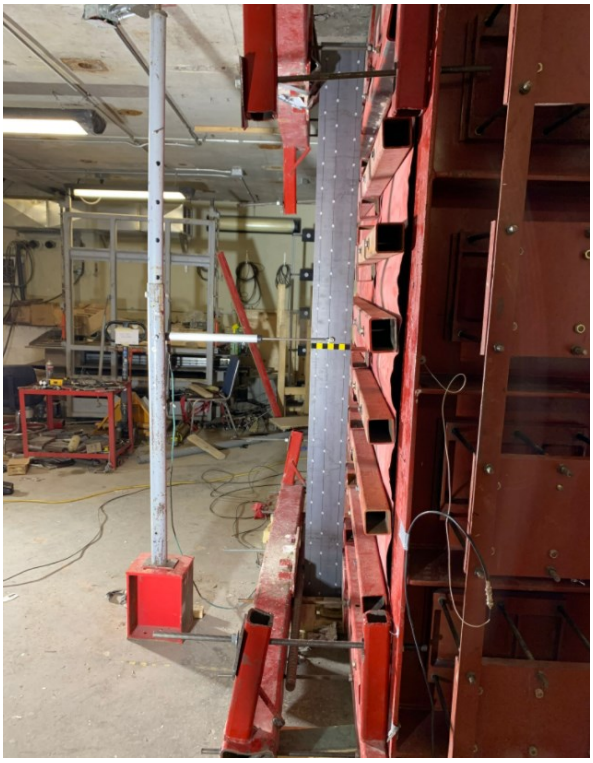

D.6.2 Mullion 3H – After test

D.6.2.1 Damage progression at Blast Shot – 1 (26 kPa – 207 kPa-msec)

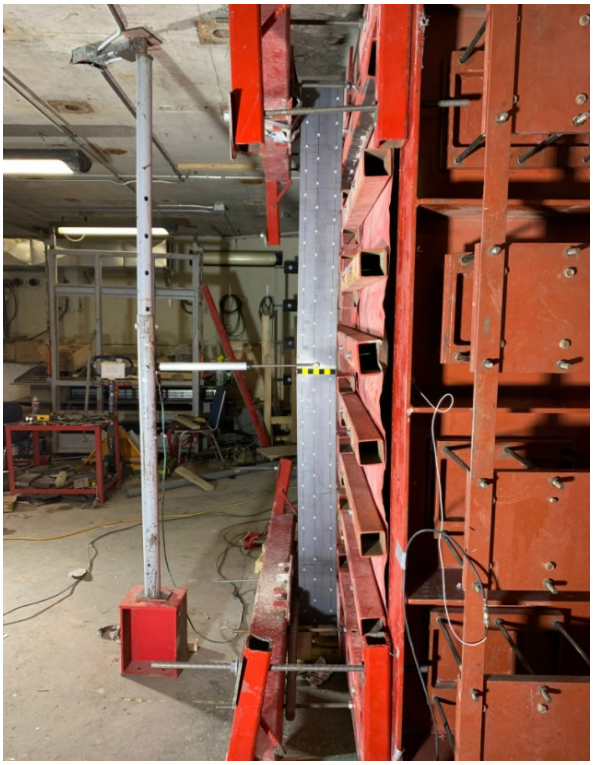

D.6.2.2 Damage progression at Blast Shot – 2 (51 kPa – 428 kPa-msec)